INAUGURAL DISSERTATION/ THESE

zur
Erlangung der Doktorwürden
der
Naturwissenschaftlichen-Mathematischen Gesamtfakultät
der

Présentée pour obtenir
Le GRADE de DOCTEUR EN SCIENCES
de

RUPRECHT-KARLS-UNIVERSITÄT HEIDELBERG

und/ et

L'UNIVERSITE PARIS XI ORSAY

vorgelegt von/ par

Diplom-Biochemikerin Sylvia Gabriele Münter
aus/ née à Heidelberg

Tag der Disputation/ Date de la Soutenance: 20.07.2004

THEMA/ SUJECT:

Analyzing the role of a cellular mechanism in HIV infection
and
Evaluation of novel antiviral compounds

Prüfungskommission/ Commission d'examen:

Prof. Dr. Hermann Irngartinger	
Prof. Michel Jacquet	
Prof. Dr. Dr. Jürgen Debus	Gutachter/ Rapporteur
Dr. Ulf Nehrbass	Gutachter/ Rapporteur

Publication list:

Knoblauch H, Busjahn A, **Münter S**, Nagy Z, Faulhaber HD, Schuster H, Luft FC. (1997); Heritability analysis of lipids and three gene loci in twins link the macrophage scavenger receptor to HDL cholesterol concentrations. *Arterioscler Thromb Vasc Biol*. 1997 Oct;17(10):2054-60.

Bajramovic JJ, **Münter S**, Syan S, Nehrbass U, Brahic M, Gonzalez-Dunia D. (2003); Borna disease virus glycoprotein is required for viral dissemination in neurons. *J Virol.* 2003 Nov;77(22):12222-31.

Roux P, **Münter S**, Frischknecht F, Herbomel P, Shorte SL. (2004); Focussing light on infection in four dimensions. *Cell Micobiol.* 2004 Apr;6(4):333-43. Review.

Münter S, Vazquez-Martinez R, Matunis MJ, David-Watine B, Nehrbass U, Shorte SL. Nuclear envelope dynamics are driven by high turnover actin polymerization (submitted).

Presentations at international meetings:

29.08. -04.09.2002	EMBO YIP PhD course Heidelberg: Poster presentation and oral presentation.
18.06.2003	First Congress of young researchers at the Pasteur Institute: Oral presentation.
13-17.12.2003	ASCB 2003 Annual Meeting San Francisco: Poster presentation.

Preamble

First of all, I would like to thank Ulf Nehrbass and Jürgen Debus having accompanied me during my doctoral thesis and for the help and inspiring discussions during the last four years.

Furthermore, I thank Professor Irngartinger for accepting me as a student under his supervision in the Department of Chemistry at the University of Heidelberg. Also, I appreciated a lot his help and advice concerning the chemical syntheses I completed in his laboratory.

I would like to express my thankfulness to Professor M. Jacquet having accepted to be part of the evaluation committee of my thesis in the *cotutelle* program between Paris and Heidelberg.

Especially, I want to thank Spencer Shorte for the ongoing help and the knowledge I achieved in fluorescent microscopy; moreover for the excellent supervision related to important constituents of my thesis and many motivating scientific conversations.

I thank all the members in the BCN lab for their encouragement during my work, the fantastic working atmosphere (even if sometimes a bit to enthusiastic about the sound) and the innumerable relaxing moments we spent in the lab … and (just to name one) in the "Breguet"; Mr. Pubmed and the better half of the "genius couple of science" for critical reading of this manuscript and all the scientific (besides many other) conversations; Ivan for the lessons in self-defense; Sophie and Brigitte for ongoing english-french and french-french translation efforts ; Edith Gouin and Laurent Blanchoin for outstanding collaboration and help during my thesis; Denise Guetard for the help and introduction to working secrets in a P3 laboratory; Klaus Braun for his supervision and help in the very first steps of my work; Rüdiger Pipkorn for the help with PNA syntheses; the mass spectrometry people at the DKFZ and the Department of Chemistry at Heidelberg University for the vast amount of samples they measured for me; Ms. M. Decraene and Ms. Dr. M. Schaade for their support in administrative questions … and without whom my "convention de *cotutelle*" would have never existed.

Also I want to thank all my friends (and at this point especially the Nocke family) for the pleasurable moments and keeping me up during the last years.

Finally the most special thank to my father, my brother and Felix.

Für meinen Vater
und
meine Mutter
(Du hast den Raum mit Sonne geflutet)

TABLE OF CONTENTS:

INDEX OF FIGURES AND TABLES:

Abbreviations:

ADP	adenosine diphosphate
ADF	actin-depolymerizing factor
AIDS	acquired immunodeficiency syndrome
Arp2/3 complex	actin related protein complex
ATP	adenosine triphosphate
BDV	borna disease virus
Bhoc	benzohydryloxycarbonyl
bp	base pair
CCPs	cell-penetrating peptides
CD	cytochalasin D
CD-BODIPY	cytochalasin linked to the fluorescent compound BODIPY
CNS	central nervous system
cPPT	central polypurine tract
DDT	dithiothreitol
DIPEA	diisopropylamine
DMEM	Dulbecco's Modified Eagle Medium
DMF	*N,N*-dimethyl formamide
DMSO	dimethyl sulfoxide
DNA	deoxyribonucleic acid
dsDNA	double stranded DNA
DsRed	red fluorescence protein (isolated from the reef coral *Discosoma sp*.)
EDC	1-ethyl-3-(3-dimethylaminopropyl)carbodiimide
EDTA	ethylenediaminetetraacetic acid
ELISA	enzyme-linked immunosorbent assay
F-actin	filaments or filamentous-actin
FITC	Fluorescein isothiocyanate
Fmoc	N-(9-fluorenyl) methoxycarbonyl
G-actin	monomers or globular-actin
GDP	guanosine diphosphate
GFP	green fluorescent protein
GP	glycoprotein
GTP	guanosine triphosphate
HAART	highly active anti-retroviral therapy
HIV	Human immunodeficiency virus
HPLC	high-performance liquid chromatography
IFs	intermediate filaments
Jaspl	Jasplakinolide

kb	kilo base pair
kDa	kilodaltons
LatA	LatrunculinA
LTR	long terminal repeat
mAb	monoclonal Antibody
mRNA	messenger RNA
MTOC	MT-organizing center
MTs	microtubules
n.a.	numerical aperture
NC	nucleocapsid
NE	nuclear envelopes
NLS	nuclear localization sequence
NMR	nuclear magnetic resonance
NRTI	nucleoside reverse transcriptase inhibitor
NUANCE	NUcleus and ActiN Connecting Element
NPC	nuclear pore complex
PAGE	Polyacrylamide gel electrophoresis
pAntp	*Drosophila* Antennapedia homeoprotein
PBS	phosphate buffered saline
PIC	pre-integration complex
PNA	peptide nucleic acid
PSF	point-spread-function
POM121	a transmembrane nuclear pore complex protein
RNA	ribonucleic acid
RNase H	Ribonuclease H
SIV	Simian immunodeficiency virus
SV40 T	simian virus 40T antigen
TFA	trifluoroacetic acid
TM	transmembrane
tRNA	transfer RNA
SDS	sodium dodecyl sulfate
SU	surface
Vpr	viral protein R
WASP	Wiskott-Aldrich syndrome protein
ψiC or ‘J bases’	pseudoisocytosine

1. Introduction

1.1 The Human Immunodeficiency Virus (HIV)

1.1.1 History and origin of the virus

The human immunodeficiency virus (HIV), a retrovirus belonging to the genus of *lentiviridae*, is the causative agent of acquired immunodeficiency syndrome (AIDS). The debate around the origin of HIV has sparked considerable interest and controversy since the beginning of the epidemic. The first cases of AIDS occurred in the USA in 1981, but they provided little information about the source of the disease. On June 05, 1981, the Centers for Disease Control and Prevention in the United States published the first report on an extremely rare form of pneumonia in five people whose immune systems had been completely destroyed. Subsequently, science progressed at a phenomenal rate. Within two years the virus responsible for the illness was identified (Barre-Sinoussi et al., 1983) and later named HIV. By 1985, serological screening was in place to prevent further infection through blood transfusion and blood products. In 1986, clinical trials began on the first anti-HIV drug, AZT (Zidovudine, a nucleoside reverse transcriptase inhibitor (NRTI)). Unfortunately, disappointment followed as researchers realized that the virus was capable of changing its genetic code with astonishing speed. The seven years that followed were marked by discouragement, because the virus spread like wildfire without a relief in sight. Then, at the 1993 International Conference on AIDS in Berlin, the results of a clinical study combining two NRTIs ("bitherapy"), AZT and ddC (Zalcitabine) or ddI (dideoxynosine), were presented, giving birth to renewed hope. But once again, these treatments would prove insufficient. Finally, in early 1996, basic research on the biology of HIV resulted in the creation of a whole new class of extremely powerful medications, inhibiting the function of a protein essential for viral maturation (protease inhibitors). When combined with AZT and ddI ("tritherapy") (Richman, 2001), for example, these new medications yielded spectacular results, which led to a 60% reduction of AIDS mortality in the United States (Weiss, 2001).

By now, due to phylogenetic analyses it is generally accepted that the virus crossed species in the first half to the 20th century. Human immunodeficiency virus-type 1

(HIV-1), the most common cause of AIDS, is closely related to SIVcpz (simian immunodeficiency virus) isolated from the chimpanzee subspecies *Pan troglodytes*. Analogously, HIV-2, a less pathogenic strain (but still causing AIDS), is most closely related to SIVsm from sooty mangabeys (Hahn et al., 2000). Additionally there is geographical coincidence with the natural habitat of these primates and the areas of HIV-1 and HIV-2 endemics respectively. One hypothesis to explain the outbreak of AIDS is the direct exposure to infected animal blood (by hunting or other means), which resulted in zoonotic transmission of SIVcpz and SIVsm to humans. This theory is also supported by a study of David Ho and coworkers, who could isolate fragments of an HIV-1 RNA in a patient serum sample (ZR59) drawn back in 1959 in Western Africa (Zhu et al., 1998). This RNA sequence is fitting perfectly into the predictions of the phylogenetic analyses and therefore supports with "hard data" this theory. The particular social, economic, and behavioral changes that occurred in the early and mid-20th century provided the circumstances whereby these viruses could expand and reach epidemic proportions all over the world.

A competing hypothesis (Curtis, 1992; Hooper, 1999; Stricker and Elswood, 1997) suggested that attenuated oral poliovirus (OPV) vaccination trials carried out in the Belgian Congo in the late 1950s were responsible for the cross-species transmission of SIVcpz that initiated the epidemic. These ideas rely on the assumption that chimpanzee kidneys were used in vaccine preparation and therefore caused a direct exposure of humans to infected matter. But two years later three independent laboratories could not find any evidence to support this hypothesis (Berry et al., 2001; Blancou et al., 2001; Rambaut et al., 2001). In none of the original vaccine vials tested, SIV nucleic acids, which could have been responsible for a cross-species transmission, were found.

1.1.2 Status quo of the epidemic

Despite being one of the best-studied pathogens during the last two decades, HIV continues to spread over the world. It is estimated that some 6000 people are infected on a daily basis. In Africa, the epidemic gives little sign of relief, in Asia it is spreading, and in other regions of the world there is growing disquiet about the trends being observed. The global HIV/AIDS epidemic killed more than 3 million people in 2003, and an estimated 5 million acquired the human immunodeficiency virus (HIV). This is bringing the number of people living with the virus up to 40 million. Sub-

Saharan Africa remains by far the region worst affected by the HIV/AIDS epidemic. In 2003, an estimated 26.6 million people in this region were living with HIV, including the 3.2 million who became infected during the past year. Countries in East Asia and the Pacific are on the whole still keeping HIV at bay, with some 130,000 new infections this year. Overall, the two regions combined are estimated to have 6.4 million people living with HIV/AIDS and compared to Africa, infection rates in the general population are still low.

In high-income countries it is estimated that 1.6 million people are living with HIV. A total number of about 170,000 HIV infections have been reported in 17 countries of Western Europe by the end of 2002. However, this number considerably understates the cumulative number of HIV infections because the three countries with the most extensive epidemics (France, Italy and Spain) do not yet have national HIV reporting systems. In Germany about 2000 new infections and 600 deaths are recorded every year. Due to widespread access to antiretroviral treatment the AIDS mortality decreases and the total number of people living with HIV continues to rise in Western Europe and the United States (WHO, 2003).

1.1.3 Retroviruses

Retroviruses comprise a large and diverse family of enveloped RNA viruses defined by common taxonomic denominators that include structure, composition, and replicative properties (Coffin, 1992). The virion RNA is 7-12 kb in size, it is linear, single-stranded, nonsegmented, and of positive polarity. The hallmark of the family is its unique replicative strategy, which includes as essential steps reverse transcription of the virion RNA into linear double-stranded DNA and the subsequent integration of this DNA into the genome of the cell. The discovery of this retroviral characteristic had an important impact on our concept of genetic information, its molecular forms, transmission, and evolution. In the early years of molecular biology, no exceptions to the unidirectional and presumed irreversible flow of genetic information from DNA to RNA to protein were known. This unidirectional flow came to be known as the "Central Dogma." It was this Central Dogma that had to be revised when the replication of retroviruses was understood (Baltimore, 1970; Temin and Mizutani, 1970). Furthermore, a significant percentage of the mammalian genome appears to be the product of reverse transcription, containing sequences derived from ancient retroviral integration.

The reverse transcription of retroviruses is not a singular, odd exception but rather a paradigm for a process that is shared by viral and nonviral genetic elements occurring in yeast, Drosophila and eventually even in plants (Boeke and Chapman, 1991; Boeke and Corces, 1989; Evgen'ev et al., 1992; Peterson-Burch et al., 2000). But the general denotation of retoviruses comprises only the well-characterized forms in vertebrates. They all have in common a virion of about 80-100 nm in diameter, enclosing two single RNA strands by a complex of viral proteins (nucleocapsid). This capsid is by itself enveloped by a lipid bilayer, derived from its host cell after budding, and incorporates and displays specific viral proteins at the surface (Figure 1).

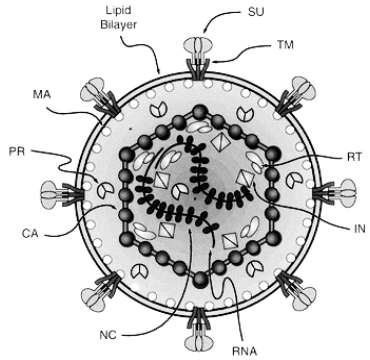

Figure 1: Schematic cross section through a retroviral particle

The viral envelope is formed by a cell-derived lipid bilayer into which proteins encoded by the *env* region of the viral genome are inserted. These consist of the transmembrane (TM) and the surface (SU) components linked together by disulfide bonds. Internal nonglycosylated structural proteins are encoded by the *gag* region of the viral genome. They are the matrix (MA) protein, capsid (CA) protein, and nucleocapsid (NC) protein. The suggested icosahedral structure of the retroviral capsid is not definitely established. Major products of the *pol*-coding region are reverse transcriptase (RT) and integrase (IN). The protease (PR) is derived from the *pro* gene between *gag* and *pol* (Coffin et al.; Retroviruses (1997).

The retroviruses were originally classified by the morphology of the virion core as visualized in the electron microscope and subdivided into seven groups (Table 1). Five of these groups represent retroviruses with oncogenic potential (*Oncoviridae*), the other two groups are *Lentiviridae* and *Spumaviridae*. Oncogenic retroviruses occur in all classes of vertebrates, and many act as natural carcinogens (e.g.: Rous sarcoma virus (RSV), Human T-cell leukemia virus (HTLV)). Lentiviruses are causing disease principally by killing or inducing loss of function of specific cells and tissues (e.g.: HIV). Relatively less is known about spumaviruses, which cause no

known disease, and interest in this category is relatively recent. The prototypical species is human foamy virus, a virus that has not been definitely linked to a specific pathology. Furthermore, retroviruses are divided into two categories, simple and complex, distinguishable by the organization of their genomes (Coffin, 1996; Murphy et al., 1994). The simple viruses encode only the Gag, Pro, Pol and Env gene products (described later) needed for the basic retroviral lifecycle. The complex viruses encode the same gene products but also an array of regulatory and accessory proteins necessary for an efficient viral propagation. All oncogenic members except the human T-cell leukemia virus-bovine leukemia virus (HTLV-BLV) genus are simple retroviruses. HTLV-BLV, lentiviruses and spumaviruses are complex.

Genus		Example / Genome
1	Avian sarcoma and leukosis viral group	Rous sarcoma virus (RSV); simple
2	Mammalian B-type viral group	mouse mammary tumor virus (MMTV); simple
3	Murine leukemia-related viral group	Moloney murine leukemia virus (MoMuLV); simple
4	Human T-cell leukemia bovine leukemia viral	human T-cell leukemia virus; complex
5	D-type viral group	Mason-Pfizer monkey virus (MPMV); simple
6	Lentiviruses	human / simian immunodeficiency virus (HIV/SIV); complex
7	Spumaviruses	human foamy virus (HFV); complex

Table 1: Classification of Retroviruses (Coffin et al.; Retroviruses (1997))

1.1.4 Genomic organization

The retroviral genomes are generally highly organized to have an optimal compaction, with the least information necessary for their own survival and propagation, on a minimal space. Retroviruses carry their genome as RNA but they replicate via a DNA intermediate. The reverse transcription of the viral RNA genome into a linear double stranded DNA form is the defining hallmark of retroviruses (Gilboa et al., 1979; Temin and Mizutani, 1970). The course of reverse transcription is complex and highly ordered, involving the initiation of DNA synthesis at precise positions, and translocation of DNA intermediates that result in duplication of

sequence blocks in the final product. The duplicated sequences are the long terminal repeats (LTRs), flanking the newly synthesized DNA on both sides, and a central stable 99 nucleotide-long plus strand overlap (the central DNA flap) (Charneau et al., 1994). Existing models for the reverse transcription propose that two specialized template switches known as strand-transfer reactions or "jumps" are required to generate the LTRs, a mostly non-coding sequences with regulatory function during reverse transcription and after provirus integration, and the central DNA flap, whose function is still a matter of debate.

The viral genes *gag*, *pro*, *pol*, and *env* occupy the body of the DNA. *gag* encodes the internal structural proteins of the virus. Gag (from the original name "*g*roup-specific *a*nti *g*en," reflecting what were believed to be the antigenic properties of this protein) is proteolytically processed into the mature proteins MA (matrix), CA (capsid) and NC (nucleocapsid). *pol* encodes the enzymes reverse transcriptase (RT), which contains both DNA polymerase and associated RNase H activities, and integrase (IN). *pro* encodes the viral protease (PR), which acts late in assembly of the viral particle to process proteolytically the proteins encoded by *gag*, *pro*, and *pol*, and in some cases also *env*. *env* encodes the surface (SU) glycoprotein and the transmembrane (TM) protein of the virion, which form a complex that interacts specifically with cellular receptor proteins. Although the order of the genes common to all retroviruses [*gag*, *pro*, *pol*, and *env*] is invariant, the relationship of their reading frames is not. The gene expression in retroviruses is equilibrated in a subtle way through reading frame shifts and splicing (Hayward, 1977; Mellon and Duesberg, 1977; Weiss et al., 1977). Accessory genes are located in a variety of places downstream from *pol;* they commonly partially overlap *env* and U3 (a part of the LTR), as well as each other, perhaps reflecting the evolutionary pressure implied by the limit to the size of an RNA molecule that can be packaged into a virion. All accessory genes are expressed from singly or multiply spliced RNAs (Figure 2).

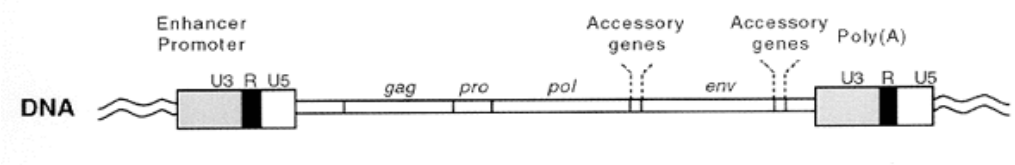

Figure 2: Genetic organization of generalized provirus

The proviral DNA as it is inserted into host DNA, with the long terminal repeats (LTRs) composed of U3, R, and U5 elements at each end abutting cellular sequences. Sequences in the LTR that are important for transcription, for example, enhancers, the promoter, and the poly(A) addition signal, are marked. The *gag*, *pro*, *pol*, and *env* sequences are located invariably in the positions shown in all retroviruses. Accessory genes are located as shown, and also overlapping *env* and U3 and each other, and occasionally in other locations (Coffin et al.; Retroviruses (1997).

1.1.5 Virion proteins of HIV

Gag precursor

The Gag protein is the precursor to the internal structural proteins of all retroviruses. Gag proteins must interact with each other, as well as with components in the plasma membrane, the genomic RNA, and probably with Env proteins to direct the assembly and budding of virions from the plasma membrane. Even in the absence of other viral proteins, expression of Gag leads to budding of particles resembling real virions. In wild-type viruses, Gag is cleaved late in the budding process by the viral protease (PR) to yield the mature proteins MA, CA, and NC that are common to all retroviruses as well as some other small proteins or peptides particular to the retrovirus species. Because proteolytic cleavage occurs late in assembly, during or after the last stages of budding, virions contain equimolar mixtures of the mature proteins. There are approximately 1200 to 1800 molecules of each Gag protein in a virion, which together represent about three quarters of the protein component of the virus (Craven et al., 1991).

MA protein

In all retroviruses, the amino-terminal domain of Gag gives rise to the MA protein (*m*embrane-*a*ssociated, or *ma*trix) that builds a roughly spherical shell around the viral core. The finding that most Gag protein precursors are modified by myristylation at their amino termini provided a major clue to MA function (Henderson et al., 1983). Myristate is a 14-carbon fatty acid that is added cotranslationally to many cellular proteins associated with membranes (Grand, 1989). Mutagenesis of the myristylation sites in MA leads to a block in the budding of particles and an accumulation of Gag inside the cell. Hence this modification seems to be essential for retroviral assembly. The three-dimensional structure of HIV-1 MA protein has been elucidated by nuclear

magnetic resonance (NMR) (Massiah et al., 1994) and X-ray crystallography (Hill et al., 1996). The lentiviral MA protein is trimeric in the crystal, with a globular amino-terminal domain and a smaller carboxy-terminal domain projecting away. The strongly positively charged regions on one side of each of the globular domains come together to form a kind of platform that might connect the cytoplasmic tail of the multimeric Env transmembrane complex to the MA protein shell. The MA protein contains a nuclear localization sequence (Bukrinsky et al., 1993a) and has been found to accompany the newly synthesized viral DNA into the nucleus (Bukrinsky et al., 1993b). It is therefore possible that MA plays a role in nuclear import of the PIC, yet it is not clear whether this feature is essential for the viral lifecycle.

NC protein

The nucleocapsid (NC) protein is a small basic protein, typically about 60-90 amino acid residues long containing one or two copies of a Cys-His motif CX_2CX_4 HX_4C (CCHC). These sequences bind a single Zn^{2+} ion and fold around the ion in a characteristic structure that is smaller and rather different from the better-known zinc-finger structures, which have a role in binding of certain proteins to nucleic acids. Indeed, NC has been shown to bind Zn^{2+} ions tightly (Bess et al., 1992) and in virions it is closely associated with the viral RNA. Probably the entire RNA molecule is coated with NC, in a stoichiometry of about one NC molecule per six nucleotides of RNA. Deletions or major alterations of the CCHC result in the absence of viral RNA in virions or alterations of the specificity of RNA packaging. Thus, this NC motif probably interacts with the "packaging sequences" near the 5'end of retroviral genomic RNAs when it is still part of the Gag precursor (Berkowitz et al., 1995). NC also contains sequences that act as "assembly domains" (Wills and Craven, 1991), which are required for assembly or budding of the virion. The assembly domains are independent of the CCHC and are likely to coincide with the stretches of basic residues.

In addition, NC promotes annealing of complementary RNA sequences (Prats et al., 1988). For example, it stimulates reverse transcription by facilitating the annealing of the primer tRNA to the primer-binding site. Under various conditions *in vitro*, NC can stimulate the dimerization of RNAs, and association between tRNA and its complementary sequence at the primer-binding site. Thus NC can help to promote primer tRNA placement during virion assembly. Furthermore it is known, that NC

can bind to double stranded nucleic acid, and thus it is probably retained on the viral DNA after reverse transcription.

CA protein

The largest cleaved part of the Gag precursor is the CA protein with approximately 200-270 amino acid residues in size. The CA protein contains the only highly conserved motif amongst gag proteins, the major homology region (MHR). The exact structural function of CA in the mature viral particle has not been elucidated, but the protein is believed to form a shell surrounding the ribonucleoprotein complex that contains the genomic RNA, as originally suggested in the 1970s. The possibility that other Gag proteins, perhaps in lower amounts than CA, also form part of the shell, has not yet been ruled out. This shell is most appropriately referred to as the "capsid." The capsid together with the components it encloses is then referred to as the "core." The biological function of the capsid shell is not known. Other prototypic enveloped RNA viruses, such as vesicular stomatitis virus (VSV, a rhabdovirus), hepatitis B virus (a hepadnavirus) and influenza virus (a myxovirus), do not have such a separate shell between the viral membrane and its associated matrix protein, and the RNA genome and its associated nucleocapsid protein. In all of these viruses, the nucleocapsid proteins are much larger than retroviral NC proteins, and thus perhaps carry out the functions of CA and NC together. The proteolytic cleavage event that severs the connection between the retroviral NC and CA, which is probably involved directly in morphological maturation of the virus, may be necessary for a subsequent step in the infectious cycle, for example, proper disassembly upon infection.

p6

In HIV-1 and other lentiviruses, a polypeptide of approximately 60 amino acids is cleaved from the Gag protein downstream from NC in a region partially overlapping the *pro* reading frame. This "p6" domain appears to have a role in release of virus in the final steps of budding and incorporation of the Vpr proteins into the virion. Viral particles from mutants with p6 deleted or altered remain tethered to the plasma membrane (Gottlinger et al., 1991).

Proteins derived from *pol* and *pro*

All infectious retroviruses carry three enzymes, reverse transcriptase (RT), integrase (IN) and protease (PR) (Katz and Skalka, 1990). The RT protein also contains an additional enzymatic activity, RNase H, which has been mapped to a separate, contiguous portion of the polypeptide, and the conventional designation "RT" always implies the protein with both reverse transcriptase and RNase H activities. The three enzymes are translated together as a Gag-Pro-Pol precursor, which is processed late in assembly to yield the mature forms of the enzymes. Since RT, IN, and PR are essential for viral replication and have characteristics that distinguish them from related cellular enzymes, they all have become targets for drug intervention in AIDS.

The reverse transcriptase, the most famous retroviral enzyme, is a relatively slow DNA polymerase, incorporating under standard conditions only 1 to 100 nucleotides per second, depending on the template. The enzyme also exhibits low fidelity and therefore the misincorporation rate under physiological conditions is on the order of 10^{-4} errors per base pair incorporated. RTs do not exhibit a proof reading nuclease activity and thus misincorporated bases are not removed as they are by host DNA polymerases.

The RNase H, an endonuclease, was identified initially as an activity of RT that degrades the viral RNA used as a template when permeabilized virions were incubated under conditions where RT could function (Molling et al., 1971). The "H" refers to the specificity of this enzyme for RNA/ DNA hybrids. Although always part of the RT polypeptide, RNase H forms a distinct subdomain.

The actual integration of the viral DNA into a target is mediated *in vivo* by the viral IN protein. Purified IN has the ability to recognize the ends of the newly synthesized linear double-stranded viral DNA, to remove two nucleotides from the 3'end of each strand, and to join this DNA ends to the genomic DNA. These activities are consonant with the role IN has in viral replication *in vivo*.

Many viruses encode proteases, which typically have roles in processing of the primary translation product and maturation of the viral particle. PR acts late in assembly and budding, or perhaps immediately after budding, to cleave the domains of Gag and Gag-Pol, causing profound morphological changes and converting the particle into an infectious virus (Vogt, 1996). The dimerization is crucial for its enzymatic activity, is likely to be involved in the regulation of proteolysis of Gag and Pol proteins, and is therefore essential for proper virion formation.

Proteins derived from *env*

Like all animal viruses that carry a lipid envelope, the surface of retroviral virions is studded with glycoproteins (envelope or Env proteins), whose function is to mediate the adsorption to and the penetration of host cells susceptible to infection. Therefore the Env protein is the primary determinant of cellular tropism. All retroviruses contain two different types of Env proteins, called SU (surface subunit; gp120) and TM (transmembrane subunit; gp41) that are derived from a common precursor polypeptide. Typically, both SU and TM proteins are glycosylated at multiple sites. At the plasma membrane, the SU/ TM oligomers are incorporated into the budding viral particle. The cytoplasmic "tail" distal to the membrane-spanning segment of TM remains on the internal side of the viral membrane. It has been suggested that the cytoplasmic tail of TM is in contact with the MA domain of the Gag protein in virions, but the nature of this contact is unknown.

Retroviruses enter via membrane fusion into the target cell. HIV and SIV recognize the same receptor, CD4, but for postbinding steps of membrane fusion and virus entry various members of the chemokine receptor family, notably CCR5 and CXCR4, are needed. Due to the specific receptor expression in host cells, HIV is mostly found in helper T-cells, in dendritic cells, macrophages and in certain cells in the brain.

Rev

The regulatory protein Rev is a small, 13-kDa sequence-specific RNA binding phosphoprotein. Rev mediates the export of unspliced and singly spliced viral RNAs from the nucleus, thus permitting the expression of the Gag, Pol and Env gene products. It binds to the Rev responsive element (RRE) present in the HIV-1 *env* gene, and by interacting with Crm1, a member of the karyopherin family of nucleocytoplasmic-transport factors, it acts to export the viral RNAs through the nuclear pore (Cullen, 2003).

Tat

Tat is a unique RNA-binding transcriptional activator that binds to the hairpin structure TAR (trans-activation response element), encoded in the LTR of nascent RNA. Through this interaction, the protein promotes the assembly of transcriptionally active complexes at the LTR (Berkhout et al., 1989) and increases the rates of elongation by RNA polymerase II. Several studies have suggested direct roles for

RNA polymerase II, general transcription factors, and various transcriptional cofactors implicated in the Tat trans-activation mechanism (Kashanchi et al., 1994; Sune and Garcia-Blanco, 1995).

Nef

Nef (negative factor, "historical name") is a 24- to 35-kDa protein unique to the primate lentiviruses HIV and SIV. Among the various HIV gene products implicated in modulation of cell signaling, Nef appears to be the most potent. The *nef* gene, expressed rapidly and abundantly following infection, is a major virulence factor both *in vitro* and *in vivo.* Rhesus macaques infected with simian immunodeficiency virus (SIV) rarely progress to disease if the viral *nef* gene is deleted. In humans, members of a cohort of individuals infected with a *nef*-deleted form of HIV have remained disease-free for many years (Miller et al., 1994). Nef leads, like Vpu, to loss of the CD4 receptor, in this case directly from the cell surface and down-regulates MHC class I levels, thereby inhibiting the cytotoxic T-lymphocyte-mediated lysis of HIV-1 infected cells. Finally, Nef may enhance virion assembly and release through unknown mechanisms.

Vif and Vpu

The *vif* (viral infectivity factor) gene is needed for efficient replication of the virus in primary CD4 cells. Vif enhances infectivity of virus produced in certain nonpermissive cells. The recent identification and characterization of its target has transformed the Vif protein, into an exceedingly hot topic. Vif's main function is now identified as blocking the action of an antiviral protein, APOBEC3G, a cytidine deaminase that attacks the viral DNA by degrading its genome before it can establish a successful infection (Mangeat et al., 2003; Zhang et al., 2003).

The *vpu* gene product is found only in HIV-1 and very closely related viruses but not in other primate or nonprimate lentiviruses. Vpu, a small integral membrane protein, folds into two distinct structural domains with different biological activities: a transmembrane (TM) helical domain involved in the budding of new virions from infected cells, and a cytoplasmic domain encompassing two amphipathic helices, which is implicated in CD4 degradation. CD4 is directly bound by Vpu and then targeted for proteolysis in the cytosolic ubiquitin-proteasome pathway. However, the molecular mechanism by which Vpu facilitates virion budding is not yet understood.

Viral protein R (Vpr)

The accessory protein Vpr is a 14kDa protein incorporated in high levels into the viral particle due to an interaction with the p6 domain of Gag. Therefore Vpr is a part of the viral pre-integration complex (PIC). The function of Vpr is not understood in detail, but numerous effects on the cell have been reported. Vpr causes a strong cell cycle arrest in the G2 stage, which provides a replication advantage for the virus since proviral transcription is highest during this stage. The protein was shown to act in *trans* to increase the expression of viral proteins and to stimulate the expression of heterologous genes driven by the LTR as well as other promoters (Cohen et al., 1990; Forget et al., 1998; Goh et al., 1998). Vpr increases efficient replication of both HIV-1 and HIV-2 in macrophages and, in addition to MA, is implicated in targeting of the newly made viral DNA to the nucleus (Heinzinger et al., 1994). This targeting function appears to be critical for the establishment of HIV infection in some nondividing cells, which is a characteristic feature of lentiviruses. Additionally, upon expression of Vpr in mammalian cells it is localized at the nuclear pore complex (NPC), which could also play a functional role in the viral lifecycle (Le Rouzic et al., 2002).

The possible involvement of Vpr with the nuclear import is actually a controversial matter of debate. One theory for PIC nuclear translocation is based on the interaction of different viral proteins with the cellular import machinery. The karyophilic nature of the HIV PIC is attributed to three viral proteins MA, IN, and Vpr. While MA and IN provide their nuclear localization signals (NLS) for the interaction with karyopherin α, the cellular receptor for nuclear-targeted proteins, Vpr regulates this process by increasing affinity of karyopherin α-NLS interaction. Without Vpr, viral NLS-proteins and the HIV-1 PIC are weak or nonfunctional karyophiles (Popov et al., 1998a). Others recently reported that Vpr expression in mammalian cells causes herniations and large holes in the nuclear envelope, which may facilitate nuclear entry of the viral PIC (de Noronha et al., 2001).

1.1.6 The retroviral life cycle

Retroviruses replicate through a complex life cycle and introduce a persistent infection (Figure 3).

In general the retroviral infection is divided into an early and a late phase. The early phase starts with the attachment and specific receptor binding followed by a complex mechanism of membrane fusion between the viral particle and the host cell membrane. Fusion leads to "microinjection" of the HIV-1 capsid into the infected host cell. Once inside, the capsid travels via microtubule tracks in an energy-dependent fashion to the vicinity of the nuclear envelope (McDonald et al., 2002) where the RNA genome is reverse transcribed into a double-stranded DNA and the pre-integration complex (PIC) is assembled. Components of the PIC include the double-stranded DNA version of the viral genome as well as the reverse transcriptase, matrix, integrase, and Vpr proteins. Preliminary evidences point out that all these steps take place inside the viral core and that only immediately before translocation into the nucleus uncoating of the capsid happens.

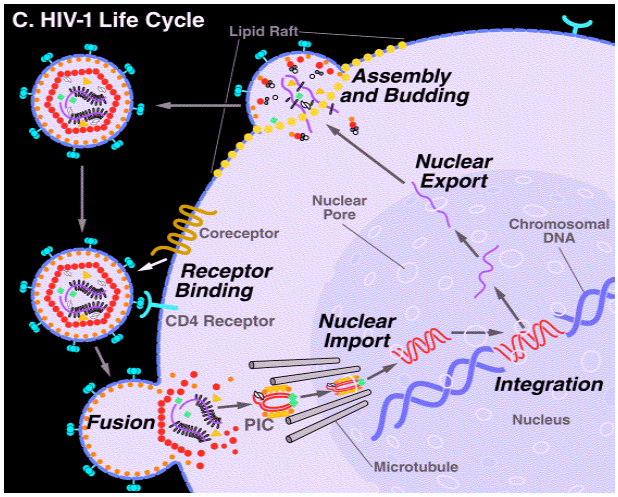

Figure 3: The HIV life cycle

HIV associates with the CD4 and cognate coreceptor, initiating membrane fusion. The pre-integration complex (PIC) facilitates conversion of viral RNA into cDNA and sheds several proteins while it traverses the cytoplasm along microtubules towards the nucleus. The PIC, or at least the components required for retroviral integration, somehow enters the nucleus to gain access to host chromosomal DNA. After integration, genomic viral RNA is exported along with the immature viral particle components, which assemble, and bud together out of the cytoplasm through lipid rafts (Sherman and Greene, 2002).

After nuclear import, the viral DNA is inserted into chromosomal DNA with the aid of virion integrase to form a stable provirus. With integration, the provirus achieves

the status of a cellular gene, thus it is expressed and replicated by cellular enzymes in concert with chromosomal DNA. All past-integration events are classified into the late replicative cycle. Transcription of the provirus generates spliced and unspliced mRNAs and full-length progeny RNA genomes that are then exported from the nucleus with the assistance of the early transcript Rev. In the cytoplasm, viral mRNAs are translated on cellular ribosomes. The translation products, together with progeny RNA, are assembled at the cell periphery into viral particles that are released from the cell by budding of the plasma membrane. Budding of viruses is followed by proteolytic cleavage of virion polyproteins inside the new viral particle by the viral protease as well as cellular proteases to generate mature and infectious progeny.

1.2 Peptide Nucleic Acids (PNAs)

With respect to the epidemical state in the third world the urgent need of an efficient therapy or treatment for HIV infected people seems to be obvious. Best current projections suggest that an additional 45 million people will become infected with HIV in low- and middle-income countries until 2010. Still no vaccine is available and massive side effects and/or therapy resistances occur in the low percentage of patients that can afford the highly active anti-retroviral therapy (HAART). For the more than 40 million HIV-infected people living in developing countries (25-28 million in sub-saharan Africa), medication remains theory. Consequently, the quick development of cheap anti-HIV drugs that are resistant to tropical climates is imperative (Piot et al., 2001). Historically, vaccines have been the most efficient and cost effective means for the control of infectious diseases, resulting in the eradication of smallpox and the control of polio, yellow fever, and measles (Deming et al., 1997; Garenne, 1993; Hull et al., 1997; Perraut et al., 2000).

Therefore a lot of research effort is spent into the development of an efficient vaccine against HIV. The most studied attempts are recombinant protein trials or viral vector systems, as Adenoviruses, Adeno-associated Viruses (AAV) or Measles viruses. In parallel there are also studies on live attenuated simian immunodeficiency virus (SIV), but, as retroviruses integrate into the host genome, this approach is controversially discussed in the field. To date, after more that two decades of research, only one HIV vaccine, a recombinant surface protein (gp120), went through a trial process, which includes preclinical testing followed by three clinical phases, with human volunteers. The objectives of this large scale vaccine study was to prevent HIV infection in people who are at high risk for HIV infection but also to see if the vaccine helps to slow the rate of disease progression in infected persons. Unfortunately, the study did not show a statistically significant reduction of HIV infection within the tested population, which was the primary endpoint of the trial. This demonstrates that vaccine design is a very challenging problem of HIV research. Additionally, therapy resistance to the highly active anti-retroviral therapy (HAART)

is reported. Therefore it is still crucial to continue the research effort to develop new anti-HIV therapies.

Hopeful tools for therapy purpose are peptide nucleic acids (PNAs) (Nielsen et al., 1991) that were developed only recently. PNA are DNA mimics in which the sugar phosphate backbone of natural nucleic acid has been replaced by a synthetic peptide backbone (N-(2-aminoethyl) glycine) to which the nucleobases are linked through methylene carbonyl linkers (Nielsen et al., 1994a) (Figure 4).

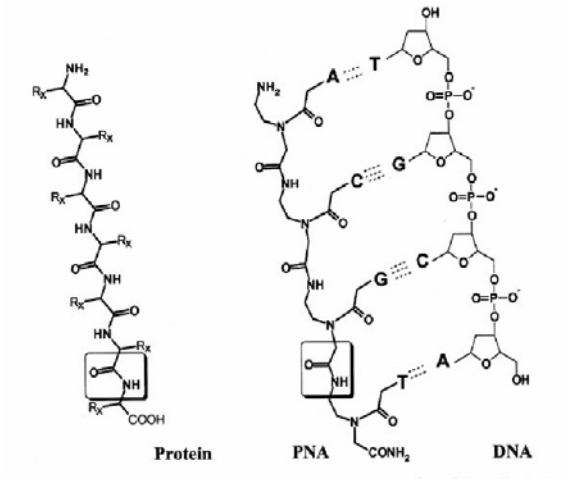

Figure 4: Structure comparison peptide, PNA and DNA

This simple and yet entirely new synthetic molecule has interesting and non-prototype chemistry. By strict chemical means, PNA, is neither a peptide nor a nucleic acid, since its backbone is an achiral uncharged polyamide. However, this atypical backbone gives PNA most appreciated advantages over other DNA analogues like phosphorothioates etc., as PNA oligonucleotides are not recognized by proteases or nucleases and are therefore extremely stable in biological fluids (Demidov et al., 1994). DNA recognizing proteins do not interact with the PNA oligomers of the same nucleotide sequence, probably due to the lack of electrostatic interactions with the backbone. Despite its achiral and neutral backbone, PNA are found to form very stable duplexes with Watson-Crick complementary single stranded DNA and RNA targets (Egholm et al., 1993). Duplexes between PNA and DNA or RNA are in general thermally more stable than the corresponding DNA-DNA or DNA-RNA duplexes mostly due to the lack of electrostatic repulsion (Jensen et al., 1997). All the described qualities make PNAs potential candidates for new anti-HIV drugs.

1.2.1 Chemical synthesis and properties of PNAs

The backbone of PNA carries 2-aminoethyl glycine linkages in place of the regular phosphodiester backbone of DNA (Egholm et al., 1992), and the nucleotide bases are connected to this backbone at the amino nitrogens through a methylene carbonyl linker (Fig. 4). Being achiral, peptide nucleic acids can be synthesized without need of any stereoselective pathway.

Since peptide nucleic acids and DNA have no functional groups in common except for the nucleobases, the chemical stability of PNA differs significantly. Unlike DNA, which depurinates on treatment with strong acids, peptide nucleic acids are fairly acid stable. However, some chemical instability can derive from the free amino functionality at the NH_2 terminus, where a slow N-acyl transfer of the nucleobase acetic acid or a cleavage of the amino-terminal PNA unit by ring closure can take place, particularly under basic conditions. PNAs are charge-neutral compounds and hence have poor water solubility compared to DNA. Neutral PNA molecules have a tendency to aggregate to a degree that is dependent on the sequence of the oligomer. PNA solubility is also related to the length of the oligomer and purine:pyrimidine ratio.

PNAs hybridize to complementary DNA and RNA sequences in a sequence-dependent manner, following the Watson-Crick hydrogen bonding scheme (Egholm et al., 1993). The various duplexes of PNA feature a high thermal stability compared to double stranded DNA (dsDNA) with decreasing values from pure PNA-PNA duplex over PNA-RNA to PNA-DNA heteroduplexes. This high thermal stability of the PNA hetreoduplexe compared to the corresponding DNA-DNA duplexes can be attributed to a more favorable entropic contribution. It is important to mention that for PNA-DNA and DNA-DNA duplexes, enthalpic changes ΔH are rather equal. It has been suggested that the entropic contribution is possibly related to the ion release associated with the formation of a hybrid duplex (Ratilainen et al., 1998). Moreover PNA-DNA hybridization is severely affected by base mismatches and PNA can maintain sequence discrimination up to the level of a single mismatch, which lowers considerably the thermal stability of a heteroduplex.

Multi-stranded triplex structure containing both Watson-Crick and Hoogsteen base-pairing is also possible and has an even higher thermal stability. But the binding of homopyrimidine PNA to dsDNA usually does not result in a conventional triplex complex (i.e. Hoogsteen binding in the major groove of the DNA-DNA helix), but

rather in a triplex invasion complex in which one PNA binds to the homopurine DNA stretch by ordinary Watson- Crick base pairing preferably in the antiparallel orientation (the PNA N-terminal faces the 3' end of the DNA strand), and another PNA binds the PNA- DNA duplex by Hoogsteen binding (preferably in parallel to the homopurine containing DNA strand). The strand invasion is favored by the presence of internal A-rich regions in a duplex DNA and by moderately low ionic strength (high salt stabilizes the DNA duplex). Because cytosines require protonation in the N^3 position in order to make Hoogsteen interactions with N^7 of guanine residues, this particular structure involving CGC^+ triplets shows pH dependence and is most stable in the non physiological pH range of 5.0- 5.5. It has been found that the synthesis of PNAs with changes of cytosine to pseudoisocytosine (ψiC or 'J bases') in the Hoogsteen strand abolishes the pH dependence of the triplex without affecting the stability of the interaction (Figure 5). Moreover, the stability of the invasive PNA_2 - dsDNA complex has been improved by chemical linking of the two strands of PNA thus forming a so called bis-PNA (Egholm et al., 1995).

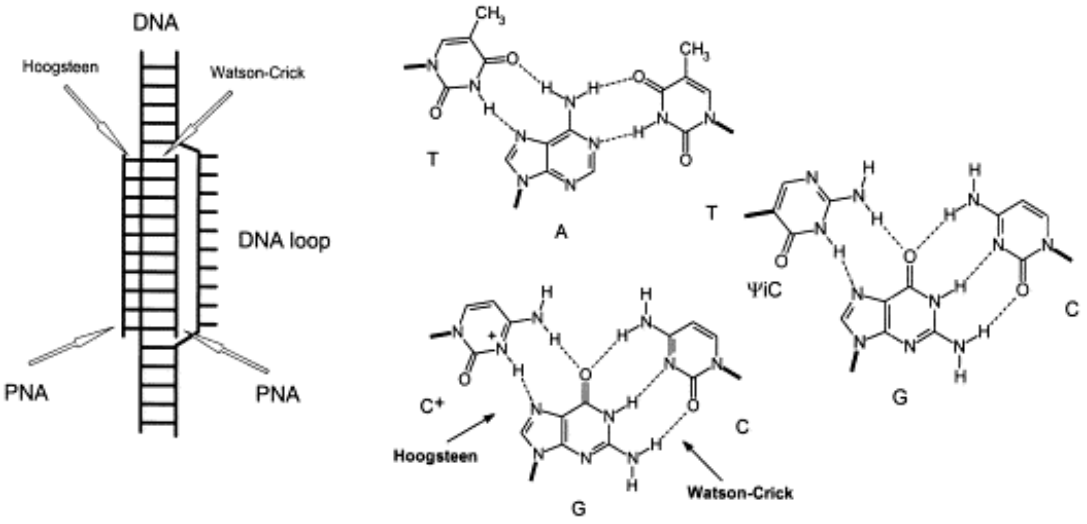

Figure 5: PNA_2 binding to dsDNA by triplex strand invasion

Triplex invasion by homopyrimidine PNA oligomers. One PNA strand binds via Watson-Crick base pairing (preferably in the antiparallel orientation), while the other binds via Hoogsteen base pairing (preferably in the parallel orientation). It is usually advantageous to connect the two PNA strands covalently via a flexible linker into a bis-PNA, and to substitute all cytosines in the Hoogsteen strand with pseudoisocytosines which does not require low pH for N3 'protonation'.

1.2.2 Antigene and antisense application of PNAs

Peptide nucleic acids are promising candidates for gene therapeutic drug design. In principle, two general strategies can be adapted to design gene therapeutic drugs. Oligonucleotides or their potential analogs are designed to recognize and hybridize to complementary sequences in a particular gene whereby they should interfere with the transcription of that particular gene (antigene strategy). Alternatively, nucleic acid analogs can be designed to recognize and hybridize to complementary sequences in mRNA and thereby inhibit its translation (antisense strategy). PNAs have been described to have significant effects on replication, transcription, and translation processes.

Inhibition of replication

An important effect of PNA is the possibility to inhibit the elongation of DNA primers by DNA polymerase. Further, the inhibition of DNA replication should be possible if the DNA duplex is subjected to strand invasion by PNA under physiological conditions or if the DNA is single stranded during the replication process. Efficient inhibition of extrachromosomal mitochondrial DNA, which is largely single-stranded during replication, has been demonstrated. The PNA-mediated inhibition of the replication of mutant human mitochondrial DNA is a novel and potential approach toward the treatment of patients suffering from ailments related to the heteroplasmy of mitochondrial DNA. Here, wild-type and mutated DNA are both present in the same cell. Experiments have shown that PNA is capable of inhibiting the replication of mutated DNA under physiological conditions without affecting the wild-type DNA in mitochondria (Taylor et al., 1997). Others could show that a bis-PNA bound to the template strand significantly reduces the DNA unwinding activity of the UL9 helicase, a herpes virus DNA helicase that is necessary for viral replication. This inhibitory effect on the template strand can be explained by a model in which translocation of the UL9 helicase in 3'→ 5' direction is impaired by the PNA binding (Bastide et al., 1999).

Inhibition of transcription

Peptide nucleic acids are capable of arresting transcriptional processes by virtue of their ability to form a stable triplex structure or strand displacement complex with DNA. Such complexes can create a structural hindrance to block the stable function

of RNA polymerase and thus are capable of working as antigene agents. Evidence from *in vitro* studies supports the idea that such complexes are indeed capable of affecting the process of transcription involving both prokaryotic and eukaryotic RNA polymerases (Nielsen et al., 1994b; Praseuth et al., 1996). PNA targeted against promoter regions can form a stable PNA-DNA complex that restricts the DNA access of the corresponding polymerase. PNA strand displacement complexes, located far downstream from the promoter, can also efficiently block polymerase progression and transcription elongation and thereby produce truncated RNA transcripts. The PNA_2/ DNA triplex arrests transcription *in vitro* and is capable of acting as an antigene agent. But one of the major obstacles for PNAs as an antigene agent is that the strand invasion or the formation of strand displacement complex is rather slow at physiological salt concentrations. Amelioration can be achieved by introducing the earlier described pH-independent pseudoisocytosines into the Hoogsteen strand of bis-PNAs. It has been found that under physiological salt conditions, binding of PNA to supercoiled plasmid DNA is faster compared to linear DNA (Bentin and Nielsen, 1996). This is relevant to the fact that the transcriptionally active chromosomal DNA usually is negatively supercoiled, which can act as a better target for PNA binding *in vivo*. In addition there is evidence that the binding of PNA to dsDNA is enhanced when the DNA is being transcribed. This transcription-mediated PNA binding occurs about threefold as efficiently when the PNA target is situated on the nontemplate strand instead of the template strand. As transcription mediates template strand-associated $(PNA)_2$/ DNA complexes, which can arrest further elongation, the action of RNA polymerase results in repression of its own activity (Larsen and Nielsen, 1996). More recently, it has been shown that a 8mer PNA directed against angiotensinogen, which is critical in the control of blood pressure, resulted in a significant decrease in plasma angiotensin I and systolic blood pressure upon intraperitoneal (i.p.) injections in hypertensive mice *in vivo* (McMahon et al., 2002).

Inhibition of translation

The basic mechanism of the antisense effects by oligodeoxynucleotides is considered to be either a Ribonuclease H (RNase H) mediated cleavage of the RNA strand in oligonucleotide-RNA heteroduplex or a steric blockage of the translation machinery. Ideally, this renders the mRNA non-functional and therefore results in the inhibition of synthesis of the specific protein. PNA/ RNA duplexes cannot act as substrates for

RNase H, but the antisense effect of the peptide nucleic acid is based on the steric blocking of either RNA processing or translation. Even though the PNA/ RNA duplex is not a substrate for RNase H, the possibility that PNA can induce degradation of targeted mRNA by alternative pathways cannot be excluded (Larsen et al., 1999).
Duplex-forming PNAs can effectively inhibit translation initiation *in vitro* when targeted to the region spanning the AUG initiation codon. Triple helix-forming PNAs can also hinder the translation process. Bis-PNA structures are capable of forming internal triple helical constructs. In principle, if targeted against the coding region of mRNA, PNA_2/RNA triple helix-forming derivatives can also cause a stop in translation, which can be easily verified by the detection of a truncated protein (Knudsen and Nielsen, 1996). Thus, in general, duplex-forming PNAs can inhibit translation in vitro if they are targeted towards the ribosome-binding site, whereas triplex-forming PNAs are effective when targeted against polypurine targets downstream of the translation initiation site. Moreover, it is observed that the target position on the mRNA drastically influences the efficiency of antisense PNAs, so that targets shifted just a few nucleotides can have varied effects on translation. The design of a PNA therefore most likely has to be optimized for each target with respect to length and, in the case of bis-PNAs, pyrimidine content (Doyle et al., 2001). Since the discovery of PNA, a lot of studies in different fields report about antisense effects of this new tool *in vivo*, what comprises in living cells as well as in animal models (Liu et al., 2004; McMahon et al., 2001; Sazani et al., 2002). The reported ability of PNA to affect gene expression by sequence-specific true antisense activity validates their application as potential therapeutics.

1.2.3 Cellular uptake of PNA

The strong potential of PNA as antisense and antigene agent was soon established in cell-free in vitro systems, but development ex vivo and in vivo was rather slow. The reason has been the lack of efficient ways to introduce PNA into cells. The large hydrophilic and uncharged molecule does not cross lipid membranes easily, which is the major challenge to be overcome before PNA can be used as a therapeutic drug. Brute techniques like microinjection, electroporation or detergent mediated cell permeabilization were used to demonstrate effects of PNA treatment in living cells, but all mentioned methods are not feasible for therapeutic purpose.

Several proteins, such as HIV-1 Tat, *Drosophila* Antennapedia homeoprotein (pAntp), and HSV-1 VP22 have been shown to traverse the cell membrane by a process called protein transduction in an energy- and receptor- independent manner (Elliott and O'Hare, 1997; Frankel and Pabo, 1988; Green and Loewenstein, 1988; Joliot et al., 1991). Short peptides derived from the respective protein-transduction domains (cell-penetrating peptides CCPs) can be internalized in most cell types and, more importantly, allow the cellular delivery of conjugated biomolecules. Since this discovery a lot of research effort has been spend to investigate the mechanism allowing these proteins to overcome cell membranes. However, internalization of CPPs and their cargo is not well understood yet and has recently been the subject of controversies.

1.2.4 Therapy approach against HIV

Since HIV integrates into the host cell genome a highly sequence specific antigene approach could be an alternative to existing antiviral treatments. Moreover, antisense approaches against targets in the early viral live cycle have the advantage to neutralize HIV before integration.

Until now, the main hurdle to overcome in PNA therapy approaches was the efficient delivery of the drug in reasonable quantities without any noxious side effect. This objective seems to be achievable with the above mentioned transport peptides. Klaus Braun (DKFZ, Germany) has developed a complex transport shuttle for the PNA delivery, that shows high efficiency at remarkably low doses (Braun et al., 2002). By coupling the PNAs via a cleavable disulfide bond to a 16 amino-acid fragment in the third helical domain of antennapedia protein (pAntp), efficient cellular transport was ensured. The entry into the cytoplasm then results in the reductive splitting of the disulfide bond and liberates the PNA from sterical binding hindrance due to the transport peptide. Subsequently, for a therapy aimed to inhibit transcription, a next barrier, the nuclear membrane, has to be overcome. Nuclear import mechanism of macromolecules is energy-dependent and carrier-mediated. Karyophilic proteins bear one or more nuclear targeting signal peptides called nuclear localization sequences (NLS) (Kalderon et al., 1984), mostly short basic peptides, which ensure, the translocation through the nuclear pore complex (NPC). Thus, the nuclear localization sequence (NLS) of the simian virus 40 (SV40) large T antigen was covalently linked to the N-terminus of the PNA construct, spaced by two lysine residues. Functional

and efficient delivery of the PNA linked to the transport peptides could be shown recently in a study targeting anti cancer compounds into the nucleus of a carcinoma cell line (Braun et al., 2003).

According to these, at the time, preliminary results, we designed a set of 16- to 18-mer PNAs directed against crucial sequences for an effective viral propagation in the HIV genome. Targets in both, the early and late replicative cycle, were selected and genomic databases were searched for highly conserved sequences in-between different HIV clades.

1.3 The actin cytoskeleton

1.3.1 Basic actin biochemistry

The actin nucleation machinery is very complex because a lot of different regulatory proteins play an important role in the equilibrium between the monomeric and polymerized state of actin. However the comprehension of this process is essential to understand the interplay between the hosts actin cytoskeleton and pathogens like several viruses or bacteria.

Actin is the most abundant protein in many eukaryotic cells. It exists in two forms: monomers (G-actin or globular-actin) and filaments (F-actin or filamentous-actin). The globular monomers form a double helical polymer, which is arranged head-to-tail to give the filament a molecular polarity. The filaments are decorated with the motor protein myosin and due to arrowhead pattern of the complex seen with electron microscopy one end is called the barbed end and the other the pointed end. This polarity is essential for the mechanism of actin assembly in living cells. Filament growth is favored at the barbed end. This leads to a strong orientation of the actin filaments outward with respect to the cell surface (Small et al., 1978). The rate-limiting step of actin assembly is the instability of actin dimers and trimers, but once started, filament growth is very rapid. Another determinant for growth is the diffusion of monomers and the rate that subunits collide with the end, only 2% of such collisions are in correct orientation for binding (Drenckhahn and Pollard, 1986). The elongation rate is directly proportional to the monomer concentration in a given solution. The critical concentration for filament growth is the ratio of rate constants for dissociation and association (k-/k+), the dissociation equilibrium constant for subunit binding at the end of a polymer. In living cells all actin (Mg-ATP actin) polymerizes above the critical concentration of 0.1μM at the barbed end (where growth is favored) and 0.7μM at the pointed end. The polymerization per se does not require Mg-ATP, bound in a deep cleft it rather stabilizes the actin monomer (De La Cruz et al., 2000). Hydrolysis of ATP by polymerized actin and thus the dissociation of the γ-phosphate seems to be an indicator for the aging of filaments and triggers the disassembly processes inside living cells. The ATP hydrolysis is not reversible

(Carlier et al., 1988) and very fast with a half time of only ~2s (Blanchoin and Pollard, 2002). In contrast phosphate dissociation is much slower (Carlier and Pantaloni, 1986), and therefore new assembled filaments are marked with ADP-P_i-actin as a relatively long-lived intermediate, which has the same properties as ATP-actin. After the γ-phosphate is split of, ADP-actin subunits dissociate faster from the barbed end than ATP-actin subunits, but both ATP- and ADP-actin dissociate slowly at the pointed end (Pollard, 1986). Therefore in the steady state ATP-actin associates at the barbed end and ADP-actin dissociates from the pointed end. These kinetc constants are leading to very slow treadmilling of subunits from the barbed end to the pointed end. This means, that actin filaments are continually built-in at one end, where new actin-ATP complexes are added, and at the same time slowly falling apart at the opposite end, where the actin-ADP form dissociates. The whole structure slowly steps through the cell, in an ATP hydrolysis dependant mechanism, but never gets any longer or shorter.

At the steady state, treadmilling in a pure actin solution under physiological conditions is rather slow, whereas cells can advance or react quickly to external stimuli. Therefore, the key point for this physiological behavior is a rich variety of regulatory proteins. Cells feature more than 60 classes of actin binding proteins (Pollard, 1999). These proteins are actin, ADF (actin-depolymerizing factor)/ cofilin (Bamburg et al., 1999), capping protein (Cooper and Schafer, 2000), Arp2/3 complex (Pollard and Beltzner, 2002), an activator of Arp2/3 complex (Weaver et al., 2003), and profilin (Schluter et al., 1997). There are to many proteins participating in the complex actin nucleation machinery to be mentioned here, but the cartoon below (Figure 6) shows a selection of the essential players in the process. (Pollard and Borisy, 2003).

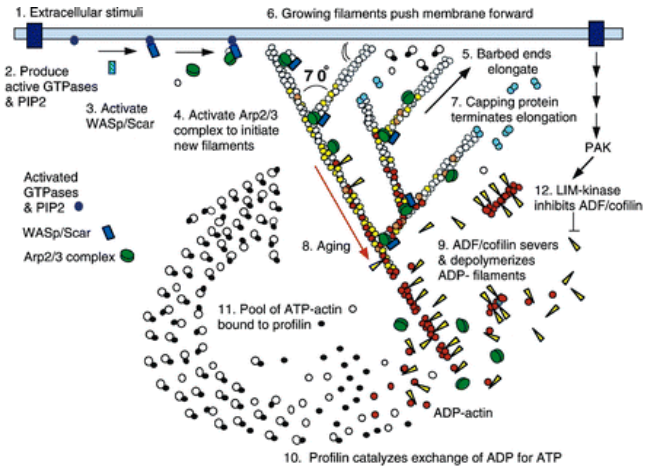

Figure 6: Actin treadmilling model for actin polymerization at the plasma membrane

(1) Extracellular signals activate receptors. (2) The membrane associated signal transduction pathways produce active Rho-family GTPases and PIP2 that (3) activate WASp/Scar proteins. (4) WASp/Scar proteins bring together Arp2/3 complex and actin monomer on the side of a preexisting filament to form a branch. (5) Rapid growth at the barbed (+) end of the new branch (6) pushes the membrane forward. (7) Capping protein terminates growth within a second or two. (8) Filaments age by hydrolysis of ATP bound to each actin subunit (white subunits turn yellow) followed by dissociation of the γ phosphate (subunits turn red). (9) ADF/cofilin promotes phosphate dissociation, severs ADP-actin filaments and promotes dissociation of ADP-actin from filament ends. (10) Profilin catalyzes the exchange of ADP for ATP (turning the subunits white), returning subunits to (11) the pool of ATP-actin bound to profilin, ready to elongate barbed ends as they become available. (12) Rho-family GTPases also activate PAK and LIM kinase, which phosphorylates ADF/cofilin. This tends to slow down the turnover of the filaments. (Redrawn from a figure in (Pollard et al., 2000)).

1.3.2. Viral cytoplasmic locomotion

An important characteristic of eukaryotic cells is the requirement for cytoplasmic transport. Cellular size and complexity is dependant on the effectiveness of its transport mechanism. During mitosis and meiosis, genetic material is segregated into daughter cells, whereas during interphase, endocytosed material or newly synthesized mRNAs, proteins and lipids are transported to their final destinations (Fuchs and Yang, 1999; Sheetz, 1999). Cytoplasmic transport and cell morphology depend on a complex network of three cytosolic filaments: microtubules (MTs), intermediate filaments (IFs) and microfilaments (actin). The cytoskeleton is highly dynamic and reorganizes constantly as the cell responds to external stimuli, changes shape, migrates over the extracellular matrix or divides. There is considerable synergy and crosstalk between the different cytoskeleton filaments and the network is regulated by a growing abundance of actin- and microtubule-binding proteins, kinases and phosphatases, which are controlled by several signaling cascades (Gundersen and Cook, 1999; Schmidt and Hall, 1998). Rather than allowing intracellular molecules to diffuse freely in the cellular volume, the cytoplasm imposes a substantial barrier to transport. Free diffusion of molecules larger than 500 kDa is restricted due to molecular crowding effected by the presence of organelles, the cytoskeleton and high protein concentrations in the cytoplasm. Diffusion coefficients measured for cytoplasmic vesicles or microinjected beads are 500- 1000 times lower compared with diffusion in aqueous solution (Luby-Phelps, 2000). For a 100bp DNA fragment,

diffusion in the cytoplasm is approximately five times lower than diffusion in water, and diffusion of a 250bp fragment and a 2000bp fragment is 17 and >100 times lower (Lukacs et al., 2000). Thus, the very restricted diffusive mobility of beads, vesicles and free DNA molecules in the cytoplasm suggests that movement of virions, subviral particles and viral genome-protein complexes cannot rely on passive diffusion and their cytoplasmic transport must therefore be an active process.

For many virus species penetration into the cell cytoplasm is insufficient to permit replication. Specifically, all DNA viruses, except for pox viruses, as well as some viral families that bear RNA genomes, including retroviruses and influenza viruses, replicate in the nucleus. Only in the nucleoplasm these viruses gain access to the cellular factors they require for amplification and transcription of their genome as well as posttranscriptional processing of viral mRNA. Therefore, these viruses not only have to cross the plasma membrane but must also traverse the cytoplasm and then enter the cell nucleus. The entry of many different viruses, including adenovirus, HIV and vaccinia, is actin dependent (Iyengar et al., 1998; Li et al., 1998; Locker et al., 2000). Moreover a number of viruses appear to have evolved to use a common retrograde transport mechanism that involves recruitment of cytoplasmic dynein, a microtubule minus-end-directed motor, to move towards the microtubule organization center (MTOC) (Kaelin et al., 2000; Sodeik et al., 1997; Suomalainen et al., 1999). MTs are the cytoskeletal highways responsible for long distance transport of host as well as viral cargo, whereas actin filaments are implicated in short distance motility.

In a recent study done by Tom Hope and colleagues (McDonald et al., 2002), it is shown, that HIV infection is reduced twofold if cells are infected in the presence of the MT-depolymerising drug nocodazole. Moreover, after microinjection of a dynein function- blocking antibody, the relative transport towards the nucleus was significantly reduced. Cytoplasmic dynein and kinesins, respectively, are so-called motor proteins for transport either to the minus-ends of MTs at the MT-organizing center (MTOC), or toward the plus-ends in the cell periphery. Yet a complete block of the HIV pre-integration complex (PIC) at the plasma membrane could only be achieved with drugs depolymerizing both the actin and the microtubule network. This result is consistent with evidence that actin can be used to gain access to the microtubule network. Generally, actin seems to play a role at several crucial steps during the viral life cycle. Depolymerization of actin prior to viral infection impairs CD4 and co-receptor clustering necessary for membrane fusion and entry (Iyengar et

al., 1998). Subsequently, the cytoskeleton provides a cofactor or acts as a scaffold for the appropriate localization and activation of the PIC and, ultimately, for efficient infection (Bukrinskaya et al., 1998). Furthermore, the nucleocapsid (NC) domain of the retroviral Gag protein directly binds actin (Liu et al., 1999) and it has been reported that this interaction may be responsible for the incorporation of cytoplasmic actin into retroviral particles (Wilk et al., 1999).

1.3.3 Routing of HIV particles from the MTOC to the nuclear envelope

It is now accepted that HIV travels along microtubule tracks through the cytoplasm towards the nuclear envelope (McDonald et al., 2002). Yet little is known about how viral particles move from the MTOC to nuclear pores as well or how nuclear actually functions. As described earlier (chapter 1.1.5) there are several viral proteins present in the PIC presumed to play a role in these procedures. A very good candidate to fulfill both tasks seems to be Vpr. The karyophilic protein is present in the viral particle and stays associated to the PIC during routing towards the nuclear envelope. It has been shown that Vpr is shuttling between cytoplasm and nucleus, directly interacts with the human nucleoporin hCG1 and therefore accumulates at the nuclear membrane (Le Rouzic et al., 2002). Moreover, recent studies show that Vpr expression in mammalian cells caused herniations and large holes in the nuclear envelope (NE) (de Noronha et al., 2001). De Noronha et al. propose a model in which Vpr enters the nucleus and disrupts the nuclear membrane from inside. Though it seems that Vpr facilitates the entry of the viral DNA into the nucleus, yet the underlying mechanism remains unclear. Interestingly, Vpr also alters the actin cytoskeleton in yeast and mammalian cells (Gu et al., 1997; Matarrese et al., 2000; Zhao et al., 1998). In $CD4^+$ T lymphocytes, Vpr induces a significant increase of polymerized F-actin and rearranges the filamentous structures (actin cables or stress fibers). The pool of G-actin remains unchanged while an increase of the total actin content was detected in Vpr-expressing cells (Matarrese et al., 2000).

These features suggest that Vpr may mediate the transition from the MTOC via the actin cytoskeleton to the nucleoporins and thus facilitates nuclear import of the PIC. To test this hypothesis, we investigated whether Vpr induced nuclear abnormalities are linked to actin polymerization dynamics inside living cells and if a direct interaction of the protein with actin can take place in vitro.

The presumption of actin being involved in the transition of the PIC from the MTOC to the nuclear envelope and maybe even in nuclear import can be supported by studies describing a distinct pool of actin surrounding the nuclear envelope (NE). These perinuclear actin filaments comprising a fine basket-like structure in the vicinity of the NE-membrane have been reported for numerous cell types (Clubb and Locke, 1998; Riparbelli et al., 1993). However, little is know concerning the polymerization dynamics likely to determine the functionality of this actin pool. Visualization with specific drugs that label actin filament is often dependent on cell fixation whilst in living cells, using green-fluorescent protein conjugates, the bright stress fibers drown the fine structures of the perinuclear actin basket out. As we wanted to investigate a dynamic phenomenon in the context of the viral infection we had to set-up a new method to label actin inside living cells.

1.3.4 Visualization of dynamic actin inside living cells

Actin comprises 10 percent by weight of the total cellular proteins of muscle cells. Even in nonmuscle cells, actin makes up 1 -5 percent of the whole protein content. A typical cytosolic concentration of actin in nonmuscle cells is 0.5mM, however, the local actin concentration can be tenfold higher in special structures like microvilli or filopodia (tiny extensions protruding from the plasma membrane). This predominance of actin compared with other cell proteins is a common feature of all cytoskeletal proteins, because they form structures that must cover large spaces in cells.

Due to this high concentration of actin in eukaryotic cells, the visualization of dynamic actin assembly is very challenging. Upon expression of actin linked to fluorescent conjugates (such as the green fluorescent protein), fine and dynamic structures are barely perceivable due to the high level of overall fluorescence. To overcome this problem, we developed a new method, which only enlightens a distinct pool of actin, taking advantage of a drug interfering with the actin polymerization. Several natural toxins are known to perturb the equilibrium between actin monomers and filamentous structures. The most commonly used are cytochalasin D, latrunculin and phalloidin with different effects each. Cytochalasin D, a fungal alkaloid, binds to the free barbed (+) end of actin filaments and thus blocks further addition of subunits. Latrunculin, a toxin secreted by Red Sea sponges, binds monomeric actin and inhibits it from adding to a filament end. Exposure to either toxin shifts the monomer-polymer equilibrium in the direction of dissociation. When these drugs are added to living

cells, the actin cytoskeleton disappears and cell movements like locomotion and cytokinesis are inhibited. In contrast, phalloidin prevents actin filaments to depolymerize. Isolated from *Amanita phalloides* (a mushroom), phalloidin binds at the interface between monomer subunits in actin filaments and locks them irreversible together. Even when actin is diluted below its critical concentration, phalloidin-stabilized filaments will not depolymerize.

As cytochalasin D is binding to free barbed ends of actin filaments it seemed to be the most appropriate drug to investigate dynamic actin polymerization. Additionally, cytochalasin D appears to be somewhat membrane permeant and therefore can potentially be used to manipulate actin polymerization *in vivo*. Applying a fluorescent analogue of cytochalasin D in concentrations that inhibit polymerization gives a very bright signal only minutes after adding to the cell medium. Yet, our intention for using cytochalasin D was not to abolish polymerization but just to visualize the pool of high turnover actin. Therefore we dropped the drug concentration to nanomolar ranges, which are still giving a bright signal of actin polymerization hotspots but do not impair the normal cellular metabolism. Hence using this approach we could examine a new aspect of the actin cytoskeleton inside living cells.

1.4 Objectives of the work

Nuclear import of the HIV pre-integration complex (PIC) an essential step in the early viral lifecycle still remains elusive. Lentiviruses, such as HIV, have the feature to translocate their genome in an active process into cell nuclei, even in non-dividing cells. Amongst the proteins, put forward to be implicated in this process, the viral protein R (Vpr) seemed to be an interesting candidate. Several studies showed that Vpr induces aberrant nuclear morphologies and transient disorganization of the cytoskeleton (Gu et al., 1997; Matarrese et al., 2000; Zhao et al., 1998). Therefore we investigated the role of this particular protein in the nuclear import process to get further insights into host pathogen interactions.

Furthermore we tested a novel antisense strategy based on PNAs to inhibit HIV replication and viral spread. A broad spectrum of sequences in the HIV genome has been targeted to study their potential relevance for antiviral effect. This approach is a powerful new method to investigate the cell biology of the virus. Additionally, PNAs could constitute new antiviral compounds, which can be further developed for therapeutical approaches.

2. Material and Methods

2.1 PNA and peptide synthesis

PNA oligomers can be prepared following standard solid-phase synthesis protocols for peptides (Merrifield, 1986; Merrifield, 1963). The scheme for protecting the N-(2-aminoethyl) glycine backbone of PNA monomers (PE Bioscience, Germany) is based on the N-(9-fluorenyl) methoxycarbonyl (Fmoc) chemistry while the exocyclic amines of the nucleobases (A, C, G, T and ψiC) are equipped with the benzohydryloxycarbonyl (Bhoc) protecting groups. The solid phase synthesis of PNA, as well as that of the peptides, was performed in a fully automated synthesizer Syro II (MultiSyn Tech, Germany) on a TentaGel N resin (Rapp Polymere, Germany) using the Fmoc strategy (Figure 7) (Merrifield, 1963).

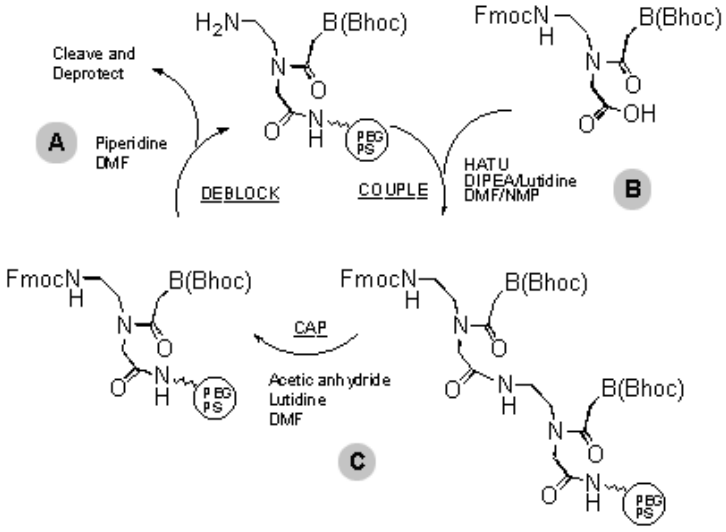

Figure 7: Scheme of the Fmoc peptide synthesis

A: The Fmoc protecting group is base-labile, and removable with 20% piperidine in dimethyl formamide (DMF). The following activation and coupling (acylation) must be maximally efficient to ensure the quality of PNA products. **B**: Optimal conditions are highly dependent on the nature of the activation reagent and the monomer-activated species. Thus we used HATU (O-(7-azabenzo-triazol-1-yl)-1,1,3,3-tetramethyluronium hexafluoro-phosphate) as the coupling reagent. The activation is accomplished by mixing monomer, HATU, and base solution containing DIPEA (diisopropylamine) and lutidine. HATU activated carboxylic acids have demonstrated enhanced coupling efficiency in peptide synthesis and are especially suited for hindered amino acid and other difficult couplings. **C**: Monomers, that have been deblocked and activated but did not react with the resin in step A and B must now be capped, to ensure the sequence accurateness of the ongoing synthesis.

The postsynthetic modification of PNA uses coupling of a desired group to an introduced lysine or cysteine residue in the PNA. Amino acids can be coupled during solid-phase synthesis or compounds containing a carboxylic acid group can be attached to the exposed amino-terminal amine group to modify PNA oligomers.
Therefore at the N-terminus of the PNA we introduced a spacer of 2 lysines (KK), to prevent spatial binding hindrance of the following nuclear localization sequence (NLS), derived from the simian virus 40T antigen (PKKKRKV) (attached only to PNAs designed for anti gene therapy) and/or one cysteine to enable linkage with a transport peptide. To promote cellular import of the PNAs, the 16 amino acid residues (RQIKIWFQNRRMKWKK) derived from the third helix of the antennapedia homodomain (pAntp(43–58)) of *Drosophila* were linked via a cleavable disulfide bond to the PNA construct (Derossi et al., 1996) (Figure 8).

Figure 8: Scheme of PNA transport construct

PNAs designed for anti gene therapy were synthesized from the C-terminus and directly linked to a double lysine spacer (KK) as well as the [SV40 T] NLS sequence. The synthesis was finished with a single Cystein at the N-terminus for further coupling with the cell transport peptide pAntp. PNAs meant to inhibit translation or the early events in the HIV live cycle had only the additional Cystein at their N-terminus. After purification and characterization the PNA-NLS or -Cys hybrid molecules were linked, under oxidizing conditions, over a cleavable disulfide bond to the pAntp peptide.

Postsynthesis procedures involve cleaving PNA oligomers from the solid support by treatment with trifluoroacetic acid. Then PNA is precipitated by ice-cold diethyl ether and dissolved in 0.1% trifluoroacetic acid solution. All synthesis products were purified by preparative HPLC (Shimadzu LC-8A, Japan) on a YMC ODS-A 7A S-7 µm reverse phase column (20 x 250 mm), using 0.1% trifluoroacetic acid in water (eluent A) and 60% acetonitrile in water (eluent B). Peptides were eluted with a successive linear gradient, increasing from 25% to 60% B-eluent in 49 min at a flow rate of 10 ml/min. The fractions corresponding to the purified conjugate were lyophilized. Sequences of single modules as well as the complete constructs were characterized with analytical HPLC (Shimadzu LC-10, Japan), using a YMC-Pack

Pro C18 (150 x 4.6-mm inner diameter) S-5-µm, 120A column with 0.1% trifluoracetic acid in water (eluent A) and 20% acetonitrile in water (eluent B). The analytical gradient ranged from 5% (eluent B) to 80% (eluent B) in 35 min. Finally the mass of the constructs was verified by matrix-assisted laser desorption ionization time-of-flight (MALDI-TOF) mass spectrometry (Finnigan, Vision 2000). The Cysteines of the pAntp peptide and the PNA or PNA-NLS construct were oxidized at the range of 2 mg/ml in a 20% dimethyl sulfoxide (DMSO) water solution. Five hours later, the reaction was completed. The excess DMSO was washed out with water by several freeze-drying steps (Table 2).

	Mol. Weight in [g/mol]		**Yield of PNA synthesis after pAntp coupling and purification**	
pAntp(43–58)	2350,92		**in [mg]**	**in [µmol]**
PNA +/- NLS		**PNA + pAntp**		
PNA I Cys	4811,4	7160,3	1,0	0,140
PNA I NLS	5933,2	8282,1	1,81	0,219
PNA II Cys (21mer)	5741,4	8090,3	2,18	0,269
PNA II NLS	6045,3	8394,2	0,6	0,071
PNA III Cys (21mer)	5879,4	8228,3	0,64	0,078
PNA III NLS	6183,2	8532,1	0,34	0,040
PNA III NLS (21mer)	7001,0	9349,9	0,93	0,099
PNA IVa Cys	5039,7	7388,6	0,99	0,134
PNA IVb Cys	4831,4	7180,3	1,86	0,259
PNA Va NLS (21mer)	6910,0	9258,9	2,24	0,242
PNA Vb NLS	6025,2	8374,1	2,09	0,250
PNA Vc NLS	6095,2	8444,1	1,11	0,131
PNA VI Cys	4781,4	7130,3	1,69	0,237
PNA VIIIa NLS	6022,2	8371,1	1,53	0,183
PNA VIIIb NLS	6077,2	8426,1	2,22	0,263
Random Cys	4924,5	7273,4	1,65	0,227
Random NLS	6046,1	8395,1	0,67	0,080

Table 2: Molecular Weight and yield of the completed PNA synthesis

Table highlights molecular weights (in g/mol) of all synthesized PNA constructs before and after coupling to pAntp. All PNAs were synthesized as 18mers, if not stated differently. On the right part of the table the yield in [mg] and [µmol] of the final synthesis product is shown.

After synthesis, PNAs were stored lyophilized at 4˚C and dissolved in phosphate buffered saline (PBS) prior to use. The aliquot in use was kept at 4˚C and when

necessary further diluted in PBS or cell culture medium (DMEM); the stock solution was stored at 20˚C.

2.2 Experimental systems to test viral production in early and late life cycle

Virus and cell lines

The virus used in this study was derived from the pLAI3 infectious molecular clone (Charneau et al., 1992), which carries the complete sequence of the HIV-1 LAI isolate (Wain-Hobson et al., 1991).

The indicator cells used are HeLa-CD4+ cells that carry the *lacZ* gene under the control of the HIV-1 LTR (Charneau et al., 1994). Additionally the HIV-1 coreceptor CCR5 is expressed on the surface of the HeLa-CD4+ cells, therefore cells can be infected by T cell-adapted HIV-1 strains (including primary isolates), that need this coreceptor for infection, (Verrier et al., 1997). HeLa P4-CD4+/CCR5 (HP4) cells were grown in Dulbecco's Modified Eagle Medium (DMEM (GIBCO)) supplemented with 10% fetal calf serum and 500 µg/ml of G418 (GIBCO).

Persistently infected cells were obtained by infection of HP4 cells with the HIV-1 LAI isolate and several passages in culture medium under G418 selection pressure. Conservation of viral infection was regularly tested with a p24 ELISA assay.

Virus infections and assay readout protocols

HP4 cells plated in 96-well plates were infected for each experiment in triplicate with equivalent amounts of pLAI3 molecular clone (0.5ng of p24 viral antigen per well), in the presence of 20 µg/ml of DEAE-dextran.

The inhibition by PNAs targeting early life cycle stages was revealed by the activity of the reporter gene *lacZ*. The ß-galactosidase activity was measured 48 hours after infection using a chemiluminescent ß-gal reporter gene assay (Roche) according to the instructions of the manufacturer. HP4 cells (~$2x10^4$ cells/well) were treated at stated concentrations with PNAs in 96 microwell plates and subsequently infected with virus as described above. After 48 hours incubation time, cells were washed and lysed for five minutes in a buffer containing 0.5% Triton X-100 and a protease inhibitor cocktail. In a photometric assay the enzymatic hydrolysis of the ß-galactisidase substrate o-nitrophenyl-ß-D galactopyranoside (ONPG) is measured. ONPG is colorless but on hydrolysis resulting in o-nitrophenol that is yellow in alkaline solution (pH 7.5). The substrate is added in excess to the lysates. After 15

min the reaction is stopped with a concentrated solution of Na_2CO_3, which shifts the pH to ~11, inactivates ß-galactisidase, and maximizes the absorbance of o-nitophenol at 420 nm. The optical density of the solution at 420 nm is read on a Wallac (Victor2) spectrophotometer and calibrated against the absorbance of a standard curve.

PNA inhibition of late replicative steps was tested on persistently infected cells (described before). Cells were treated at stated concentrations with the different PNAs and the supernatants were tested for viral load using an HIV-1 core profile enzyme-linked immunosorbent assay (ELISA), quantifying the amount of p24 capsid protein (Kit; PerkinElmer Life Science). Briefly, an aliquot of cell culture supernatant was diluted 1/10 in sample diluent and lysed with 0.5% Triton X-100. Then dependent on expected viral load, further dilution (in general 1/1000 or 1/10000) were prepared. 200µl of each sample were tested in duplicate by adding it directly to a monoclonal antibody-coated microplate. The captured antigen is complexed with biotinylated polyclonal antibody to HIV-1 p24, following by a streptavidin-HRP (horseradish peroxidase) conjugate. The resulting complex is detected by incubation with ortho-phenylenediamine-HCl (OPD), which produces a yellow color, whose intensity is directly proportional to the amount of HIV-1 p24 captured. The absorbance of each microplate well is determined using a microplate reader (Bio-Rad) at a wavelength of 492 nm with the reference at 620 nm and calibrated against the absorbance of an HIV-1 p24 antigen standard or standard curve.

2.3 Cell culture

Cell lines

HeLa (ATCC), NIH-3T3 mouse fibroblasts, baby hamster kidney cells (BHK1; expressing functional, green fluorescent protein (GFP) conjugated nucleoporin POM121) and HeLa cells expressing the LaminA protein fused to the red fluorescent protein (DsRed), were cultured in complete DMEM (DMEM Glutamax (Invitrogen), 10% FCS, 100U/ml streptomycin, 100µg/ml penicillin) at 37°C in an atmosphere of 95% air / 5% CO_2 and subcultured every 4-5 days. To subculture, cells were washed twice with PBS, without Ca^{2+} and Mg^{2+} (Invitrogen), and then detached from their plastic support with 1x Trypsin-EDTA (0.25% Trypsin; 1mM EDTA, Invitrogen) for 5 min at 37˚C. To store the cells in liquid nitrogen, we froze them progressively (about 1°C per hour) in culture medium supplemented with 10mM HEPES (Invitrogen) and 10% DMSO (Sigma) at pH 7.4.

Transient plasmid expression

The expression of Vpr-GFP was achieved by transient transfection of the plasmid pVprGFP (derieved from pEGFP-N1 (Clontech Inc.); containing Vpr between Pst I-Bam HI) with Fugene6 (Boehringer-Mannheim) according to manufacturer protocol. The nuclear pore labeling in HeLa cells was achieved by transfection with a plasmid (pcPOM121-GFP) containing POM121-GFP (pcDNA1Neo (cut by Xho I and Xba I)) (Imreh et al., 1998; Soderqvist et al., 1997) (kind gift of E. Hallberg, University College, Huddinge).

Synchronization

Populations of mitotic cells were either produced by a single overnight (~18 hours) thymidine block (2.5mM, Sigma) (Fang et al., 1998) or by an overnight incubation (17h) with Aphidicolin (an inhibitor of DNA replication) (0.5µg/ml, Sigma).
After the blocking, cells were washed with PBS and grown in fresh medium without thymidine or Aphidicolin for ~8 hours prior to use.

2.4 Molecular biology techniques

Agarose gel electrophoresis

This is a method to separate DNA strands according to size, allowing to determine the size of the separated strands by comparison to strands of known length (marker). Due to the negative charges of its phosphate backbone, the DNA moves toward the positive electrode in an electric field. An optimal separation, between small and big fragments, is achieved by using an appropriate agarose concentration (between 0.8% and 1.5%). The agarose is dissolved in TAE buffer (2M Tris, 250mM Na-Acetate, 50mM EDTA; PH 7.8) by boiling. After cooling down to ~50˚C, ethydium bromide (intercalating agent to stain nucleic acids; upon exposure to UV light it will fluoresce a red-orange color) was added (0.5µg/ml,) and the solution is filled into a gel rack. DNA was diluted in 4x sample buffer (50mM EDTA, 50% v/v Glycerin, small amount of bromophenol blue to stain) and injected into gel slots. For separation, a current of 60V-100V was applied in gel racks filled with TAE buffer.
When DNA was prepared for further use (i.e. in ligation), the band was cut out of the gel and purified using a Qiagen Gel-Purification kit protocol. The purified DNA was then dissolved in TE-buffer (10mM Tris, 1mM EDTA; pH 8).

Molecular cloning

For cloning purpose, target DNA was cut with restriction enzymes (or restriction endonucleases). These are enzymes that cut double stranded DNA in a sequence specific manner without damaging the nuclear bases. The chemical bonds cleaved by restriction enzymes can be reformed by other enzymes known as DNA ligases. Therefore restriction fragments carved from different chromosomes or genes can be spliced together. The DNA digestion was performed according to the manufacturer's manual in the appropriate buffer and at the indicated temperature. The amount of enzyme used per digestion was adjusted to the amount of DNA to be cut in the preparation; in general 0.5 units/µl per preparation (1 unit of any enzyme is the amount capable to cut completely within one hour 1µg DNA under optimal salt and temperature conditions).

Ligation of DNA fragments

The *in vitro* combination of two DNA fragments was achieved with a DNA-ligase, an enzyme able to *ligate* two strands, by the formation of covalent phosphodiester bonds. For the reaction, DNA-vector and insert were added in equimolar concentration (0,5-1µg) mixed in a total volume of 20µl with 1µl T4-DNA-Ligase and 2µl 2x Ligase-buffer and incubated for at least 4 hours at 16˚C.

Polymerase Chain Reaction (PCR)

The Polymerase Chain Reaction (PCR) provides an extremely sensitive means of amplifying small quantities of DNA *in vitro*. The technique was made possible by the discovery of *Taq* polymerase, the DNA polymerase purified from the bacterium *Thermus aquaticus* living in hot springs. This DNA polymerase is stable at the high temperatures needed to resist several cycles of strand separation at high temperatures.
PCR is based on the DNA polymerization reaction. A sense/antisense primer-pair, framing the region of interest, and dNTPs are added along with a DNA template and the DNA polymerase. The original template is melted (at 94˚C), the primers are annealing (at ~45-55˚C) and the polymerase produces two new strands (at 72˚C), doubling the amount of DNA present. This provides two new templates for the next cycle. The DNA is again melted, primers anneal, and the Taq polymerase generates 4 new strands which results in an exponential amplification of the template.

Reactions were performed in a total volume of 100µl with a DNA content of 10-20ng (purified Plasmid DNA), 1µl *Taq* Polymerase, 10µl 10x buffer (purchased with the enzyme), 2µl of a 10mM dNTP stock solution and ~2-3µl of each primer of a 10µM stock solution.

The annealing temperature was calculated according to: [4x(GC) + 2x(AT)] x18/length of primer. To gain the final annealing temperature we subtracted another 5˚C from the calculated result. Anneling time was calculated knowing that the *Taq* Polymerase is adding ~ 1000 nucleotides/ minute.

2.5 Microscopy

Immunostaining

Cells or isolated nuclei were fixed for 20 min with 4% paraformaldehyde in cytoskeleton buffer (10mM MES, 3mM $MgCl_2$, 138mM KCl, 2mM EGTA and 0.32M sucrose, pH 6.1), then permeabilized for 5min with 0.5% Triton X-100 in PBS and incubated successively with appropriate fluorescent markers as indicated: phalloidin Alexa-488 (staining actin filaments (F-actin); Molecular Probes) (1/200, 20 min); Hoechst 33342 (Sigma-Aldrich) (0.001mg/ml, 10 min,); monoclonal antibody mAb414 (staining the NPC; Babco, USA) (1/5000 in PBS supplemented with 10% horse serum, overnight at 4˚C), followed by secondary, anti mouse CY3 conjugated, antibody (Jackson ImmunoResearch Laboratories, Inc.) (1/200 in PBS supplemented with 10% horse serum, one hour at RT).

Treatment of cells with "cytoskeleton drugs"

HeLa cells expressing POM121-GFP were incubated for 30 minutes with either 1µM Cytochalasin D (CD) (Sigma), 1µM LatrunculinA (LatA) (Molecular Probes) or 200nM Jasplakinolide (Jaspl) (Molecular Probes) at 37°C (additionally DMSO vehicle control according to stock solution of all drugs). Following the drug treatment, cells were fixed and co-stained with Hoechst 33342 as described above. In two independent experiments, at least 200 nuclei were counted and analyzed for each experimental setup (samples and controls respectively).

For the live cell experiments the CD-BODIPY loading solutions were freshly prepared by serial dilution of a 1mM stock solution (in DMSO) into experimental medium to give the stated final concentrations. Facile staining of cells was achieved by continuous incubation of cells in this solution for twenty minutes. With very low

concentrations, cells could be maintained for several hours before any deleterious effects were observed. Co-visualization using bright-field transmission observation was used routinely to ensure that observed cells were flat, adherent and healthy. The cell permanent, minor groove binding, AT selective, fluorescent DNA stain HOECHST 33342 (Sigma) was added to the experimental medium where stated (final concentration 1µg/ml) in order to reveal chromatin distribution inside living cells.

Microinjection.

HeLa cells expressing POM121-GFP were microinjected with either 10µM actin-Alexa568, or Dextran-Rhodamine 70kDa (2.5mg/ml) using a Femtojet/Injectman micromanipulator (Eppendorf, Hamburg, Germany).

Live cell image acquisition

For live cell imaging, cells grown on MatTek's glass bottom microwell dishes (MatTek Corporation, 35mm) were exchanged into OptiMEM medium (Gibco BRL). On the microscope stage, cells were maintained at 37°C with a Zeiss "Tempcontrol 37-2 digital" heating chamber.

"High-resolution" fluorescent imaging in living cells was performed using two different types of microscope customized to achieve maximal spatial resolution; either a wide-field fluorescence imaging or a high-speed spinning disk confocal system. The wide-field system was built around an upright microscope (DM-RXA, Leica, Germany) equipped with a Nomarski filter. For high-resolution imaging, a 100x oil immersion, infinity corrected objective (PL APO, Leica) was used. The light-gathering ability of a microscope objective is quantitatively expressed in terms of the numerical aperture (n.a.), which is a measure of the number of highly diffracted image-forming light rays captured by the objective. Higher values of numerical aperture allow increasingly oblique rays to enter the objective front lens, producing a more highly resolved image. The n.a. of the objective we used was 1.4, and we calculated the maximum spot resolution and focal depth to be ~0.2µm and ~0.25µm respectively (Taylor and Salmon, 1989). Fluorescent emission was detected directly using a 12-bit digital integrating CCD camera (*C4742-95,* Hamamatsu, Japan). No signal binning was used in order to maintain maximum *x-y* spatial resolution. Image acquisition control and processing used *OpenLab* software (Improvision, UK). The high-speed spinning disk confocal system (*UltraView RS*- Perkin-Elmer, USA)

equipped for dual wavelength acquisition, and built around a Zeiss (Germany) inverted *200M* microscope. Cells were visualized using a Hamamatsu ERII firewire detector and a 100x *NeoFluor* 1.3 n.a. objective yielding pixel resolution ~208nm (2x2 binning), and fast axial sampling used a piezo-objective drive stepping at 200nm.

Time-lapse acquisitions with cells only expressing GFP were achieved using a standard Zeiss Axiovert 200M microscope equipped with a *Plan-Fluar* 100x objective, n.a. 1.45. The microscope is controlled by Till Vision (Till photonics, Germany) designed for fast live cells imaging and equipped with a xenon lamp, polychromator for precise wavelength selection and a Till Photonic Imago QE CCD camera.

Images from some experiments on fixed cells were acquired using an upright Zeiss Axioplan2 microscope, with the Zeiss Axiovision 4.1 software and an integrated ApoTome applet. (63x PlanApochromat n.a. 1.3, equipped with an Axiocam MRm b&w camera).

Deconvolution and reconstruction

All axial image datasets were identically treated. First using geometric light reconstruction (deconvolution) based on a calculated point-spread-function (PSF) estimate. Deconvolution is necessary for the recovery of an object from an image that is degraded by blurring and noise. In microscopy, the blurring is largely due to diffraction limited imaging by the instrument and the noise is usually photon noise. The PSF (the image of a single point object) can be obtained by recording the image of a sufficiently small object like a fluorescent bead. Most lenses are not perfect optical systems. As a result, visual stimuli that pass through the lens will undergo a certain degree of degradation, meaning the lens will introduce a small amount of blur. So if the relative intensity of this point of light were plotted as a function of distance, one would obtain a Gaussian distribution. This curve is called the "point spread function" (PSF) and this function is essential for the deconvolution algorithm. Following the calculation of the PSF, the “maximum likelihood estimate” iterative algorithm is applied both algorithms are available through *Huygens* software (*Scientific Volume Imaging*, Netherlands), and tuned using the commercially available plug-in “Nipkow-disk”. Second, the deconvolved results were then 3D reconstructed

and partly analyzed using the "Co-loc" option of *Imaris* (Bitplane, Switzerland). All two-color, three-dimensional rendering and reconstruction used the same software.

CD-BODIPY *in vitro* measurements

Purified, native and fluorescent (*FITC*) conjugated rabbit skeletal muscle actin (Cytoskeleton, Denver, *U.S.A.*) in 2µl stock aliquots (10mg/ml; 222µM; containing 2mM Tris-HCl, 0.2mM $CaCl_2$, 0.2mM ATP, 0.5mM DTT, 2% sucrose, and 0.005% NaN_3 (pH8.0)) was prepared at working dilutions (0.5-0.75 mg/ml; 11-17µM) by addition of low salt buffer (5mM Tris-HCl, 0.2mM Na-ATP, 0.5mM DTT, 0.2mM $CaCl_2$, pH8.0). For each experiment, a single fresh actin stock was used. Stock and aliquots were maintained at 4°C. Drugs were added, yielding the final concentrations stated. Samples were vigorously mixed by pipette, vortexed and then left on ice for 1 hour before being clarified (100 000xg, 4°C, 30min). Supernatants were added to 5x concentrated *high* salt polymerization buffer giving final concentrations of 100mM KCl and 10mM Mg-ATP in the low salt buffer. After mixing, a 5 µl droplet was sealed under a glass cover slip on a microscope slide and incubated at 37°C for at least 3 hours to allow actin to fully polymerize to a steady state (Carlier et al., 1986) before semi-quantitative observation using fluorescence microscopy. Each experiment (triplicate samples) was performed at least twice yielding comparable results.

2.6 Biochemistry

SDS-PAGE

Polyacrylamide gel electrophoresis (PAGE) is used to separate heterogenous protein mixtures (Laemmli, 1970). The polyacrylamide gel matrix is formed by the co-polymerization of two monomers: acrylamide and bis-acrylamide. The acrylamide polymerizes into long chains, which are crosslinked at intervals by the bis-acrylamide, forming polyacrylamide. The porosity of the matrix can be altered by changing the percentage of acrylamide in the mixture; higher percentage of acrylamide gives better separation of small proteins. The gel is composed of two components one low concentrated stacking gel, to concentrate the sample, and a separating gel on the bottom with the required matrix pore size. In order to most accurately separate proteins according to their sizes, the proteins must be denatured. The anionic detergent sodium dodecyl sulfate (SDS) is used as the denaturing agent in gel and

sample buffer. SDS is an amphipathic molecule with a long hydrophobic tail and a small negatively charged head group. The hydrophobic portion of the molecule coats the protein, disrupting the secondary, tertiary, and quaternary structures. Another consequence of treatment with SDS is that the proteins are artificially coated with negative charges. Therefore, in an electric field, they migrate toward the positive pole. Since the proteins are denatured and the negative charge on the proteins is exceedingly large, the primary factor determining the rate of migration of the protein through the matrix is the size of the protein.

Samples were resuspended in sample buffer (250mM Tris, pH 6.8, 2% SDS, 20% glycerol, 0.08% bromphenol blue, 2mM EDTA and 20mM dithiothreitol (DDT)) and boiled for 5 minutes at 100˚C. The gels were run on a Biorad gel electrophoresis apparatus in buffer containing 25mM Tris, 0,2M glycine and 1% SDS, pH 8.5 at ~100V- 150V. After the run, the gel was either further processed for immunoblotting or stained with coomassie blue stain (0.25% coomassie blue R-250 (w/v) in 45% Ethanol and 10% acetic acid) for 20 minutes and destained with a solution containing 45% ethanol and 7.5% acetic acid to reveal proteins directly on the gel.

Immunoblot (Western Blot)

Proteins separated in an SDS-PAGE can be transferred to a solid membrane for western blot analysis. For this procedure, an electric voltage is applied to the gel, so that the separated proteins migrate through the gel onto a nitrocellulose membrane (Schleicher & Schull Optitran BA-S 83) in the same pattern as they were separated on the SDS-PAGE. After the transfer in a wet apparatus (Biorad) in buffer containing 48mM Tris, 39mM glycine and 20% v/v ethanol, the transfer efficiency was checked by coloring of the membrane with Ponceau S Solution (Sigma; 0,1% w/v ponceau S and 5% acetic acid diluted in 1/5 in water). Ponceau S is staining all proteins on the nitrocellulose membrane with a detection limit of 250ng and has the advantage to be easily removable by washing with destilled water. Subsequently the membrane was blocked (in order to prevent non-specific protein interactions between the membrane and the antibody) with 5% (w/v) milk in PBS for 15 minutes at RT (or overnight at 4˚C) and incubated with a specific primary antibody which recognizes only the protein of interest (diluted at indicated concentration in 5% milk/PBS) overnight at 4˚C (or 1 hour at RT). The membrane was then extensively washed with PBS (3 x 10 min) and incubated with a secondary peroxidase-conjugated antibody, specific for the

species in which the primary antibody was raised, (also diluted at indicated concentration in 5% milk/PBS) for 1 hour at room temperature. Again the membrane was washed with PBS (3 x 10 min), developed according to manufacturer's instructions using a reaction Kit (Chemiluminescence HRP substrate; Pierce) and exposed to an X-ray film (hyperfilm ECL 18x24, Amersham) for the appropriate time period (30 seconds to several minutes, depending on the intensity of the band).

2.7 Actin polymerization assays

Bead coating and motility assay

Carboxylated polystyrene beads (Polysciences), 0.5µm, were first washed in storage buffer (0.1M NaH_2PO_4, 0.1M Na_2HPO_4, pH 7,4) and then incubated in protein solution either containing 1mg/ml chemically synthesized Vpr protein (in H_2O, 5mM DTT) or, as controls, 1.8mg/ml ActA or 2mg/ml ovalbumin. In all cases, conditions were such that the amount of protein was saturating. For example, 2µl of 0.5µm beads (2.5% solids) were added to 10µl of protein solution. Beads were incubated in protein solution for 1 hour at 4˚C on a rotating wheel then pelleted and washed in buffer B (20mM Tris-HCl, pH 7.8, 100mM KCl, 1mM $MgCl_2$, 0.2mM ATP, 0.1% Tween 20, and 0.2% BSA) and resuspended in 30µl of buffer B. Protein-coated beads were stored on ice or at 4°C and were used within 1 week.

For visualizing bead motility, coated beads (0.5µl) were added to *Xenopus laevis* egg cytoplasmic extract (10µl) supplemented with tetramethylrhodamine-labeled actin (0.5µl of 60µM rho-actin (Cytoskeleton, USA)), creatinine phosphate (0.65µl of 500mM stock) and ATP Mg^{2+} (1µl of 10mM stock). The assay mix was allowed to incubate on ice for 1 hour. Then, a 2µl sample was removed and squashed between a microscope slide and a 22-mm-square glass coverslip, sealed with vaseline:lanolin:paraffin (at 1:1:1), and incubated at RT for 30 minutes in the dark before observing on the microscope. All observations were performed on the wide-field fluorescence imaging system built around an upright microscope (DM-RXA, Leica, Germany). Image acquisition control and processing used *OpenLab* software (Improvision, UK).

Actin polymerization

Actin, isolated from rabbit skeletal-muscle (received from L. Blanchoin), was stored in its Ca^{2+} bound form in Ca-G buffer (5mM Tris-HCl pH 7.5, 0.2mM ATP, 0.2mM $CaCl_2$ and 0.2mM DTT) at 4˚C. Immediately before polymerization, Ca-ATP-actin was converted to Mg-ATP-actin by incubation with one-tenth of a volume of 10x exchange buffer (2mM EGTA and 0.2mM $MgCl_2$) in Mg-G buffer (Ca-G buffer with addition of 1mM $MgCl_2$) for 5 min at 4°C. The actin was then polymerized by addition of a 1:9 dilution of 10x KMEI (500mM KCl, 10mM $MgCl_2$, 10mM EGTA, 100mM Tris-HCl, pH 8) (Blanchoin et al., 2000).

After 20 min of polymerization at RT in presence of one molar equivalent rhodamine-phalloidin, the actin was diluted to a final concentration of ~10nM in fresh fluorescence buffer (50mM KCl, 1mM $MgCl_2$, 100mM DDT, 20µg/ml catalase, 100µg/ml glucose oxidase, 3mg/ml glucose, 0.5% methylcellulose, 10mM imidazole pH 7.0). Two microlitres were applied to glass coverslips coated with 0.01% (w/v in H_2O) poly-L-lysine and the actin filaments were viewed with the same microscope as stated above (DM-RXA, Leica, Germany).

Pyrenyl-actin polymerization assay

Pyrenyl-actin was produced by labeling the Cys374 residue in actin monomers with pyrene-iodoacetamide. Before polymerization, Ca-ATP-(pyrenyl) actin was converted to Mg-ATP-(pyrenyl) actin as already described. The (pyrenyl) actin (in general 2µM) was mixed with the stated proteins at RT in Mg-G buffer, and one-tenth of a volume of 10x KMEI was added to initiate polymerization. Pyrene fluorescence of samples (200µl) was monitored using a spectrofluorimeter with excitation at 365 nm and emission at 407 nm.

Actin polymerization on crude nuclear envelopes and western blot analysis

Rabbit skeletal muscle actin was polymerized, at indicated concentrations, for 30 min with the protocol described above in the presence of isolated NE-membrane. (Isolated NE membranes were obtained in collaboration with the group of M. Matunis. The ghost membranes were prepared according to the protocol in (Cronshaw et al., 2002).) Aliquots of this reaction mix were then put onto a glass cover-slip, where the nuclei were let to adhere and then fixed with 4% paraformaldehyde for 20 min, whereupon

immunostaining with mAb414 (Davis and Fink, 1990) (1/5000) and phalloidin-Alexa488 (Molecular Probes) was performed (see above).

For cosedimentation assays, actin (4µM final) was polymerized in the presence of isolated NE-membranes (same protocol) followed by a low speed centrifugation with an Eppendorf 5417C at 1200*g*. Supernatants were transferred to fresh tubes and pellets were washed once in 1x KMEI and resuspended in 20µl 1x KMEI. Equal volumes of the supernatants and the pellets were subjected to western blot analysis. The different fractions were subjected to SDS-PAGE (10% gel) and immunoblotted with purified mAb414 (1/5000) or an anti-actin antibody (sigma) (1/1000). To remove the proteins at the surface of the isolated NE, we incubated the crude NE-membranes for 1h at 4°C with $MgCl_2$ (2M final) and washed them twice in their conservation buffer (10% sucrose, 20mM triethanolamine, 0.1mM MgCl2, 1mM DTT, pH 7,5). After $MgCl_2$ treatment the nuclear envelopes (NEs) were subjected to the co sedimentation assay described above.

To study the direct interaction of actin with the nuclear membrane, NEs were additionally pre-incubated overnight at 4°C separately with mAb414 (1/4000), anti Nuance mAb (directed against an actin binding protein on the nuclear membrane; 1/50) and anti c-myc (Santa-Cruz, Biotechnology; (1/2000)). Cosedimentation assays and SDS PAGE were then performed as described above, with 2µM actin.

3. Results

3.1 Part I: Implication of the host cell in HIV infection

3.1.1 The viral protein R (Vpr) induces nuclear membrane invaginations

In contrast to other retroviruses, lentiviruses are able to infect non-dividing cells. Despite the importance of this characteristic for HIV infection, the nuclear import of the PIC (pre-integration complex) is still poorly understood. In addition to the central DNA flap, several NLS containing-proteins have been proposed as being implicated in the process (Bukrinsky et al., 1993a; Gallay et al., 1997; Heinzinger et al., 1994; Popov et al., 1998a; von Schwedler et al., 1994; Zennou et al., 2000). Amongst the NLS-bearing proteins, the small (14 kDa) Vpr protein (Bukrinsky and Adzhubei, 1999) is a promising candidate. Erroneously, this protein was classified as accessory yet it turned out to be necessary but not essential for HIV replication in non-dividing cells. However, the fact that the *vpr* gene is conserved in primary isolates of HIV-1 strongly suggests a crucial role. As an integral part of viral particles, Vpr is imported into the cells during infection (Coffin, 1996) and stays associated with the PIC at least until the genomic DNA is delivered into the nucleus (Miller et al., 1997). Furthermore, Vpr interacts with POM121 and hGC1, two components of the nuclear pore complex (NPC) (Fouchier et al., 1998; Le Rouzic et al., 2002). The binding to the NPC may be important to explain the requirement of Vpr for HIV nuclear import in non-dividing cells.

The nucleus is separated from the cytoplasm by two concentric membranes known as the nuclear envelope (NE). The NE is punctuated by holes known as nuclear pore complexes (NPCs), which provide the main pathway for transport of cellular material across the nuclear-cytoplasmic boundary. When HeLa cells were transfected with a vector containing Vpr fused to the green fluorescent protein (GFP), the tagged protein was clearly localized to the nuclear envelope and more precisely displayed the characteristic punctuated NPC staining (Figure 9).

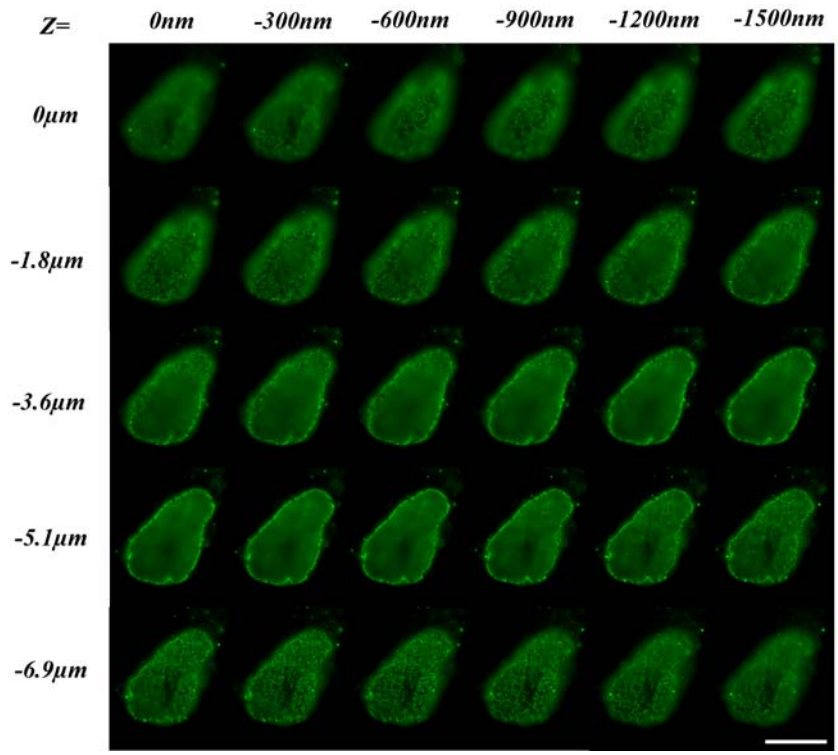

Figure 9: "Z-stack" from nuclear associated Vpr-GFP inside a living HeLa cell.

The panel shows a fluorescent image recorded from the nucleus of a living HeLa cell expressing Vpr-GFP. Vpr-GFP expression reveals the characteristic punctuated staining of NPCs. Note the membrane invagination appearing at the bottom of the nucleus. The image series (*left to right*) shows images selected at z-axis intervals of 300nm, descending through the sample. The scale bar (*bottom right*) is 10µm. Images were recorded using a *TILL-Photonics* imaging system mounted on a *Zeiss Axiovert200M* microscope.

The shape of the eukaryotic cell nucleus as defined by the nuclear envelope (NE) is usually not a smooth symmetric spherical or ovoid shape. Instead, it contains asymmetric structural domains in the form of deep membrane folds, or "invaginations". These structures are widely reported (Bourgeois et al., 1979; Hochstrasser and Sedat, 1987; Park and De Boni, 1992) and appear to be a common feature of eukaryotic nuclei.

Using an inverted fluorescent microscope for living cell imaging, Vpr-dependent deformation of the nuclear envelope could be recorded. Surprisingly, nuclear membrane ruffling was enhanced compared to control experiments, in which cells were transfected with the GFP-conjugated nucleoporin POM121 (a transmembrane nuclear pore complex (NPC) protein). In Vpr expressing cells, we also observed an

enhanced frequency of nuclear membrane invaginations. We quantified this observation in fixed cells. Invaginations were counted ~8 hours after transfection with Vpr-GFP or the control plasmid POM121-GFP. The statistical analysis resulted in a 40% increase of invagination frequency in cells expressing Vpr. Moreover we observed, that the induction of invaginations was only transient, because invagination counting after 24 hours following transfection resulted in a non significant increase (data not shown). From this point forward we conducted *in vivo* imaging experiments of Vpr expressing cells at early time points after transfection.

Besides membrane ruffling and the increase of invaginations in fixed cells, we also recorded highly dynamic processes, with invaginations appearing and disappearing within few minutes (Figure 10).

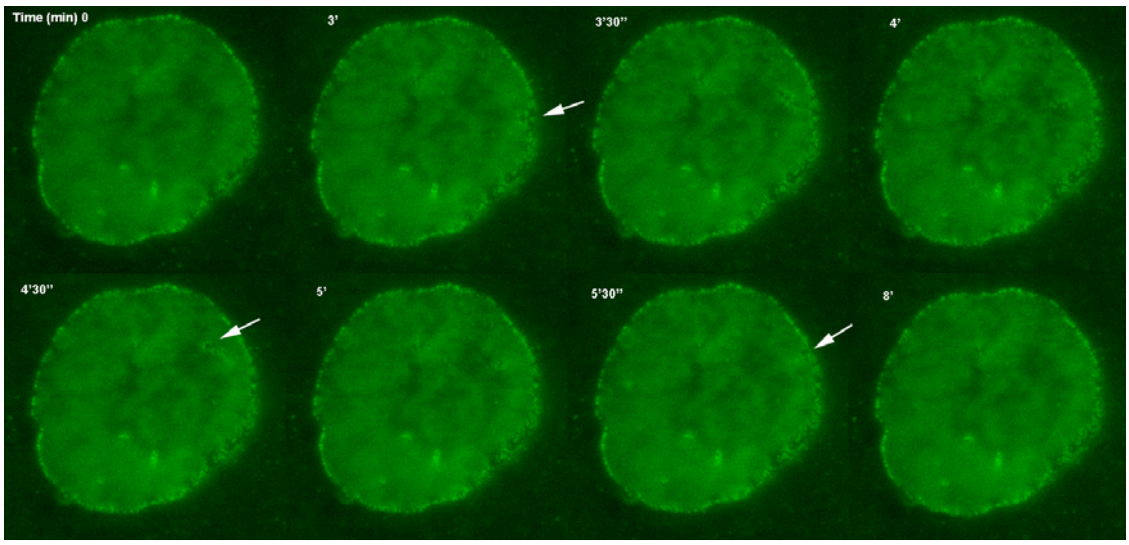

Figure 10: Dynamic invagination of nuclear envelope in cell expressing Vpr-GFP

The panel above shows the nucleus of a HeLa cell transiently expressing Vpr-GFP. The cell was recorded for about 15 minutes on a single plane with one image recorded every 30 seconds. In the first timeframes the nuclear membrane is rather stable. But then preceded by membrane ruffling at a distinct area of the NE (indicated by arrowhead in the second frame) a highly dynamic invagination appears and disappears (arrowheads) within a total time of 3 minutes.

The fast and directed fluctuation of the nuclear membrane observed at a locally distinct area, is a very interesting observation in the context of the yet unanswered question of HIV pre-integration complex (PIC) entry into the nucleus. However, the functions of nuclear membrane invaginations are not well understood. NE

invaginations appear as fine tubular projections of the double membrane, which permeate inwards upon the nuclear space, and can exhibit dynamic structural fluctuations (Broers et al., 1999; Ellenberg et al., 1997; Fricker et al., 1997). To date, the molecular basis for *de novo* formation and dynamic structural organization of invaginations has remained elusive.

3.1.2 Actin-polymerization and NE-membrane structural plasticity

To gain a primary understanding of the structural plasticity and dynamics of nuclear envelope (NE) membranes we used a paradigm based on the POM121-GFP fusion protein expressed in Hela cells. Inside fixed cells, NE invaginations were observed as discrete membrane infolds reaching from the nuclear membrane into the nucleoplasm (Figure 11).

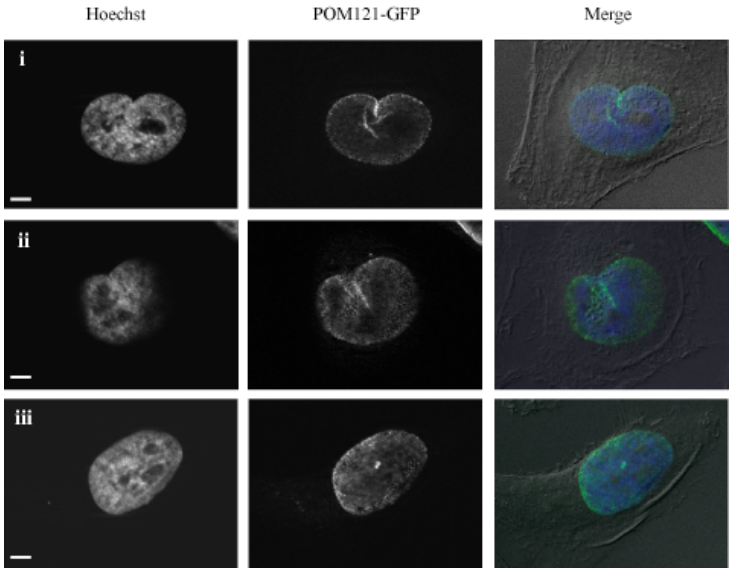

Figure 11: Nuclear invaginations visualized in fixed cells

Wide field fluorescence images of fixed HeLa cells expressing POM121-GFP co stained with Hoechst. Two different kinds of invaginations can be shown. In the first two examples (i, ii) invaginations are seen as large membrane folds and the third panel (iii) highlights an invagination seen as a spot at the nuclear envelope surface (scale bars: 5µm).

As evidenced by DNA staining (Hoechst labeling), NE-membrane invaginations were observed mostly in interphase cells, demonstrating that this phenomenon is quite distinct from mitotic invaginations, which precede the nuclear envelope breakdown (Beaudouin et al., 2002).

Depending on the serendipitous point-of-view, the green POM121-GFP channel allowed NE-membrane invaginations to be observed as distinct striations (Figure 11 (i & ii)), or isolated points (Figure 11 (iii)) that penetrated through the depth of the nucleus. Simple three-dimensional image reconstruction and iso-surface rendering emphasized how these deep membrane folds entered the nucleoplasm (Figure 12).

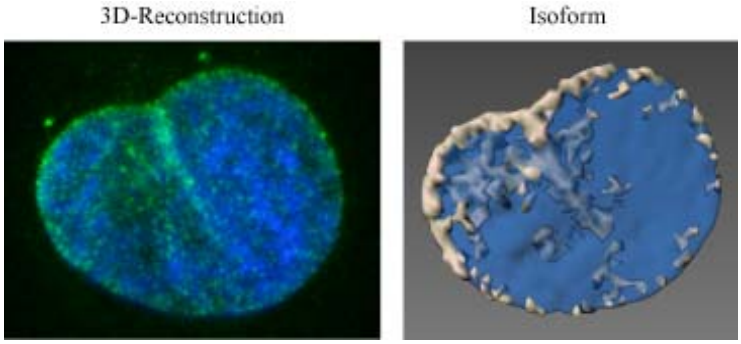

Figure 12: 3D reconstruction

The reconstruction of a stack (Figure 11 (ii)) shows the projection of the invaginating nuclear envelope membrane into the nuclear space, and (*right*) its iso-surface rendering. Note how in the iso-surface rendering the invagination penetrates deep into the interior of the nucleus.

We made similar observations in a variety of distinct cell types (including NIH-3T3, BHK1, HEK293, HeLa cells) consistent with the view that the phenomenon is a common feature of interphase nuclei (Clubb and Locke, 1998; Collings et al., 2000; Fricker et al., 1997). Next, we proceeded to visualize the dynamics of NE-membrane structural plasticity using living Hela cells expressing POM121-GFP, and detected continuous NE-membrane "ruffling". We also observed rotational nuclear movements as previously described (Bard et al., 1985; Paddock and Albrecht-Buehler, 1986), but this global movement of the entire nucleus was distinct and different to the micron-domain movements associated with NE-membrane ruffling. In addition, a second major dynamic activity, albeit more rare than NE-membrane ruffling, was the *de novo* formation of NE-membrane invaginations. Sometimes, NE-invaginations were highly transient and disappeared within minutes (Figure 13).

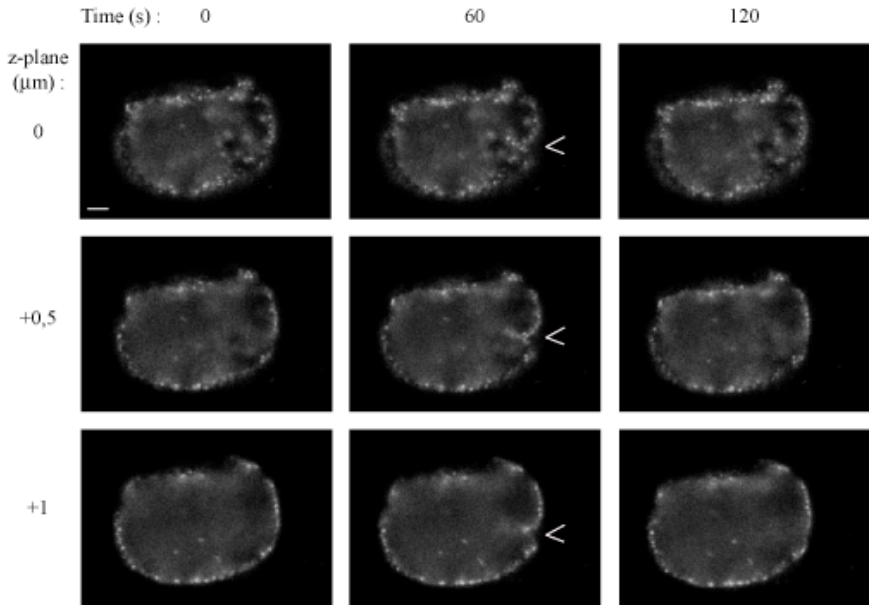

Figure 13: Highly dynamic nuclear invagination

Four-dimensional time-lapse recording showing a transient nuclear invagination inside a living HeLa cell expressing POM121-GFP. The nucleus was "through-focus" imaged (one z-stack every 60 seconds) yielding a z-stack image series over time during 20 minutes. The images are selected from three different focal planes, at comparable time-points during which a transient invagination appears during only 1 minute (arrow) and then disappears (scale bar: 5µm).

Evidently, these types of highly localized structural dynamic resembled directed movements that should most likely be driven by a cellular force-generating machinery. In this context, previous studies in fixed cells have reported NE-membrane invaginations to be filled with the candidate force-generating polymer: F-actin (Clubb and Locke, 1996; Johnson et al., 2003), prompting us to next investigate the effects of drugs known to modulate the dynamic equilibrium for actin polymerization inside living cells.

We treated HeLa cells expressing POM121-GFP with drugs that increased (Cytochalasin D (CD), and Lantruculin A (LatA)), or decreased (Jasplakinolide (Jaspl)) polymeric actin turnover. Cells were then fixed, and we measured the percentage of cell nuclei containing invaginations. With this approach, ~20% of cells possessed an increased occurrence of invaginated nuclei (arbitrary more than two) following either no-treatment (control) or vehicle (DMSO) treatment. By contrast, the percentage of cells displaying nuclear invaginations was highly increased following treatment with either CD, or LatA (~66% and 87% respectively). Treatment with the

F-actin stabilizing drug Jaspl, led only to a doubled value of cells displaying NE-membrane invaginations compared to the controls (~41%) (Figure 14).

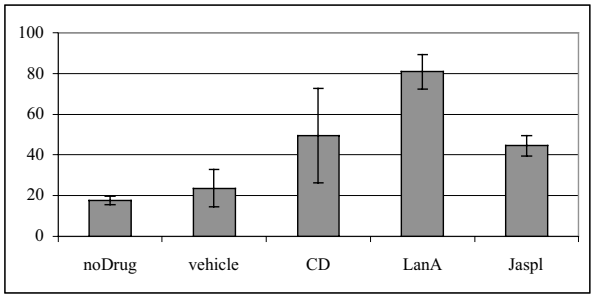

Figure 14: "Invaginated phenotype" after treatment with actin drugs in living cells

Hela cells expressing POM121-GFP were treated with the cytoskeleton interfering drugs CD (1µM), LatA (1µM) and Jaspl (200nM) (additionally vehicle (DMSO) treatment) fixed and co-stained with Hoechst 33342. In two independent experiments the phenotypes normal/round and invaginated were counted with n≥200 nuclei per experimental setup.

Taken together, the effect of CD, LatA, and Jaspl on the structure of NE-membranes, suggests a role for actin polymerization in the formation and/or stability of NE-membrane invaginations. However, it was surprising to find that both increased and decreased polymeric actin turnover yielded an increase in the number of cells displaying invaginations. This suggested a more complex relationship between actin polymerization and NE-membrane invaginations. Accordingly, to gain insight on this paradox, we next designed a method to investigate directly the polymerization state of actin in close vicinity to NE-membranes.

3.1.3 A novel method to probe for actin polymerization *in situ*

To date, there are only a limited number of probes and methods available to detect actin inside intact living cells, and none of them specifically target the visualization of actin polymerization *per se.* We therefore sought to develop a method allowing actin polymerization to be detected directly inside intact living cells, with the specific aim of revealing its association with NE-membranes. We achieved this using a fluorescent derivative of CD (CD-BODIPY). Inasmuch as CD binds specifically to free-barbed-ends of growing actin filaments, we reasoned that CD-BODIPY fluorescence should accumulate preferentially at sites of actin polymerization. To qualify, this approach

we first established the utility of CD-BODIPY as a fluorescent marker for actin. We assayed CD-BODIPY fluorescence in solutions containing fully polymerized rabbit skeletal muscle actin at 10 µM. This is a concentration far beyond the critical concentration for polymerization (Bonder et al., 1983) where ~100% of available actin is in the polymeric form (Carlier et al., 1986; Coue et al., 1987). Under these conditions, a concentration dependent, sigmoidal increase in CD-BODIPY fluorescence was observed. Similarly, addition of CD-BODIPY to cells that had been fixed and permeabilized also resulted in a sigmoidal binding curve (Figure 15 (A)). Together this suggests that the drug binds to a saturable actin-binding site in the absence of dynamic actin filament turnover. To verify these results we used a second *in vitro* assay based upon LatA. LatA specifically binds G-actin (1:1) (Spector et al., 1989), but not F-actin and the resulting net reduction in available monomers shifts the steady-state equilibrium towards depolymerization (Coue et al., 1987; Spector et al., 1989). The presence of LatA in polymerized actin solutions caused a net reduction in CD-BODIPY fluorescence (Figure 15 (B)). The effect was linear at drug concentrations between 1-10µM, and half-maximal at ~5µM, reflecting the stoichiometry expected, and strongly suggesting that CD-BODIPY fluorescence was directly dependent on binding free-barbed-end actin protomers.

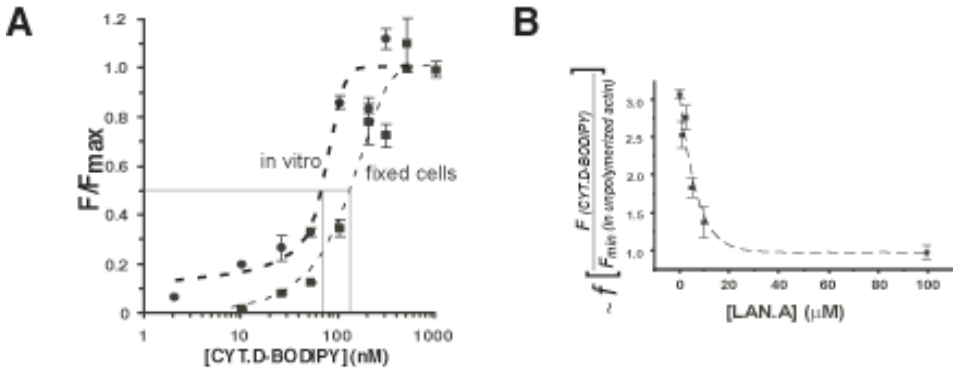

Figure 15: CD-BODIPY binds free-barbed-end actin protomers *in vitro*

Panel A: Concentration dependence of CD-BODIPY fluorescence in polymerized actin solutions (*heavy dashed line, filled circles*). The drug's dose dependent fluorescence in fixed cells (HEK293) is also shown (*fine dashed line, filled squares*). All data are normalized to fluorescence maxima at 1µM CD-BODIPY. Panel B: Measurement of the concentration dependent effect of LatA on polymerized actin using CD-BODIPY fluorescence. Data points are normalized to the fluorescence measured in

unpolymerized samples containing 10μM (ATP actin). Note that CD-BODIPY fluorescence in the presence of polymerized actin is three-fold higher than that measured in unpolymerized actin solutions.

The concentration of free-barbed-end actin protomers is expected to be a non-linear function of the total actin concentration and the steady state equilibrium for polymerization (Korn, 1982; Pollard and Cooper, 1986). In a pure solution of actin around the critical concentration, the majority of polymeric structures comprises short filaments and di/tri-meric complexes to which CD can bind. Conversely, actin concentrations superior to the critical concentration yield a diminution of these binding sites due to a predominance of long filaments. Based on these properties, we tested the ability of CD-BODIPY to report more subtle changes in the actin polymerization state using different concentrations of actin. Accordingly, CD-BODIPY (50nM) fluorescence peaked in pure solutions of actin at ~1.1μM. This approaches the critical concentration of actin polymerization expected for a reaction under similar conditions (Carlier et al., 1986). Furthermore, relative to the total amount of actin present, the CD-BODIPY fluorescence was diminished at levels at and above the critical concentration. Yet, the signal was high at levels below the critical concentration. This strongly suggests that CD-BODIPY fluorescence intensity was favored under conditions where the availability of free barbed-end protomers characteristic of polymerizing filaments was high, and not when stable polymerized F-actin filaments dominated (data not shown).

Our *in vitro* results indicate that CD-BODIPY shows similar affinity for the free-barbed-end of actin filaments, analogous to CD. In addition, and also analogous to CD, CD-BODIPY is hydrophobic, allowing it to permeate cell membranes to give a facile labeling of intact living cells. Living cells, exposed to low concentrations (1-20nM) of CD-BODIPY revealed patterns consistent with the fluorescent drug's ability to label polymerizing actin structures. In particular, we observed localization in the peripheral lamellipodia of motile cells, which is a well characterized actin-polymerization-dependent motile structure. More remarkably, CD-BODIPY labeling also showed a common fluorescence pattern comprising strong fluorescence concentrated in the nuclear region of the cytoplasm. A variety of different cell types was examined this way (including the cell lines NIH-3T3, BHK1, HEK293, HeLa cells, and human glioblastoma cells U87 and U373), and all showed this particularly pattern of CD-BODIPY labeling localized to cell nuclei (see Figure 37 in annex).

3.1.4 Polymerizing actin at the nuclear envelope *in vivo*

To examine more closely the relationship between CD-BODIPY labeling in the vicinity of cell nuclei, and specifically at the NE-membrane, we again used a co-visualization strategy in cells expressing POM121-GFP. In this approach, it was necessary to use a high-speed spinning-disk confocal imaging microscope (equipped for z-stack axial sampling of the entire cell volume), followed by image processing and geometric light reconstruction (*deconvolution*) in order to maximize three-dimensional spatial resolution, whilst minimizing out-of-focus light contamination. Intact living cells expressing POM121-GFP showed a characteristic signal distribution, comprising punctuate densities (reflecting NPC's) that demarcated precisely the NE-membrane. On the other hand, the CD-BODIPY staining appeared mostly to spread in a "patchy" pattern throughout the cell cytoplasm, but highly concentrated in a polarized region in the perinuclear cytoplasm. Most striking, a sub-cellular pool of CD-BODIPY labeling was clearly cumulated in a ring around the nucleus, co-localized with POM121 (Figure 16).

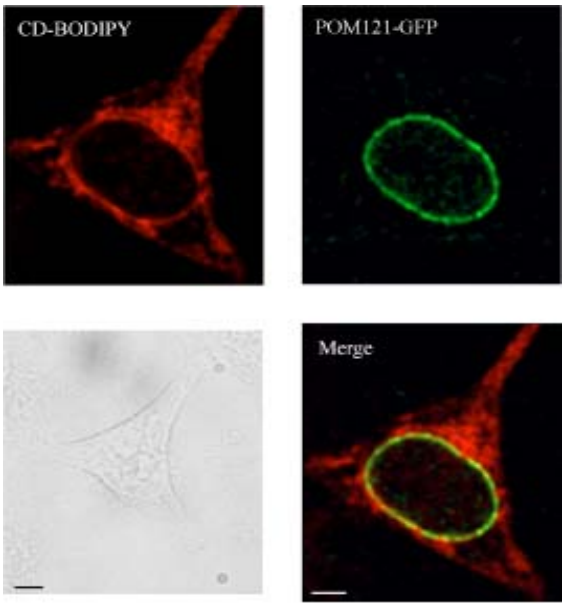

Figure 16: Co-localization of CD-BODIPY at the nuclear envelope of living cells

The panel shows one confocal section through a HeLa cell transiently expressing POM121-GFP (*green*), and stained with 50nM CD-BODIPY (*red*). Note the strong "ring" of CD-BODIPY in the region of the NE. In addition, a bright field image of the same cell is shown, and a corresponding red-green merged image confirms the spatial correlation between the NE and the ring of CD-BODIPY staining (scale bars: 5µm).

Taking full advantage of the low signal-to-noise and enhanced quality of the deconvolved confocal imaging method, we measured the extent of co-localization between CD-BODIPY and POM121 in each planar slice from the z-stack image series. These results were then analyzed as pixel intensity correlation histograms, revealing co-localization at the NE above background threshold levels for the entire stack (Figure 17).

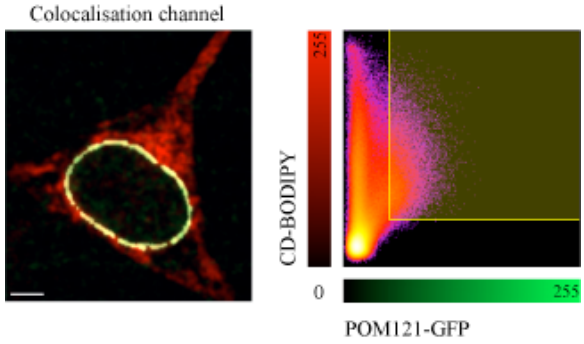

Figure 17: Co-localization analysis

The panel shows the same field as shown in Figure 16, except co-localization is represented by opaque yellow pixels based on image thresholds indicated by the yellow cut-off line (right) in the scatter gram of specific pixel intensity correlation (scale bar: 5µm).

These results suggested that NE-membranes were lined with free-barbed-end (i.e. polymerizing) actin. However, due to the unavoidable uncertainty associated with semi-quantitative analysis of fluorescence co-localization in such a small cellular sub-compartment, we sought an additional control. Again capitalizing on our confocal/ deconvolution methodology, we chose to use an approach based upon comparison with single-cell microinjection of fluorescent actin, and fluorescent dextrans. We reasoned that a high-turnover pool of actin polymerization in the vicinity of the NE-membrane should recruit microinjected fluorescent actin conjugates. This would rapidly become visible due to polymerization-dependent accumulation into this highly concentrated sub cellular compartment. We tested this, by designing a series of experiments based on single-cell microinjection of rhodamine-labeled actin into cells expressing POM121-GFP. As a systematic control we used cytoplasmic microinjection of rhodamine-labeled 70kD dextran, expected to yield a bulk cytosolic fluorescent signal, which should be excluded from the cell nucleus. For all conditions, cells were visualized using high-speed, confocal sampling followed by deconvolution

and co-localization analysis. With this approach, minutes after the microinjection, fluorescent actin revealed after three-dimensional analysis of "optical slices" an accumulation of actin-fluorescence surrounding NE-membranes (Figure 18).

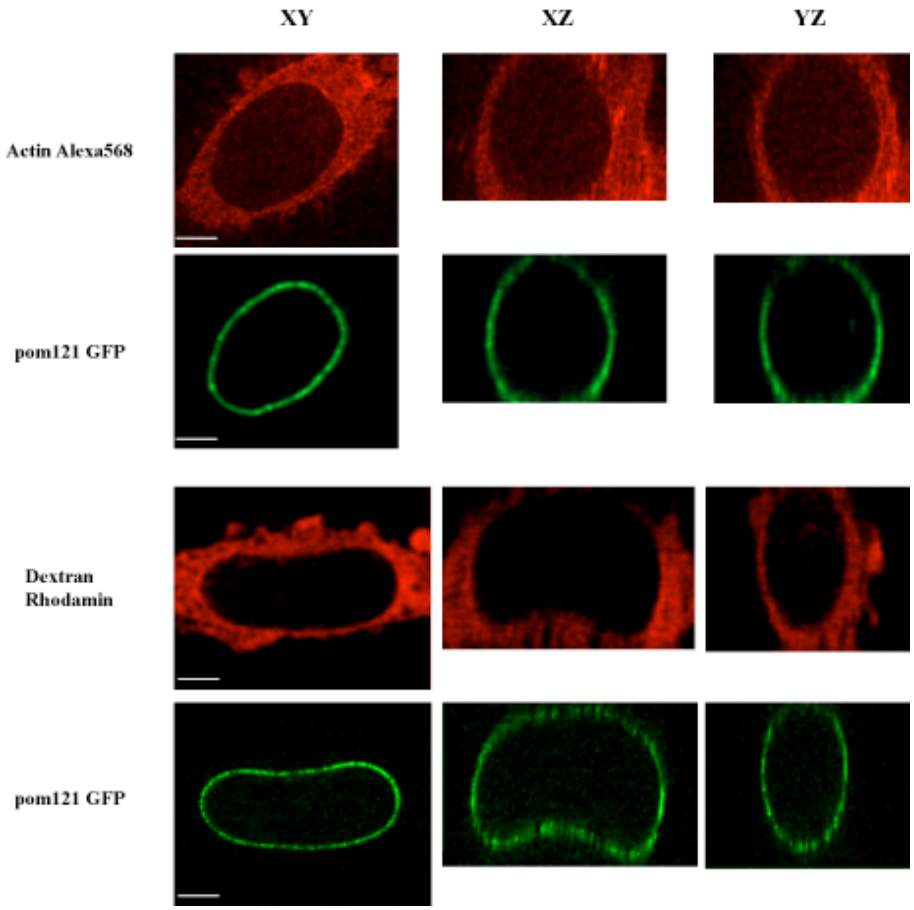

Figure 18: Co-localization of fluorescent actin and the NE inside living cells

HeLa cells transiently expressing pom121-GFP (*green*) and microinjected with either 10µM actin-Alexa568 (top rows, *red*), or 70kDa Dextran-rhodamine (bottom rows, *red*) were imaged in three-dimensions using a confocal microscope. The columns correspond to *xy*, *xz* and *yz* optical slice section views through each cell (scale bars: 5µm).

Semi-quantitative co-localization analysis (summarized in table 3) revealed that NE-membrane accumulation of both microinjected actin and CD-BODIPY was highly specific as compared with non-specific co-localization measured using microinjection of fluorescent 70kD dextran. We therefore, concluded with confidence (table 3), that NE-membranes *in situ* are abundantly decorated with actin protomers, comprising free-barbed ends characteristic of a distinct pool of high-turnover polymerizing actin.

Colocalisation	channel A (pom121 GFP)	Mean value	StDev
DextranRho inject 1	8,23		
DextranRho inject 2	22,56		
DextranRho inject 3	5,77		
DextranRho inject 4	10,99		
DextranRho inject 5	12,17	11,944	5,755
Actin568 inject 1	52,82		
Actin568 inject 2	37,32		
Actin568 inject 3	29,84		
Actin568 inject 4	38,64		
Actin568 inject 5	26,82	37,088	9,032
CD treatment 1	87,48		
CD treatment 2	63,9		
CD treatment 3	77,87		
CD treatment 4	56,64		
CD treatment 5	55,24	68,226	12,532

Table 3: Specific accumulation of polymeric actin at NE inside living cells

Three-dimensional image stacks of living cells expressing POM121-GFP and co-labeled with actin-rhodamine, dextran-rhodamine, or CD-BODIPY (exemplified in Figures 16 and 18) were analyzed for signal co-localization. Values in column two show overall percentage of POM121-GFP signal detected to be co-localized, and columns three and four show the corresponding mean and standard deviation for five cells in each condition. A *student t-test* revealed co-localization with POM121-GFP by dextran-rhodamine (control) to be significantly different from co-localization detected using either actin or CD-BODIPY labeling ($P<0.01$).

3.1.5 Actin polymerization at nuclear envelopes in vitro

Our detection of a perinuclear pool of polymerizing actin raised the question of how actin polymerization could be physically seeded from nuclear envelopes. To address this issue, we turned to the use of an in vitro assay. Crude nuclear envelopes, prepared from rat liver cells were incubated in vitro with G-actin under polymerizing conditions. Actin polymerization was quenched by fixation of the samples on a microscope cover-glass. The fixed nuclei were then double-stained using, first, monoclonal antibody mAb414 (revealing nuclear pore proteins and thereby gross NE structure) and second phalloidin (Alexa-488, revealing specifically actin filaments,

but not G-actin). We observed long, polymerized actin filaments protruding outwards from preparations of nuclei (Figure 19). Interestingly, polymerized filaments were observed at the surface of NE-membranes even at actin concentrations as low as 0.1µM, an actin concentration some ten-fold inferior to the critical concentration of polymerization. This is suggesting that NE-membranes are able to enhance polymerization by reducing the critical concentration for actin polymerization *in vitro*.

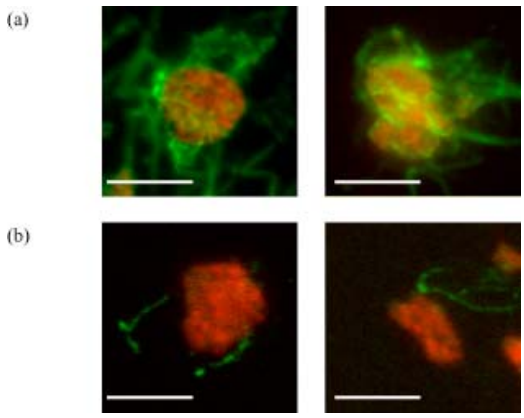

Figure 19: Isolated nuclear envelopes catalyze actin polymerization *in vitro*

The figure shows pseudo-colored images for the merged fluorescence channels of the isolated nuclei labeled with mAb414 (red) in the presence of two concentrations (1µM (a) and 0,1µM (b)) of rabbit skeletal muscle actin labeled with Phalloidin-488 (green), under polymerizing conditions. Note particularly how actin filaments radiate from nuclei in a corona and that even at 0,1µM actin concentration there are still filaments attached at the isolated nuclei (scale bars 5µm)

We next adapted our *in vitro* assay in order to distinguish the specificity of crude NE-membrane for binding with actin. To this end, actin was polymerized in suspension with isolated nuclei present, and this was followed by a low speed centrifugation sufficient to separate crude NE-membrane into the pellet, but leaving soluble G- and F- actin in the supernatant. A Western-blot analysis of supernatant and pellet fractions showed that the nuclear pellet fraction co-sediments with high levels of actin, and confirmed that actin binding to nuclear envelopes had occurred. By contrast, the same experiment performed using high-salt treated isolated envelopes (to remove surface proteins from the cytoplasmic NE-membrane surface), inhibited the binding of polymerized actin (as evidenced by its absence from the nuclear pellet fraction) (Figure 20 (a)). This is suggesting that actin binding to nuclear envelopes involved

some protein components, and not non-specific, hydrophilic binding to lipid membranes.

Following, we investigated candidate proteins possibly involved in the mechanism of actin recruitment to the NE. Based upon the in vitro biochemical assay, we tested the ability of the anti-nucleoporin mAb414 to displace actin binding to isolated NE-membranes. As a control, we used an anti-c-myc antibody and observed that mAb414 caused a strong inhibition of actin recruitment into the nuclear pellet. This is indicating that in our system actin binds specifically to the cytoplasmic face of the NE-membrane, via its interaction with one (or more) nucleoporins. Parenthetically, we also tested the effects of anti-NUANCE Ab (Zhen et al., 2002). NUANCE is a non-nucleoporin, NE-membrane localized protein that is reported to bind actin, and enhances actin-polymerization. Incubation with anti-NUANCE antibodies also caused a net reduction in the total actin signal associated with NE-envelopes, compared with control conditions, but was much less effective than mAb414 (Figure 20 (b)).

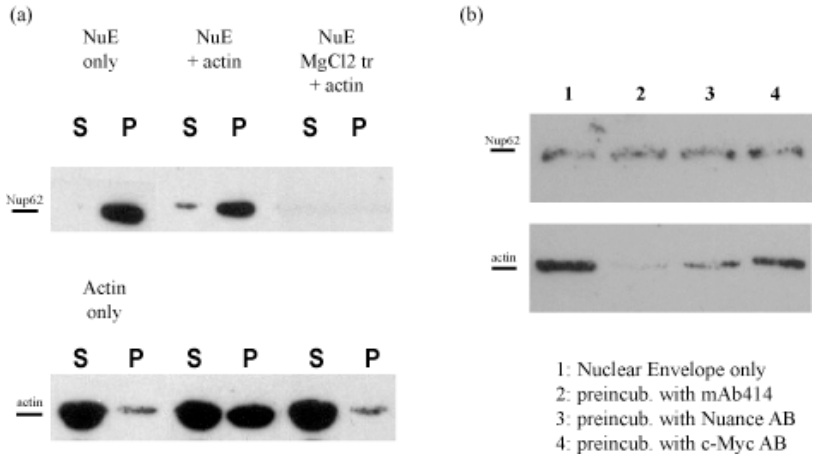

Figure 20: Western Blot analysis of NE/ actin interaction *in vitro*

Co sedimentation assay (*a*) (S: Supernatant; P: Pellet), gel-photos show Western blot analysis using either mAb414 (upper panel), or anti-actin-Ab (lower panel). The first six lanes (*a*) show corresponding analysis of S/P results from: isolated NE-membrane alone or actin alone (lower panel), envelopes plus actin, and finally envelopes pre-treated with 2M $MgCl_2$ and then exposed to polymerizing actin. (actin concentration here 4µM). In panel (*b*), pellet-fractions for the co-sedimentation assay with antibody pre-treated nuclear envelopes followed by actin polymerization (2µM actin) were shown. The upper panel shows a Western blot revealed with mAb414 and in the lower panel actin in the same sample. Note the complete displacement of actin recruitment following pre-treatment with mAb414 (*lane2*), and the diminished levels of actin binding following pre-

incubation with αNUANCE mAb, compared with the lack of effect following pre-treatment with *c-myc* antibodies

Taken together the results from our in vitro analysis suggest strongly that some direct interaction occurs between actin and nuclear protein component(s) present on the cytoplasmic face of intact NE-membranes.

3.1.6 Polymerizing actin is integral to NE-membrane invaginations

Microinjected fluorescent actin was sometimes observed to accumulate at the "mouth" of NE-invaginations, but was difficult to detect deeper inside NE-membrane invaginations (Figure 21).

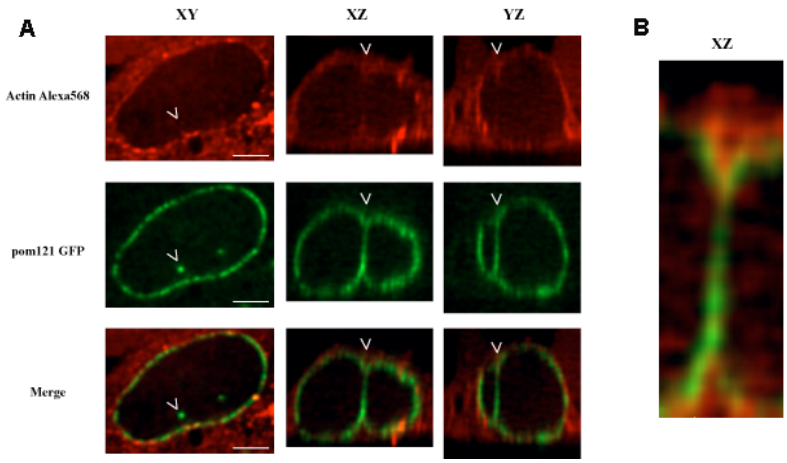

Figure 21: NE-membrane invaginations in actin microinjected living cells

Panel A: Shows an example of a HeLa cell transiently expressing pom121-GFP (*green*) that was microinjected with 10µM actin-Alexa568 (*red,* top row), and imaged in three-dimensions using confocal microscopy. The columns correspond to *xy*, *xz* and *yz* optical slice section views through the cell for each channel, and the red-green channel merge (third row). Note that in the *x,y* a single point (*white cursor in merged image*) is observed, but in *x,z y,z* sections this same structure is seen as a long fine channel crossing the whole nucleoplasm (*white cursors*) (scale bars 5µM). **Panel B:** Three-dimensional rendering showing *x,z* projection of detail around the NE-membrane invagination (left). Note the accumulation of *red*-fluorescent actin in the mouth of the NE-membrane invagination.

By contrast, CD-BODIPY labeling reached much higher levels, and revealed more clearly that actin polymerization extends deep into the cytoplasmic confines of the fine tubular membrane infolds. We took advantage of this fact, in order to co-

visualize the underlying chromatin in the nuclear matrix, revealing a close association of chromatin to actin filled invaginations. Moreover, combining CD-BODIPY, Hoechst and POM121-GFP, NE-membrane invaginations were observed as an exquisitely organized compartment comprising a fine tube of NE-membrane, around which chromatin in the nuclear matrix was aligned, and through which cytoplasmic polymerizing actin permeated the core. Combined with our results showing that cytoskeletal actin binds directly to NE-membranes and actin's localization to NE invaginations fits well with the idea that actin polymerization is the driving force for the formation of invaginations (Figure 22).

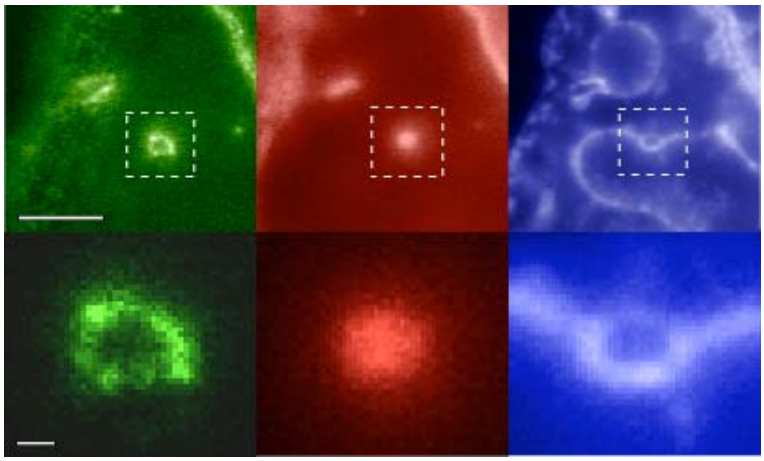

Figure 22: Cytoplasmic actin polymerization extends into nuclear invaginations surrounded by NPC's and chromatin

The panel shows images of a BHK1 cell stably expressing POM121-GFP (*green*), and delineating the opening of a nuclear invagination observed from above as a ring pattern. The cell was co-labeled with CD-BODIPY (*red*) and HOECHST (*blue*) (scale bar: 5µm). The second row of images are enlarged from the boxes (*dotted line*) indicated in the top row, highlighting one of the invaginating structures. Note how the actin polymerization is clearly delineated to be inside the ring of POM121-GFP labeled nuclear membrane, and that chromatin labeling reflects this organization (scale bar: 1µm).

These results provide a new basis for the understanding of the dynamic relationship between cytoskeletal actin and nuclear envelope structure. Primarily, they demonstrate how a highly localized sub-cellular pool of polymerizing actin is directly recruited by NE-membranes *in situ*. Furthermore, these data strongly suggest that

high-turnover actin, surrounding the NE-membrane, is involved in the formation of NE-membrane invaginations.

Due to the analogy of these NE-invaginations and those observed after Vpr expression we investigated the possibility of actin being implicated in the Vpr-induced NE deformations. Moreover, it has been shown recently that HIV exploits the cytoskeleton to reach the nucleus (McDonald et al., 2002). Given that Vpr is binding to nucleoporins, stays associated to the PIC until nuclear entry and is implicated in NE dynamics (according to our observation), suggests a scenario in which Vpr links the gap between the cytoskeleton and the NPC to support the nuclear entry.

3.1.7 Interaction of Vpr with actin

We sought to discern the capacity of Vpr to polymerize actin in a complex experiment. The intracellular pathogenic bacterium, *Listeria monocytogenes,* captures the host cell's actin polymerization machinery to assemble a comet tail of actin filaments and to push itself through the cytoplasm (Dramsi and Cossart, 1998). Only one defined part of the bacterial membrane protein, ActA, is required for the actin-based motility (Lasa et al., 1997; Pistor et al., 1995). ActA binds actin monomers, recruits the Arp 2/3 complex and stimulates actin nucleation (Welch et al., 1998). Therefore, we attempted to produce recombinant *Listeria*, in which Vpr replaces the actin polymerization domain of ActA. Subsequent to this, we wanted to investigate, whether upon infection of cells, the recombinant bacteria were still capable of inducing actin polymerization and thus being propelled through the cytoplasm. Unfortunately, we were not able to obtain the mutated strain, because the engineered bacteria were not viable. This mortality might be due to the amino acid coding, which differs substantially between Listeria and the human coding, which is used by HIV.

We decided to change the approach to *in vitro* assays. The *in vitro* polymerization of actin has been extensively studied and therefore several assays to test the impact of single proteins on actin polymerization exist. First we tested if Vpr coated beads can form actin comet tails in *Xenopus laevis* oocyte extracts when a fluorescent analog of actin (actin-rhodamine) is added in the assay. The coated beads recruited actin at their surface, yet the fluorescence was dim and no actin comet tails could be seen (data not shown).

As no clear conclusion could be reached in the bead-assay we switched to a fluorometric study. Herein, actin polymerization is followed by the change in

fluorescence intensity of a pyrenyl-labeled form of G-actin (N-(1-pyrenyl)iodoacetamide labeling). This actin analogue is excited at 365 nm and the emission can me measured at 407 nm. Upon polymerization of pyrenyl-labeled actin, the fluorescence intensity is about 25-fold enhanced, due to interactions of the stacked fluorophores (Kouyama and Mihashi, 1980). Pure actin monomers initiate new filaments with very low efficiency because formation of dimers and trimers is highly unfavorable compared with polymer elongation (Pollard and Cooper, 1986). Thus, cells use other factors to initiate filaments. The Arp2/3 complex, an abundant assembly of seven subunits (Machesky et al., 1994), is one such factor. As positive control we utilized the Wiskott-Aldrich syndrome protein (WASP), a key regulator of cytoskeletal reorganization, and added the necessary nucleation factor Arp2/3 in the corresponding experiment. In Figure 23, the characteristic actin polymerization curve for WASP/ Arp2/3 (in green) at an actin concentration of 2µM is shown. The same diagram shows Vpr (in blue and black; with or without Arp2/3 complex respectively), the Arp2/3 complex alone (in orange) and actin without any additional proteins (in red).

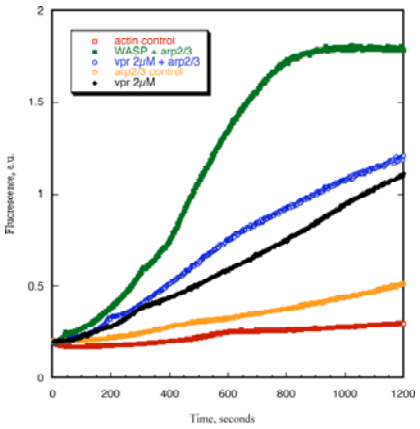

Figure 23: In vitro actin polymerization visualized in a pyrene-actin assay

Actin polymerization was visualized by the change in fluorescence emission of pyrene-actin. The green curve represents the actin polymerization for the strong activator couple WASP/ Apr2/3 complex. The effect of Vpr with or without the Arp2/3 complex is plotted in blue and black respectively. In red and orange we plotted the controls for actin alone and actin together with the Arp2/3 complex. Vpr revealed an effect on the elongation of actin filaments. However, Vpr could not reduce the lag phase of actin polymerization.

In parallel, we polymerized actin filaments in the presence of the proteins stated above. After polymerization was completed, the filaments were visualized following phalloidin-rhodamine staining under a fluorescence microscope. Both experiments pointed towards an elongation effect of Vpr on actin. Yet, in both assay we used a chemically synthesized protein of Vpr. Performing the control experiment it turned out that the elongation effect was due to a byproduct of peptide syntheses: trifluoroacetic acid (TFA). Normally the quantity of TFA present should not harm any experimental setup, but actin polymerization is extremely sensible to pH changes. As TFA is a very strong acid even traces are enough to change the actin polymerization behavior. Therefore we could reproduce the plotted effect for Vpr upon addition of equivalent amounts of TFA to 2µM actin in the pyrenyl-actin assay (data not shown). Having only the chemically synthesized protein at our disposal to perform *in vitro* assays we preferred to concentrate on the *in vivo* experiments (described in 3.1.2).

3.2.8 Visualization of viral Vpr-GFP particles

To study viral dynamics *in vivo* and to investigate the interaction of viral particles with polymerizing actin inside living cells, we developed a novel assay system. The imaging based strategy allows visualization of early and late events of the postinfection, preintegration episode of the HIV life cycle. For this purpose HeLa cells, expressing the laminA protein fused to DsRed, were infected with viral particles labeled with GFP (obtained from A. Boese; see annex). We followed these particles in live cell experiments on a high-speed image acquisition, fluorescence microscope (Figure 24 (A)). After the image acquisition, the particles were tracked using dedicated software (developed by A. Genovesio). The algorithm of the tracking program allows to follow *in vivo* single viral particles in three-dimensions. Figure 24 (A) shows an example, where a viral particle (green spot) was tracked. The particle was moving in a very directed manner towards the nuclear membrane and disappeared once it reached in close vicinity the nuclear envelope. The second part of the figure (Figure 24 (B)) shows a deconvolved and reconstructed stack where several trajectories of the GFP-labeled particles were traced.

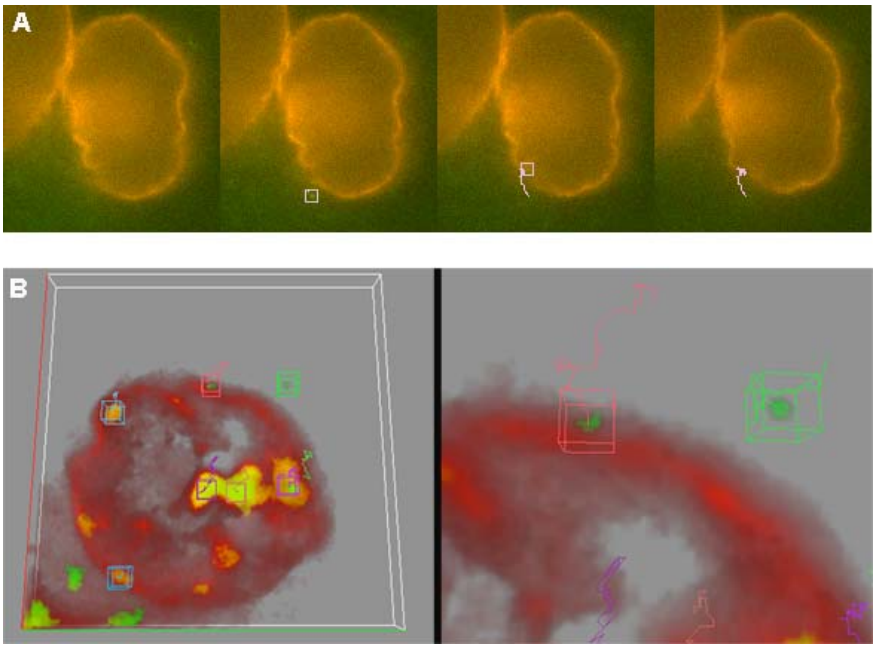

Figure 24: Tracking of viral particle inside a living cell

HeLa cells expressing the laminA protein in DsRed were infected with fluorescent (GFP-lacI-Vpr) viral particles. Immediately after infection 4D image acquisition was started and the movement of the GFP labeled particles was followed. After the experiment the data were deconvolved and a single particle-tracking algorithm was applied on the image series. In (A) we could track one bright spot on its very directed way in the cytoplasm towards the nucleus (directly on the microscope images). (B) The left part shows the trajectories of several viral particles after deconvolution and reconstruction of the analyzed stack. (B; right) shows a blow-up of the upper two particles close to the nuclear membrane with the traced trajectories in red and green respectively.

These results are very promising and indicate, that the developed experimental setup allows the *in vivo* tracking of viral particles. The aim of the project is now to get more insight into the routing of the PIC through the cytoplasm and the entry into the nucleus in the presence and absence of Vpr.

3.2 Part II: PNAs as candidates for novel antiviral therapies

To test the capacity of PNAs for their antiviral potential, we used two different systems. On one hand, we wanted to inhibit the replication of HIV. In a second approach (in collaboration with the laboratory of D. Gonzalez-Dunia at the Pasteur Institut) we sought to block the viral spread of borna disease virus (BDV). BDV, the etiological agent of Borna disease, is a nonsegmented negative-strand RNA virus (de la Torre, 1994; Schneemann et al., 1995) that has the unique property, among members of the order *Mononegavirales*, of transcribing and replicating its genome in the nucleus (Cubitt and de la Torre, 1994). The virus causes neurological disorder of farm animals (Ludwig et al., 1988) and there is considerable evidence that BDV also infects humans (Carbone et al., 2001; De La Torre et al., 1996) however this remains controversial.

3.2.1 Selection of target sequences for antiviral PNAs

For the definition of PNA target sequences in the HIV genome, databases (EMBL and SWISSprot available at: http://genome.dkfz-heidelberg.de/menu/biounit/) were searched for sequences highly conserved in different HIV clades. Amongst the identified sequences, we selected the ones playing an important role in different steps of the HIV replicative cycle.

The central polypurine tract (cPPT) is an essential element of reverse transcription, as it is an initiation site of second-strand DNA synthesis (Charneau and Clavel, 1991). We selected three PNAs to target this region. Another target sequence is located in the central DNA flap, a 99-nucleotide long strand overlap, which is known to be involved in the nuclear import of the viral pre-integration complex (PIC) (Zennou et al., 2000). Finally, we choose a sequence upstream of the cPPT on the DNA (+) strand to inhibit synthesis of the central DNA flap during reverse transcription.

For the inhibition of late steps in the viral life cycle another set of PNAs was synthesized, targeting Nef and NCp7 as well as one PNA directed against the start of

the Gag mRNA. The sequences were chosen, because Nef is required for high viral loads in the infected host and thus for disease progression (Renkema and Saksela, 2000). NCp7 is involved in the packing of viral RNA into the virion and the budding at the plasma membrane (Berkowitz et al., 1995; Muriaux et al., 1996). Also, mutation within the NCp7 proximal zinc finger in the HIV-1 genome is leading to a lower infectivity of the viral offspring (Ramboarina et al., 1999). Additionally, the PNAs directed against the cPPT and the central DNA flap were synthesized both in sense and antisense orientation and may therefore target the viral genome during the early as well as the late replicative cycle. The PNA sequences were synthesized according to the HIV-1 LAI isolate, a commonly used laboratory strain.

The borna disease virus (BDV) sequences were selected on the coding region of the viral glycoprotein (GP) mRNA. Sensitivity to detergents and organic solvents indicate that BDV is an enveloped virus, a suggestion also supported by electron microscopy data of cell-released BDV infectious particles (Gonzalez-Dunia et al., 1997; Kohno et al., 1999; Zimmermann et al., 1994). Viral glycoproteins (GPs) present at the surfaces of enveloped viruses mediate virus attachment to cell surface receptors, serving as primary determinants of viral tropism and facilitating penetration by triggering fusion of the viral envelope with cell membranes. The PNA sequences were chosen according to the BDV laboratory strain He/80.

As negative control, a random sequence was selected which has been verified to neither match the HIV-1, BDV nor the human genome (Table 4).

Denotation:	Target:	Polarization:	Sequence:
PNA I	cPPT	DNA (+) or RNA	N-term CAA TCC CCC CTT TTC TTT C-term
PNA II	cPPT	DNA (-)	N-term GTA TTC ATC CAC AAT TTT C-term
PNA II long	cPPT	DNA (-)	N-term GCA GTA TTC ATC CAC AAT TTT C-term
PNA III	cPPT	DNA (+)	N-term AAA TTG TGG ATG AAT ACT C-term
PNA III long	cPPT	DNA (+)	N-term AAA ATT GTG GAT GAA TAC TGC C-term
PNA IVa	DNA flap	DNA (-)	N-term TAG TAG ACA TAA TAG CAA C-term
PNA IVb	DNA flap	DNA (+)	N-term TCC CCT GCA CTG TAC CCC C-term
PNA Va	Nef	DNA (-)	N-term AGA TCT TAG CCA CTT TTT C-term
PNA Va long	Nef	DNA (-)	N-term TGT AGA TCT TAG CCA CTT TTT C-term
PNA Vb	Nef	DNA (-)	N-term GGC TAA TTC ACT CCC AAC C-term
PNA Vc	Nef	DNA (-)	N-term TAG AGA TTT TCC ACA CTG C-term
PNA VI	start of gag	mRNA	N-term cac cca tct ctc tcc ttc C-term

PNA VIIa	NCp7	DNA (-)	N-term ATT ACT ACG TCT CTC CGT C-term
PNA VIIb	NCp7	DNA (-)	N-term TAT CGG TTT TTA ACG TCC C-term
PNA	Random		N-term CAT ACT TGA CTC GTT ATC C-term
PNA-G I	G protein	RNA	N term-GCA TTG CCA GAC TAC CCC C-term
PNA-G II	G protein	RNA	N term-TCC CTA CGC CGC CTT CTC C-term

Table 4: Sequences of the designed and synthesized PNAs

The table shows a list of the 14 PNAs (I-VII), used for either antigene or antisense therapy against HIV, with the corresponding target in the HIV-1 genome, their polarization and nucleotide sequences. Also listed is the sequence of the Random PNA as well as two PNAs targeting the mRNA of the BDV glycoprotein (GP).

3.2.2 PNA synthesis and quality control

All PNAs were synthesized based on the Fmoc chemistry. They were individually coupled to cellular targeting sequences. PNAs intended to bind to the DNA (-) strand, in the case of HIV, were synthesized directly with a NLS [SV40-T] sequence that ensures an efficient nuclear import. The same holds true for the BDV molecules, because the virus is transcribed and replicated in the nucleus. Cellular import of all hybrid molecules was achieved by coupling to a cell-penetrating peptide (CCP), the transport peptide of the Antennapedia homeoprotein in *Drosophila* (pAntp) (see chapter 1.2.3) that was synthesized in parallel and coupled via a cleavable disulfide bond to the purified PNAs. To be specific, antisense molecules need to be at least 15 nucleotides long. However, due to poor synthesis efficiency, the length of PNAs is still limited. After optimization of our protocol we could ensure the syntheses of 18mer PNAs with a good yield. As the monomer coupling was directly monitored during synthesis, we could even achieve some PNAs with a good yield up to 21 nucleotides (Table 3). Thereafter, the molecules were purified on an analytical HPLC followed by laser desorption mass spectrometry to ensure purity of the final product (data not shown).

3.2.3 PNAs targeting the early replicative cycle of HIV

To investigate effects of PNAs on the early viral life cycle, we used the Hela P4 CD4+/CCR5 (HP4) cell line. This derivative of the HeLa cell line stably expresses the CD4 and CCR5 proteins crucial for HIV entry into the cell. Furthermore, they carry

the bacterial lacZ gene under the control of the HIV-1 promotor (LTR) (Charneau et al., 1994). The LacZ gene encodes an enzyme (β-galactosidase) that can produce a variety of colored or fluorescent compounds from appropriate substrates. The HP4 cells display low basal β-galactosidase expression, which is dramatically induced by the HIV-1 transactivator Tat. In this system, the β-galactosidase activity measured using a chemiluminescent assay is proportional to the amount of Tat protein produced by the integrated provirus. Accordingly, this assay is a readout of the efficiency of provirus establishment. If PNAs are able to inhibit early steps of viral replication, less integration events are expected and thus a lower level of ß-galactosidase activity in PNA treated cells compared to control or vehicle treatment (HIV-1 only or Random PNA treatment).

In the first set of experiments, PNAs resuspended in PBS were applied to the cells at different concentrations ([10pM], [100pM] and [1nM]) half an hour prior to infection with HIV-1 (LAI isolate). The ß-galactosidase activity was measured 48 hours after treatment. In HP4 cells treated at a 1nM concentration of the antisense molecules, we detected a 20-30% decrease in the ß- galactosidase readout for target sequences in the cPPT (red dashed bars: PNA I Cys/NLS and PNA II Cys/NLS; Figure 25).

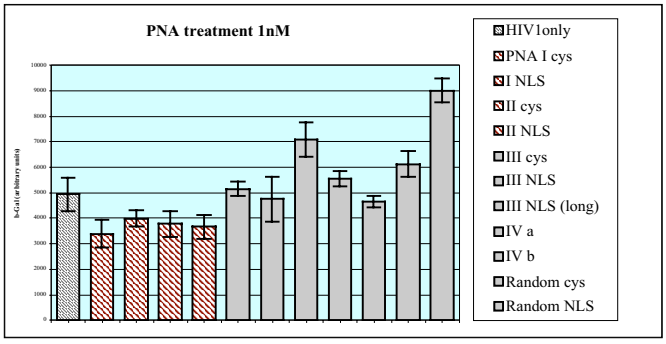

Figure 25: PNA treatment with low concentrations targeting the early HIV life cycle

The ß-Galactosidase readout of 1nM PNA treatment directed against early targets in the HIV life cycle. The experiment was done in triplicate for each data point. The ß-Gal level of cells treated with PNAs targeting the cPPT (red dashed bars) was reduced by 20-30% compared to the control (HIV-1 only). For all other tested PNAs we could not decrease the ß-Gal level in this first experiment.

Increasing the PNA concentrations up to 100nM did not improve the inhibition of early HIV integration events detected in the first experiment (data not shown).

3.1.4 PNAs targeting the late replicative cycle of HIV

The following set of experiments intended to study inhibitory effects of the PNAs on late replicative steps. A population of persistently infected HP4 cells was selected following infection with HIV-1 LAI. These cells were treated with the 14 PNAs directed against HIV and the Random PNA at two different concentrations ([100nM] and [1µM]). After incubation for 48 hours, an aliquot of the culture supernatant was tested for the amount of released HIV virions by an HIV-1 core profile enzyme-linked immunosorbent assay (ELISA) quantifying the amount of p24 capsid protein (Figure 26).

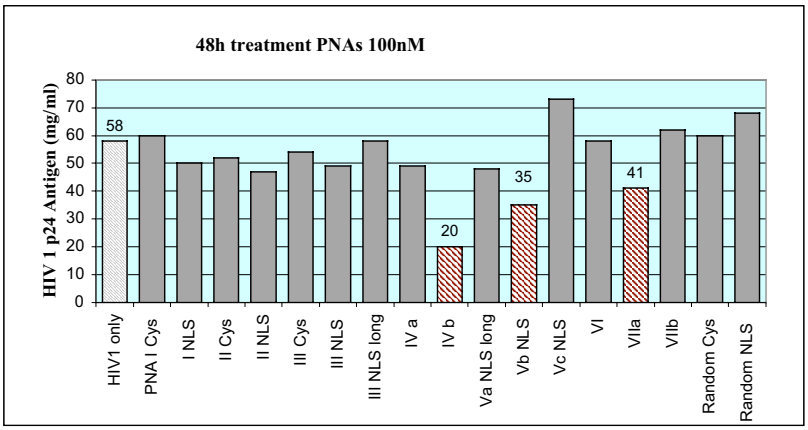

Figure 26: PNA treatment targeting late replicative cycle

Persistently (HIV-1) infected cells were treated with a PNA concentration at 100nM. After 48 hours of incubation time at 37˚C the viral offspring was detected with a p24 ELISA. Under these conditions some PNAs (IVb targeting the c-PPT, Vb targeting Nef and VIIa targeting Ncp7), inhibited to a certain amount the viral production compared to control and vehicle treatment.

In this screen, PNA IVb (targeting the central DNA flap), PNA Vb-NLS (targeting Nef) and PNA VIIa (targeting NCp7) turned out to be the most promising inhibitors of the viral production. They decreased the p24 level following treatment with a PNA-concentration of [100nM] by about 65%, 40% and 30% respectively. All other PNA sequences tested revealed a p24 level comparable to the vehicle treatment (Random PNA) (Figure 26). At higher concentrations [1µM] the overall p24 level was reduced for all PNAs. Unfortunately, this included the Random PNA treatment, which indicates an unspecific effect of the antisense molecules itself. However, again the same PNAs (IVb and Vb NLS) showed the best inhibition (data not shown).

We varied several parameters such as PNA concentration (from 100nM up to 50µM) or incubation time (24 to 144 hours) for the most promising candidates to ensure a complete tracing of the viral offspring following PNA treatment. The up-scaling of PNA concentrations lead to a dose dependant decrease of the viral production, yet again the same was true for the Random PNAs. We presumed that at some point this unspecific effect could be titrated out, but the ratio (targeted PNA/ Random PNA) remained comparable throughout all experiments. Increasing incubation time did also not result in better inhibitory effect (data not shown).

3.2.5 Infectivity test of produced viral particles

Next, we proceeded to test the infectivity of the viral offspring produced under PNA treatment. The persistently infected cells were treated twice during a three-day interval with different PNAs at high PNA concentrations (25µM and 50µM). As an additional control, we included the BDV PNA-G I to the experiment. After six days, supernatants were collected and the viral production quantified by a p24 ELISA. Subsequently, fresh HeLa P4 cells were infected with the same viral titer. As the viruses applied on the HeLa reporter cells were produced under PNA treatment, we expected a decrease of infectivity and therefore a lowering of the β-galactosidase activity in the test system (Figure 27).

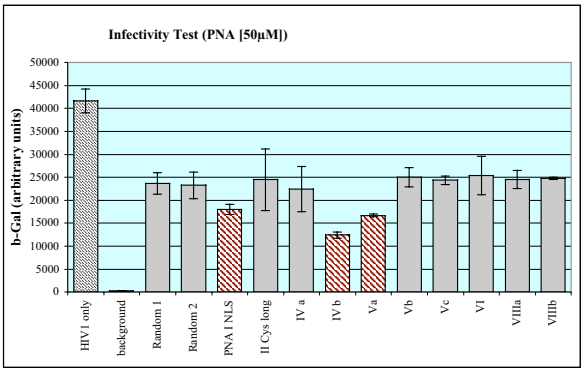

Figure 27: Infectivity test of viral particles

Under permanent PNA [50µM] treatment viral particles were produced in persistently infected HeLa P4 cells and subsequently used to infect naïve cells. This experiment aimed to test the virulence of a progeny produced under a PNA repression situation. The amount of integration events measured with the ß-Gal readout was reduced but none of the samples was completely cleared of viral particles.

Consistent with the result of earlier experiments, the PNA inhibiting the synthesis of the central DNA flap (IVb) revealed a decreased infectivity of the viral particles, produced under PNA repression, of 70% compared to the control. Also PNA I NLS (targeting the cPPT) and PNA Va (targeting Nef) treatment led to the production of viral offspring, that showed only 40% infectivity in the ß-Gal readout, compared to the controls. All other tested PNAs had no significant impact on the infectivity of virus collected from these cells.

3.1.6 PNA treatment inhibiting borna disease virus (BDV)

BDV infection is noncytolytic in all cell systems examined so far and requires cell-cell contact for its spread. Little infectious virus is released from BDV-infected cells (Carbone et al., 1993), and virus yields are very low. In addition, assembled virus is very rarely observed in infected cells and assembled viral particles have never been visualized in the brains of BDV-infected animals. BDV antigen distribution in the central nervous systems (CNS) of infected animals strongly suggests that BDV disseminates by cell-cell contact, possibly using the synaptic contacts between neurons (Gosztonyi and Ludwig, 1995). These observations, combined with the notion that ribonucleoproteins (RNP) of BDV are infectious after transfection to susceptible cells (Cubitt and de la Torre, 1994), have led to the hypothesis that dissemination of BDV in the CNS takes place as non-enveloped RNP rather than as enveloped viral particles (Gosztonyi et al., 1993). This would imply that after initial entry of BDV into its target cell, BDV glycoproteins (GPs) are dispensable for BDV dissemination.

To assess whether BDV-GP is required for neuronal dissemination of the virus, a PNA antisense approach was used. First, we analyzed whether treatment with PNAs targeted against the coding GP mRNA would lead to decreased expression levels in infected cells. In order to be able to analyze the expression levels of GP by flow cytometry, we treated Vero-BV (Vero cells persistently infected with BDV) cells with PNA constructs (BDV PNAs and Random PNA; Table 3). Due to the persistent nature of BDV infection in Vero-BV cells, the cells contained considerable levels of BDV-GP at the start of treatment. Since the half-life of BDV-GP is unknown, we chose to treat Vero-BV cells for a period of 12 days before analysis. The analysis demonstrated that upon treatment with PNA-G I, BDV-GP expression levels in Vero-

BV cells were decreased, whereas treatment with Random PNA and PNA-G II had no detectable effect (data not shown).

Next, we tested the potential of PNA treatment to inhibit BDV dissemination in acutely infected primary neurons. One day after initial infection with BDV-CRV (cell-released virus), neurons were thoroughly washed, and 1 day later, PNAs were added to the culture medium. Immunofluorescence analysis on day 10 revealed productive virus spread when cells were treated with the Random PNA, comparable to the amount of virus dissemination seen in untreated cells (Figure 28).

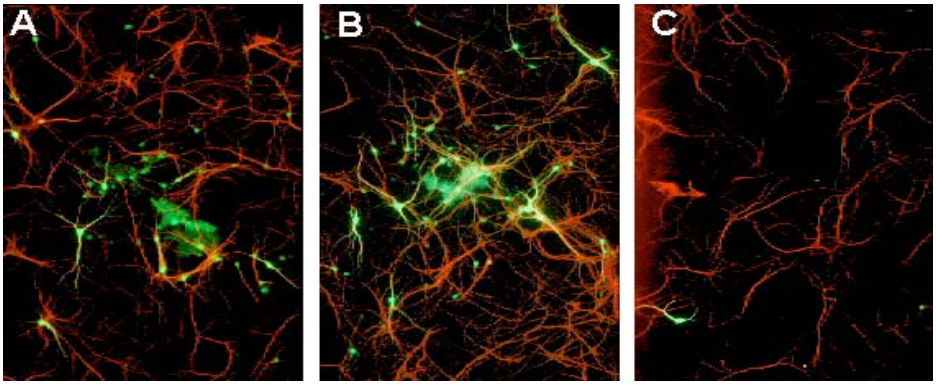

Figure 28: PNA treatment of primary hippocampal neurons following BDV infection

Primary hippocampal neurons were infected with 250 FFU (focus-forming units) of BDV-CRV/well on day 3 of culture. On day 4, the cultures were washed twice with fresh medium, after which new medium was added. On day 5 of culture, PNAs were added (A: untreated; B: Random PNA 0.5µM; C: PNA-G I 0.5µM). On day 10, samples were taken for immunofluorescence analysis and quantification. BDV-N was detected with a FITC-labeled secondary antibody and the neuronal staining was achieved with an anti-microtubule-associated protein 2 (anti-MAP-2) antibody, detected with a CY-3 secondary antibody. Original magnification x100.

In sharp contrast BDV dissemination was progressively inhibited with increasing concentrations of PNA-G I, as could also be confirmed by quantification of the BDV-N-positive neurons per well. The neurons were treated according to the same protocol as described above, immunostained, and then the number of infected neurons per well was counted on fluorescent microscopy images (as shown in Figure 28). The distribution pattern of the few BDV-positive neurons following PNA-G I treatment at [1µM] suggested that infection of these neurons was due to primary infection rather than to virus dissemination (Figure 29) (Bajramovic et al., 2003).

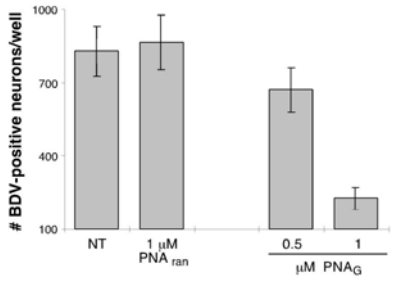

Figure 29: Quantification of inhibitory effect in infected neurons

Quantification of BDV-N-positive neurons per well on day 10 of culture. NT, not treated. Results are given for one representative experiment selected from a series of three independent experiments.

In summary we could show, that the BDV-GP is necessary for BDV dissemination in neurons. Furthermore we demonstrated that PNAs directed against the viral mRNA can efficiently inhibit viral spread in permanently infected cells as well as in primary hippocampal neurons. Given the low expression level of BDV-GP and its crucial role in viral dissemination in neurons, this protein represents an attractive target for antiviral therapy by PNA based strategies.

4. Discussion and Perspectives

My thesis work has been partitioned in two parts. Both were aiming at the understanding and inhibition of viral propagation. The first part, I will discuss, was focused on basic cellular biology to get new insights into the host-pathogen relationship. Secondly we evaluated a novel class of antiviral compounds based on PNAs.

The human immunodeficiency virus (HIV) manipulates fundamental host cell processes in sophisticated ways to achieve optimum replicative efficiency. Detailed analysis of the interplay between viral proteins and normal cellular activities has provided new insights into central questions of virology and host cell biology.
Many aspects of the HIV-1 life cycle remain largely unknown. Thus, little is understood of the events occurring immediately after entry into the cytoplasm by membrane fusion. This implies routing, decapsidation and nuclear import of the pre-integration complex (PIC). In addition to the inferred engagement of the classical nuclear import pathway (which utilizes importin-α and importin-ß), it appears that Vpr acts in a complementary fashion to augment PIC import. In particular, Vpr contains a NLS sequence and is able to interact with importin-α as well as with nucleoporins (Fouchier et al., 1998; Le Rouzic et al., 2002; Popov et al., 1998b), and may therefore serve to directly connect the PICs to the nuclear pore complex (NPC).
Upon transfection of HeLa cells with Vpr-GFP, the characteristic punctuated pattern of the NPC was stained after short expression time of the plasmid. The over expression of the viral protein induced the incidence of nuclear envelope (NE) membrane invaginations significantly. Moreover we recorded some of the invaginations being very fast, pushing into the nucleoplasm and disappearing within few minutes. These highly dynamic appearances are fairly rare, yet we also observed in all experiments enhanced membrane ruffling at the nuclear envelope (NE). Since membrane ruffling is easier to analyze than the rare but highly dynamic invaginations we are about to quantify the observation in Vpr-expressing cells compared to control conditions (see annex).
Recently, it has been shown, that Vpr can induce ruptures of the nuclear envelope that may constitute an alternative mechanism evolved by HIV to get access to the nucleus (de Noronha et al., 2001). In this context the induction of invaginations is highly intriguing, as this could precede the NE ruptures. NE invaginations have been

described before and seem to be a common feature of cell nuclei in mammalian (Beaudouin et al., 2002; Ellenberg et al., 1997), plant (Collings et al., 2000) and insect cells (Hochstrasser and Sedat, 1987). However little is known about the function and formation of NE invaginations. Therefore we investigated this common cellular phenomenon to get further insight on this possible mechanism involved in the nuclear import of HIV.

In interphase cells we observed nuclear membrane ruffling and nuclear invaginations being either stable and durable over time or in contrast highly active. Thus actin polymerization provides a good candidate for the molecular force generating mechanism that must exist to drive nuclear membrane dynamics. Due to the abundant amount of actin inside living cells we could show, only with state-of-the-art imaging techniques using spinning disc confocal acquisitions followed by deconvolution, that CD-BODIPY as well as microinjected monomeric actin is immediately localized in a fine ring around the nuclear envelope. Furthermore, actin co-localizes in a significant degree with the NE and is localized deep inside membrane invaginations. Due to CD-BODIPY labeling (respective the free-barbed-ends) the visualized actin was comprised, not from stable filaments, but rather from high-turnover polymerizing actin. These observations provide the first evidence that dynamic nuclear membrane invaginations depend on actin polymerization. This mechanism would be envisaged analogous to the established model describing plasma-membrane filopodia (microspike) formation (Mallavarapu and Mitchison, 1999; Small et al., 1978; Wang, 1985).

Filopodia are tiny extensions, protruding from the surface at the leading edge of the plasma membrane (Jacinto and Wolpert, 2001; Vacquier, 1968). They have dimensions comparable to that of the nuclear invaginations reported here. The necessary force generation for these structures comes from compartmentalized actin treadmilling (for review see (Welch and Mullins, 2002)). In this context stable NE-membrane invaginations could arise from a cascade of events beginning with enhanced actin polymerization at a highly localized site on the cytoplasmic surface of the NE-membrane (Figure 30). Qualitatively this activity results in membrane "ruffling", which manifests as a restricted and dynamic deformation of the NE. Subsequently, dynamic ruffling can propagate into a rapid (minutes) *de novo* generation of conspicuous, finger-like projections (invaginations), which either collapse in minutes, or stabilize sufficiently to last many hours.

Since many years it has been recognized that *de novo* actin polymerization happens at membrane surfaces (Tilney, 1976). In existing models it has been observed that free-barbed-ends are attached to the membranes and filament growth happens to be at the same site (Defacque et al., 2000; Mitchison and Cramer, 1996; Small et al., 1995; Tilney and Portnoy, 1989). Accepting this precedent would imply that the free-barbed-ends of polymerizing actin in NE-membrane invaginations are also oriented towards the membrane and thus at the tip of the forming structure (Figure 30).

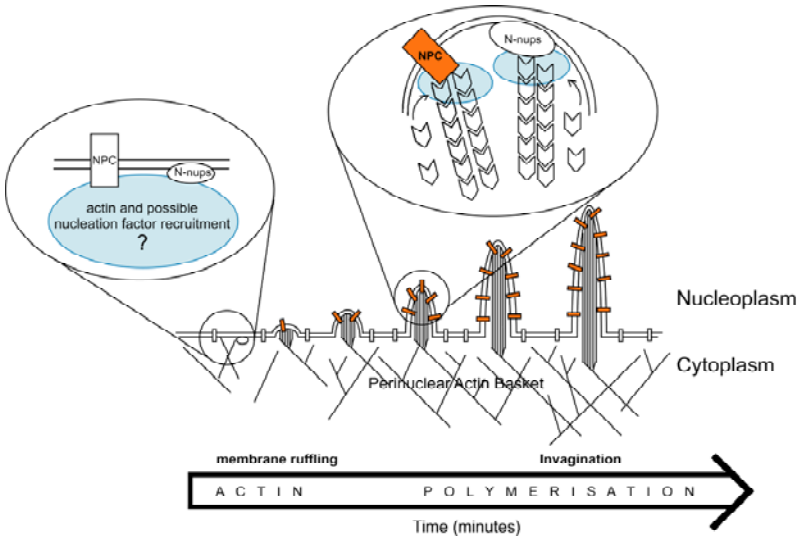

Figure 30: Scheme for *de novo* generation of nuclear membrane invaginations

Such explicit polarization requires a complexity of molecular players. In filopodia formation, the small GTPase Cdc42 is the major activator of polymerization (Ridley and Hall, 1992; Ridley et al., 1992) through numerous downstream effectors including members of the Wiskott-Aldrich syndrome protein family (WASP/N-WASP) (Symons et al., 1996), the membrane phospholipids *phosphatidylinositol 4,5 bisphosphate* (PIP_2) (Yin and Stull, 1999) and the Arp2/3 complex (Higgs and Pollard, 2000). In NE-membranes it is not yet clear whether the same molecules are involved. On this point, it is striking that Cdc42 is remarkably concentrated in a perinuclear ring pattern around the nucleus (Luna et al., 2002). Therefore this would be an interesting candidate to investigate the molecular components involved in NE dynamics.

We also found that nucleoporins, themselves are responsible for actin binding. This

could be the basis for stabilization and/ or propagation of NE-membrane invaginations. However, previous studies showed that NPC channel permeability is directly modified by the polymerization state and binding of actin (Prat and Cantiello, 1996). Moreover, knockout of a divergent actin gene (ACT2) in yeast yields defects in NPC structure and function (Yan et al., 1997). Such evidence suggests that actin binding to the NPC can result in structure/ function modulation. Actin-bound NPC's could thereby be structurally primed to answer functional requirements inside the nuclear milieu, for example, with respect to chromatin metabolism. Towards this view our visualization of chromatin deposits surrounding NE-membrane invaginations might prove to be of profound significance. Our results reveal a striking association between discrete NE-membrane invaginations and the underlying chromatin. It has been suggested that NE-membrane invaginations may play a role in the spatial organization of the NE/chromatin interface (Ellenberg et al., 1997). Furthermore this has been supported by the fact that an increased electron density similar to heterochromatin surrounds nuclear membrane invaginations (Ellenberg et al., 1997; Fricker et al., 1997) and membrane 'tracks' associated with nucleoli (Bourgeois et al., 1979; Dupuy-Coin et al., 1986). We suggest that functionally distinct NE-membrane invaginations could be encoded, in a spatially compartmentalized manner, to serve for better functions concerning the interplay of *nucleo-cytoplasmic* transport and communication.

Since actin treadmilling is involved in the shaping of the nuclear envelope this may also hold true for the Vpr-dependent invaginations. Possibly, Vpr could enhance the actin polymerization at the NE to increase the frequency of the dynamic phenomenon observed. Inducing invaginations would situate the PIC in close vicinity of a high NPC density and thus the underlying chromatin, which we have demonstrated to be associated.

We hypothesized that Vpr may interact directly with actin such as a nucleation factor. However, we could not show a direct interaction of Vpr with actin. The *in vivo* actin polymerization machinery is a very complex and equilibrated system. Therefore it might be possible that the interplay involves a third party, which has not been present in the *in vitro* experiments. We could show that the NPC is involved in actin recruitment to NE-membrane and furthermore it has been demonstrated that Vpr binds to nucleoporins. This connection might well be the key for the induction of actin polymerization. For the moment we have no evidence for this interaction being

responsible for actin polymerization initiation. However, this would be an important issue to address, in order to find new approaches to inhibit HIV infection.

Since the discovery of HIV about twenty years ago, extensive research on the viral lifecycle has transformed AIDS in a treatable yet not curable disease. Introduction of triple combination therapy, comprising protease and reverse transcriptase inhibitors, markedly reduced mortality of AIDS patients in industrialized countries. However, the virus is able to escape highly active antiretroviral therapy (HAART) due to the emergence of resistant strains (Pomerantz and Horn, 2003).

HIV infection typically results in high replication of virus with innocuous symptoms followed by a clinically latent period (which is variable depending on the infected individuals). The ability of the virus to reach and infect immunologically privileged sites such as brain and lymph nodes (Haggerty and Stevenson, 1991) complicates the treatment of HIV due to the poor accessibility of these compartments for drugs (Thomas, 2004). Latently infected resting $CD4^+$ T lymphocytes can survive for many years and cause re-emergence of virus after withdrawal of HAART (Finzi et al., 1997; Wong et al., 1997). These sanctuaries constitute a major obstacle for virus eradication in infected individuals, because currently used drugs can only fight HIV while the virus is replicating. The frequent occurrence of adverse effects and metabolic complication directly related to therapy as well as the high economic costs of HAART call for further development of HIV therapies. Therefore a PNA based antisense strategy could be a complement for currently available drugs. PNAs can target early and late replicative steps, thus block *de novo* infection and viral spread.

We designed a series of PNAs against HIV with a broad spectrum of target sequences. The length, although challenging for PNA syntheses, is important for the specificity of antisense molecules. Specific binding is achieved with 14-15mer PNAs however for strong inhibition longer PNAs are favorable (Doyle et al., 2001). Optimization of the chemical synthesis allowed us to obtain 18 to 21mer PNAs. Furthermore the efficient cellular and nuclear import of our PNA constructs, due to the attached pAntp peptide and a NLS sequence, has been verified recently (Braun et al., 2002).

The experimental settings to evaluate the virtue of the PNAs were chosen in order to be able to distinguish between effects on early and late replicative cycle. We tested

the PNA treatment upon acute HIV infection as well as on persistently infected cells. Experiments on the persistently infected cells put forth some PNAs with inhibitory potential. At a concentration of 100nM PNAs targeting the central DNA flap, Nef and NCp7 caused an up to 3-fold reduction of the viral load in the cell culture supernatants. We also applied a cocktail of the three PNAs stated above to see if a concerted action of the most promising PNAs resulted in a better inhibition. Yet the effect was not significantly improved (data not shown). Following, we increased the PNA concentrations (up to 50µM), what conducted to further lowered levels of detected p24 antigen. Yet beside this dose response relationship, we noted an unspecific effect of the random PNAs upon up scaling of the concentrations above 1µM. The ratio of specific effect versus unspecific random PNA effect stayed the same with increasing concentrations. Thus the inhibition of the antisense molecules was significantly narrowed in comparison to the random PNAs.

The best effects could be achieved while testing the infectivity of viral particles produced under PNA treatment. We expected NCp7 and Nef to be potent targets because defects in both proteins are known to produce less infective viruses (Ottmann et al., 1995; Schiavoni et al., 2004). Yet the NCp7 PNA had no significant effect however the PNA targeting Nef decreased the ß-Gal readout level to about 40%. Surprisingly, after treatment with the anti flap PNA the viral particles were 3-times less infectious. This is an interesting result, because testing the same PNA for its inhibitory effect in early replicative events showed no significant results. Thus the result could indicate that the PNA binds to the viral RNA before budding and inhibits viral infection in the next replicative round. If the binding of PNAs inside mature particles decreases infectivity, it would be attractive to synthesis PNAs with a viral targeting signal. Vpr is recruited through the interaction with p6 of Gag to the viral particle (see introduction). Therefore in analogy to cell-penetrating peptides (CCPs) it might be possible to target PNAs directly to budding viral particles. Following, infectivity of these viral particles could be tested in primary lymphocytes, the principal targets for HIV-1 in vivo, which are poor substrates for transfection.

The experiments designed to inhibit early events in the HIV life cycle were not very successful. Lack of effectiveness observed may be a result of inaccessible sites in the target. The secondary structure of the RNA plays a crucial role in the competence of the treatment. Additionally the viral RNA is coated with 1500-2000 copies of NCp7 (Darlix et al., 1995), protecting the genomic RNA against degradation by RNAses

(Tanchou et al., 1995). Traditionally antisense design has been based on the principle of trial and error. This can often be a laborious process considering that only an estimated 2-5% of randomly selected sites represent competent antisense targets (for review see (Sohail and Southern, 2000)).

Recently it has been shown that an effective PNA antisense inhibition of HIV is very challenging. Targeting different regions of the HIV-1 genome by complementary 15-mer PNAs revealed that one antisense oligomer out of 22 was potent in inhibiting the viral protein synthesis and virion assembly (Sei et al., 2000). A PNA targeted against the *gag-pol* mRNA transframe region reduced HIV-1 p24 antigen production in the culture supernatant by up to 98%. Additionally PNAs are extremely sensible to mismatches. The introduction of one or two mismatches abolished the inhibition of a 18mer PNA shown to inhibit gene expression in a luciferase gene reporter system (Doyle et al., 2001). This evidence complicates a PNA based therapy against HIV, due to its high variability which is resulting of reverse transcriptase infidelity, having an average error rate per detectable nucleotide incorporated of 1/1700 (Roberts et al., 1988).

Since small interfering RNAs (siRNA) can be used in a sequence specific manner for gene silencing in mammalian cells, they offer a good tool for intracellular immunization against HIV. Only the unsolved problem of *in vivo* delivery constitutes a major drawback versus the PNA treatment. However, it has been shown that HIV replication can be inhibited by a RNAi approach (Arteaga et al., 2003; Coburn and Cullen, 2002; Jacque et al., 2002). Das et al. demonstrated that a siRNA targeted against Nef blocked HIV replication in persistently infected cells. Yet, after several weeks of cell culture HIV-1 escape variants appeared, no longer inhibited by siRNA (Das et al., 2004). Even targeting essential viral genes with an antisense approach, the virus may become resistant as a result of silent mutations. Therefore targeting of cellular genes as the coreceptor for membrane fusion CCR5 or Cyclophilin A, an intracellular chaperone essential for infectivity, could be advantageous (Liu et al., 1996; Towers et al., 2003).

With the large spectrum of antisense/ antigen molecules directed against HIV, we wanted to cover several sensible targets for a possible therapy purpose. We could show promising effects upon treatment with some PNAs however for an anti-HIV therapy the inhibition was not strong enough. Additionally, a sequence specific antisense strategy targeting single HIV sequences is, due to the high mutation rate,

very challenging. As it has been shown, an antisense treatment can result in the inhibition of viral replication but it is likely followed by viral escape (Das et al., 2004). Yet, analogous to the current triple combination therapy a PNA based treatment could be administrated in combination to existing drugs or as a cocktail of different PNAs to prevent viral escape.

In contrast to HIV, the PNA based approach seems more potent to inhibit viral spread of borna disease virus (BDV). Although BDV is like HIV a RNA virus, yet it is not replicating via a DNA intermediate. The BDV genome is very stable, with less than 5% sequence differences in isolated strains (Binz et al., 1994; Schneider et al., 1994). This low mutation rate is highly favorable for an antisense inhibition of the virus.

We tested 2 different sequences targeted against the surface glycoprotein (GP) of BDV. Not much is known about the function of this protein. Electron microscopy data suggest that BDV is an enveloped virus (Gonzalez-Dunia et al., 1997; Zimmermann et al., 1994), however assembled particles have never been visualized in the brain of infected animals. We assessed whether the GP is required for viral dissemination. For this purpose the PNA approach represented a molecular biology tool to study the function of GP in the viral life cycle. Yet the efficient inhibition of viral spread opens the possibility of a sequence specific, PNA based, anti-viral therapy.

Although the choice of target sequences is a very delicate issue (discussed above) one of the two synthesized PNAs efficiently down regulated the GP expression. The same PNA was also potent to inhibit viral spread in an experimental system using persistently infected Vero cells as well as in primary hippocampal neurons. This result gives further evidences that enveloped viral particles are essential for BDV dissemination.

In vivo, BDV replicates and persists predominantly in neurons of the limbic system. Therefore the primary cultures of rat hippocampal neurons are an appropriate assay system to study primary infection. The efficiency of the PNA treatment in these cells is encouraging for a possible therapeutically approach. Expression level of GP *in vivo* is very low (Carbone et al., 1993) and with its crucial role for viral spread in neurons, the BDV-GP represents an attractive target for antiviral therapy by antisense strategies. Moreover well studied animal models are available to investigate BDV infection. Rats and mice can be infected experimentally, which represents a powerful tool to further investigate the potential of a PNA based antiviral therapy.

5. Summary

5.1 Abstract (english):

The human immunodeficiency virus (HIV) is the causative agent of the acquired immunodeficiency syndrome (AIDS). Despite more than twenty years of intense research still no vaccine or curing therapy has been found. For the development of novel antiviral compounds, understanding of the HIV lifecycle as well as the molecular mechanisms of host pathogen interactions are a prerequisite.

Like all viruses, HIV subcontracts cellular machineries for efficient replication and production of new progeny. A particular feature of lentiviruses is the active transport of the pre-integration complex (PIC) into the nucleus. The mechanism remains elusive, yet in the case of HIV the viral protein R (Vpr), a small 14kDa accessory protein, is one candidate possibly implicated in the process. The protein stays associated to the PIC until nuclear translocation. Furthermore it has been shown, that Vpr binds to the nuclear pore complex (NPC). This interaction might therefore be the link mediating nuclear import of the PIC. Moreover the cytoskeleton has been shown to play a major role in cytoplasmic transport of viral particles. In this context, we observed the nuclear envelope (NE) to be embedded in a perinuclear actin shell and displaying highly dynamic nuclear invaginations. We developed a novel approach to visualize actin inside living cells based on a fluorescent analog of cytochalasin D (CD-BODIPY). Due to specific binding to free-barbed-ends of short actin fibers, we could show that this compound visualizes a high turnover actin pool around the NE and inside NE-membrane invaginations of living cells. Although reported in many different cell types, the possible role of perinuclear actin filaments in the dynamic structural plasticity of the NE remains unresolved. We could show that NE-membranes alone are sufficient to nucleate polymerizing actin filaments *in vitro*, involving both actin recruitment to their surface, and filament growth. Accordingly, our results demonstrate that perinuclear actin dynamics are orchestrated by the NE itself. Therefore, by binding of Vpr to the NPC, the virus could possibly exploit this pool of polymerizing actin as a new strategy to overcome the nuclear membrane.

Furthermore, we tested peptide nucleic acids (PNAs) as new compounds to inhibit viral spread at different stages of the lifecycle. PNAs have been developed recently and dispose of several features to be a powerful tool for a novel antisense approach. We synthesized a series of PNAs directed against crucial sequences in the HIV genome and tested them under various conditions. This showed in particular, that infectivity of virions produced in the presence of PNAs was significantly diminished. In another viral system, PNAs targeted against the borna disease virus (BDV), could provide evidence for the requirement of the surface glycoprotein (GP) in BDV infection. Moreover, the treatment could effectively inhibit viral spread in primary neurons. These results demonstrate PNAs to be a powerful molecular tool and a potential antiviral drug candidate.

5.2 Zusammenfassung (deutsch)

Das Humane Immundefizienzvirus (HIV) ist der Auslöser der erworbenen Immunschwächekrankheit (AIDS). Seit mehr als zwanzig Jahren wird intensive Forschung betrieben, um mehr Verständnis für die Biologie dieses Virus zu erlangen. Dennoch konnten bisher weder ein Impfstoff noch eine das Virus vollständig eliminierende Therapie entwickelt werden. Das Verständnis des viralen Lebenskreislaufs auf der einen Seite und des Zusammenspiels von Gastzelle und Pathogen auf der anderen Seite ist eine grundlegende Vorraussetzung für die Entwicklung neuer antiviraler Strategien.

Viren nutzen zelluläre Mechanismen für ihre eigene Replikation und Vermehrung. Eine ausserordentliche Fähigkeit von Lentiviren ist der aktive Transport ihres Präintegrationskomplexes (PIC) durch die intakte Kernmembran. Die molekulare Grundlage dieses Vorgangs ist bis heute noch nicht bekannt. Im Falle von HIV gibt es allerdings Hinweise, dass das akzessorische virale Protein R (Vpr) eine Rolle bei diesem Vorgang spielt. Das Protein begleitet den PIC bei seinem Weg durch das Zytoplasma bis zu dessen Kontakt mit der Kernmembran. Vpr bindet an Komponenten des Kernporenkomplexes (NPC), und es besteht die Möglichkeit, dass Vpr durch diese Wechselwirkung den Kerntransport des PICs vermittelt.

Beim Transport viraler Partikel durch das Zytoplasma spielt das Zytoskelett eine maßgebliche Rolle. In diesem Zusammenhang stellten wir fest, dass der Zellkern von einem Geflecht an Actin umgeben ist und hoch dynamische Invaginationen der Kernmembran aufweist. Um Actin in lebenden Zellen darzustellen, haben wir eine neue Methode entwickelt, die auf der Verwendung einer fluoreszierenden Form von Cytochalasin D (CD-BODIPY) basiert. Diese Droge bindet spezifisch an das schnell wachsende Ende (free-barbed-end) von Actinfilamenten. Mit Hilfe dieses Systems konnten wir zeigen, dass die Kernmembran von stark polymerisationsaktivem Actin umgeben ist, und dass dieses Actin tief in die Invaginationen der Kernmembran hineinreicht. Ein den Zellkern umgebendes Actingeflecht wurde bereits früher beschrieben, allerdings war die Bedeutung und Auswirkung auf die Struktur des Zellkerns nicht bekannt. In dieser Arbeit konnten wir nun zeigen, dass isolierte und aufgereinigte Kernmembranen *in vitro* ausreichen, um die Polymerisierung von Actin zu initiieren. Dieser Vorgang beinhaltet sowohl die Bindung von Actin an die Kernmembran als auch das Wachstum von Filamenten. Dementsprechend demonstrieren unsere Ergebnisse, dass die Zellkernmembran *per se* in der Lage ist, dieses spezielle Actinreservoir zu manipulieren. Das HI-Virus könnte nun durch die Bindung von Vpr an den NPC das beschriebene zelluläre Phänomen ausnutzen, um durch eine lokal Induktion der Polymerisierung von Actin die Kernmembran zu überwinden.

Des Weiteren, haben wir Peptid Nuklein Säuren (PNAs) auf ihre Fähigkeit als neuartige antivirale Präparate hin untersucht. PNAs wurden erst kürzlich entwickelt und stellen dank

ihrer hervorragenden biochemischen Misch-Eigenschaften eine neue und sehr vielversprechende Möglichkeit dar, Genexpression spezifisch zu inhibieren. In dieser Hinsicht haben wir eine Reihe von PNAs synthetisiert, die gegen essentielle Sequenzen im Genom von HIV gerichtet sind, und haben ihre Wirksamkeit in einer Vielzahl von Versuchsanordnungen untersucht. Hiermit konnten wir zeigen, dass virale Partikel an Infektiosität verlieren, wenn sie in Anwesenheit von PNAs produziert werden. In einem anderen viralen Versuchssystem konnten wir unter Verwendung von PNAs, die gegen die Sequenzen des Glycoproteins des Borna Disease Virus (BDV) gerichtet sind, die Notwendigkeit des Hüllproteins von BDV für den Infektionsprozess aufzeigen. Außerdem konnte durch die PNA-Behandlung eine Ausbreitung des Virus in primären Neuronen blockiert werden. Diese Ergebnisse qualifizieren PNAs sowohl als leistungsfähige Hilfsmittel für die Grundlagenforschung als auch eine vielversprechende Möglichkeiten im Hinblick auf den Einsatz als antivirale Therapeutika.

5.3 Résumé (français)

Le virus d'immunodéficience humaine (VIH) est responsable du syndrome d'immunodéficience acquise (SIDA), et entraîne la dégénérescence du système immunitaire. Plus de vingt ans de recherche intense n'ont pas permis de développer un vaccin ou des voies thérapeutiques permettant de guérir les malades. L'étape fondamentale pour découvrir de nouvelles stratégies antivirales reste la compréhension de la pathogénie du SIDA ainsi que les mécanismes moléculaires de l'interaction du virus avec l'hôte.

Comme tous les virus, le VIH détourne les machineries cellulaires pour se répliquer et se propager. Une caractéristique des lentivirus est le transport actif du complexe de pré-intégration (PIC) dans le noyau de la cellule hôte. Le mécanisme de ce transport n'est pas connu, mais une protéine accessoire du VIH, appelée Vpr (viral protein R) pourrait être impliquée dans ce processus. En effect Vpr reste associée au PIC jusqu'à la translocation du génome à travers la membrane nucléaire. Par ailleurs, il a été montré que Vpr est capable d'intéragir avec le complexe du pore nucléaire (NPC). Cela laisse soupçonner que cette interaction est à la base de l'import nucléaire du PIC. Il a également été montré que le cytosquelette joue un rôle prépondérant dans le transport de particules virales. Dans cette perspective, nous avons observé que la membrane nucléaire est entourée d'une enveloppe d'actine périnucléaire et que la membrane forme des invaginations dynamiques. Nous avons mis au point une nouvelle approche pour visualiser l'actine dans les cellules vivantes basée sur l'utilisation d'un analogue fluorescent de la cytochalasine D, le CD-BODIPY. Ce composé se fixe sur les extrémités barbées des fibres courtes d'actine (free-barbed-ends), ce qui nous a permis de visualiser dans des cellules vivantes un réservoir d'actine qui polymérise autour de l'enveloppe nucléaire ainsi que dans les invaginations de cette membrane. Alors que la

présence de filaments d'actine périnucléaire a été décrite dans plusieurs types cellulaires, leur rôle, notamment dans la plasticité de l'enveloppe nucléaire, n'est toujours pas compris. Nous avons montré que des enveloppes nucléaires isolées suffisent à initier la polymérisation de filaments d'actine *in vitro*, un phénomène qui requiert à la fois le recrutement de l'actine à la surface de l'enveloppe nucléaire et la croissance des filaments. Nos résultats démontrent que la dynamique de l'actine périnucléaire est orchestrée par l'enveloppe nucléaire elle-même. C'est donc via la liaison de Vpr au NPC que le virus pourrait exploiter la présence de l'actine comme stratégie pour pénétrer dans le noyau en dépit de la barrière que constitue l'enveloppe.

Par ailleurs, nous avons testé l'effet des acides nucléiques peptides (PNAs) sur l'infection du virus à différents stades du cycle invasif. Les PNAs sont des molécules de conception récente dont les caractéristiques permettent l'utilisation dans une nouvelle approche antisens. Nous avons synthétisé une série de PNAs dirigés contre des séquences fonctionnellement cruciales du génome du VIH et les avons testés en explorant différentes conditions. Nous avons montré que l'infectivité des virions produits en présence de PNAs est considérablement réduite. Dans un autre système viral, les PNAs dirigés contre le Borna Disease Virus (BDV) nous ont permis de mettre en évidence le rôle de la glycoprotéine de surface (GP) lors de l'infection. De plus, nous avons montré que ce traitement inhibe la propagation de l'infection dans des cultures de neurones primaires. Les PNAs sont donc des outils moléculaires extrèmement efficaces, et des candidats prometteurs pour de nouvelles thérapeutiques antivirales.

6. References

Arteaga, H.J., Hinkula, J., van Dijk-Hard, I., Dilber, M.S., Wahren, B., Christensson, B., Mohamed, A.J. and Smith, C.I. (2003) Choosing CCR5 or Rev siRNA in HIV-1. *Nat Biotechnol*, **21**, 230-231.

Bajramovic, J.J., Munter, S., Syan, S., Nehrbass, U., Brahic, M. and Gonzalez-Dunia, D. (2003) Borna disease virus glycoprotein is required for viral dissemination in neurons. *J Virol*, **77**, 12222-12231.

Baltimore, D. (1970) RNA-dependent DNA polymerase in virions of RNA tumour viruses. *Nature*, **226**, 1209-1211.

Bamburg, J.R., McGough, A. and Ono, S. (1999) Putting a new twist on actin: ADF/cofilins modulate actin dynamics. *Trends Cell Biol*, **9**, 364-370.

Bard, F., Bourgeois, C.A., Costagliola, D. and Bouteille, M. (1985) Rotation of the cell nucleus in living cells: a quantitative analysis. *Biol Cell*, **54**, 135-142.

Barre-Sinoussi, F., Chermann, J.C., Rey, F., Nugeyre, M.T., Chamaret, S., Gruest, J., Dauguet, C., Axler-Blin, C., Vezinet-Brun, F., Rouzioux, C., Rozenbaum, W. and Montagnier, L. (1983) Isolation of a T-lymphotropic retrovirus from a patient at risk for acquired immune deficiency syndrome (AIDS). *Science*, **220**, 868-871.

Bastide, L., Boehmer, P.E., Villani, G. and Lebleu, B. (1999) Inhibition of a DNA-helicase by peptide nucleic acids. *Nucleic Acids Res*, **27**, 551-554.

Beaudouin, J., Gerlich, D., Daigle, N., Eils, R. and Ellenberg, J. (2002) Nuclear envelope breakdown proceeds by microtubule-induced tearing of the lamina. *Cell*, **108**, 83-96.

Bentin, T. and Nielsen, P.E. (1996) Enhanced peptide nucleic acid binding to supercoiled DNA: possible implications for DNA "breathing" dynamics. *Biochemistry*, **35**, 8863-8869.

Berkhout, B., Silverman, R.H. and Jeang, K.T. (1989) Tat trans-activates the human immunodeficiency virus through a nascent RNA target. *Cell*, **59**, 273-282.

Berkowitz, R.D., Ohagen, A., Hoglund, S. and Goff, S.P. (1995) Retroviral nucleocapsid domains mediate the specific recognition of genomic viral RNAs by chimeric Gag polyproteins during RNA packaging in vivo. *J Virol*, **69**, 6445-6456.

Berry, N., Davis, C., Jenkins, A., Wood, D., Minor, P., Schild, G., Bottiger, M., Holmes, H. and Almond, N. (2001) Vaccine safety. Analysis of oral polio vaccine CHAT stocks. *Nature*, **410**, 1046-1047.

Bess, J.W., Jr., Powell, P.J., Issaq, H.J., Schumack, L.J., Grimes, M.K., Henderson, L.E. and Arthur, L.O. (1992) Tightly bound zinc in human immunodeficiency virus type 1, human T-cell leukemia virus type I, and other retroviruses. *J Virol*, **66**, 840-847.

Binz, T., Lebelt, J., Niemann, H. and Hagenau, K. (1994) Sequence analyses of the p24 gene of Borna disease virus in naturally infected horse, donkey and sheep. *Virus Res*, **34**, 281-289.

Blanchoin, L., Amann, K.J., Higgs, H.N., Marchand, J.B., Kaiser, D.A. and Pollard, T.D. (2000) Direct observation of dendritic actin filament networks nucleated by Arp2/3 complex and WASP/Scar proteins. *Nature*, **404**, 1007-1011.

Blanchoin, L. and Pollard, T.D. (2002) Hydrolysis of ATP by polymerized actin depends on the bound divalent cation but not profilin. *Biochemistry*, **41**, 597-602.

Blancou, P., Vartanian, J.P., Christopherson, C., Chenciner, N., Basilico, C., Kwok, S. and Wain-Hobson, S. (2001) Polio vaccine samples not linked to AIDS. *Nature*, **410**, 1045-1046.

Boeke, J.D. and Chapman, K.B. (1991) Retrotransposition mechanisms. *Curr Opin Cell Biol*, **3**, 502-507.

Boeke, J.D. and Corces, V.G. (1989) Transcription and reverse transcription of retrotransposons. *Annu Rev Microbiol*, **43**, 403-434.

Bonder, E.M., Fishkind, D.J. and Mooseker, M.S. (1983) Direct measurement of critical concentrations and assembly rate constants at the two ends of an actin filament. *Cell*, **34**, 491-501.

Bourgeois, C.A., Hemon, D. and Bouteille, M. (1979) Structural relationship between the nucleolus and the nuclear

envelope. *J Ultrastruct Res*, **68**, 328-340.

Braun, K., Peschke, P., Pipkorn, R., Lampel, S., Wachsmuth, M., Waldeck, W., Friedrich, E. and Debus, J. (2002) A biological transporter for the delivery of peptide nucleic acids (PNAs) to the nuclear compartment of living cells. *J Mol Biol*, **318**, 237-243.

Braun, K., Wolber, G., Waldeck, W., Pipkorn, R., Jenne, J., Rastert, R., Ehemann, V., Eisenmenger, A., Corban-Wilhelm, H., Braun, I., Heckl, S. and Debus, J. (2003) The enhancement of neutron irradiation of HeLa-S cervix carcinoma cells by cell-nucleus-addressed deca-p-boronophenylalanine. *Eur J Med Chem*, **38**, 587-595.

Broers, J.L., Machiels, B.M., van Eys, G.J., Kuijpers, H.J., Manders, E.M., van Driel, R. and Ramaekers, F.C. (1999) Dynamics of the nuclear lamina as monitored by GFP-tagged A-type lamins. *J Cell Sci*, **112**, 3463-3475.

Bukrinskaya, A., Brichacek, B., Mann, A. and Stevenson, M. (1998) Establishment of a functional human immunodeficiency virus type 1 (HIV-1) reverse transcription complex involves the cytoskeleton. *J Exp Med*, **188**, 2113-2125.

Bukrinsky, M. and Adzhubei, A. (1999) Viral protein R of HIV-1. *Rev Med Virol*, **9**, 39-49.

Bukrinsky, M.I., Haggerty, S., Dempsey, M.P., Sharova, N., Adzhubel, A., Spitz, L., Lewis, P., Goldfarb, D., Emerman, M. and Stevenson, M. (1993a) A nuclear localization signal within HIV-1 matrix protein that governs infection of non-dividing cells. *Nature*, **365**, 666-669.

Bukrinsky, M.I., Sharova, N., McDonald, T.L., Pushkarskaya, T., Tarpley, W.G. and Stevenson, M. (1993b) Association of integrase, matrix, and reverse transcriptase antigens of human immunodeficiency virus type 1 with viral nucleic acids following acute infection. *Proc Natl Acad Sci U S A*, **90**, 6125-6129.

Carbone, K.M., Rubin, S.A., Nishino, Y. and Pletnikov, M.V. (2001) Borna disease: virus-induced neurobehavioral disease pathogenesis. *Curr Opin Microbiol*, **4**, 467-475.

Carbone, K.M., Rubin, S.A., Sierra-Honigmann, A.M. and Lederman, H.M. (1993) Characterization of a glial cell line persistently infected with borna disease virus (BDV): influence of neurotrophic factors on BDV protein and RNA expression. *J Virol*, **67**, 1453-1460.

Carlier, M.F., Criquet, P., Pantaloni, D. and Korn, E.D. (1986) Interaction of cytochalasin D with actin filaments in the presence of ADP and ATP. *J Biol Chem*, **261**, 2041-2050.

Carlier, M.F. and Pantaloni, D. (1986) Direct evidence for ADP-Pi-F-actin as the major intermediate in ATP-actin polymerization. Rate of dissociation of Pi from actin filaments. *Biochemistry*, **25**, 7789-7792.

Carlier, M.F., Pantaloni, D., Evans, J.A., Lambooy, P.K., Korn, E.D. and Webb, M.R. (1988) The hydrolysis of ATP that accompanies actin polymerization is essentially irreversible. *FEBS Lett*, **235**, 211-214.

Charneau, P., Alizon, M. and Clavel, F. (1992) A second origin of DNA plus-strand synthesis is required for optimal human immunodeficiency virus replication. *J Virol*, **66**, 2814-2820.

Charneau, P. and Clavel, F. (1991) A single-stranded gap in human immunodeficiency virus unintegrated linear DNA defined by a central copy of the polypurine tract. *J Virol*, **65**, 2415-2421.

Charneau, P., Mirambeau, G., Roux, P., Paulous, S., Buc, H. and Clavel, F. (1994) HIV-1 reverse transcription. A termination step at the center of the genome. *J Mol Biol*, **241**, 651-662.

Clubb, B.H. and Locke, M. (1996) F-actin forms transient perinuclear shells at the mitosis-interphase transition. *Cell Motil Cytoskeleton*, **33**, 151-162.

Clubb, B.H. and Locke, M. (1998) Peripheral nuclear matrix actin forms perinuclear shells. *J Cell Biochem*, **70**, 240-251.

Coburn, G.A. and Cullen, B.R. (2002) Potent and specific inhibition of human immunodeficiency virus type 1 replication by RNA interference. *J Virol*, **76**, 9225-9231.

Coffin, J.M. (1992) Structure and classification of retroviruses. In Levy, J.A. (ed.), *The retroviridae*. Plenum Press, New York, pp. 19-49.

Coffin, J.M. (1996) Retroviridae and their replication. In Fields, B.N.e.a. (ed.), *Virology*. Raven Press, New York, pp. 1767-1848.

Cohen, E.A., Terwilliger, E.F., Jalinoos, Y., Proulx, J., Sodroski, J.G. and

Haseltine, W.A. (1990) Identification of HIV-1 vpr product and function. *J Acquir Immune Defic Syndr*, **3**, 11-18.

Collings, D.A., Carter, C.N., Rink, J.C., Scott, A.C., Wyatt, S.E. and Allen, N.S. (2000) Plant nuclei can contain extensive grooves and invaginations. *Plant Cell*, **12**, 2425-2440.

Cooper, J.A. and Schafer, D.A. (2000) Control of actin assembly and disassembly at filament ends. *Curr Opin Cell Biol*, **12**, 97-103.

Coue, M., Brenner, S.L., Spector, I. and Korn, E.D. (1987) Inhibition of actin polymerization by latrunculin A. *FEBS Lett*, **213**, 316-318.

Craven, R.C., Bennett, R.P. and Wills, J.W. (1991) Role of the avian retroviral protease in the activation of reverse transcriptase during virion assembly. *J Virol*, **65**, 6205-6217.

Cronshaw, J.M., Krutchinsky, A.N., Zhang, W., Chait, B.T. and Matunis, M.J. (2002) Proteomic analysis of the mammalian nuclear pore complex. *J Cell Biol*, **158**, 915-927.

Cubitt, B. and de la Torre, J.C. (1994) Borna disease virus (BDV), a nonsegmented RNA virus, replicates in the nuclei of infected cells where infectious BDV ribonucleoproteins are present. *J Virol*, **68**, 1371-1381.

Cullen, B.R. (2003) Nuclear mRNA export: insights from virology. *Trends Biochem Sci*, **28**, 419-424.

Curtis, T. (1992) *Rolling Stone*, p. 54.

Darlix, J.L., Lapadat-Tapolsky, M., de Rocquigny, H. and Roques, B.P. (1995) First glimpses at structure-function relationships of the nucleocapsid protein of retroviruses. *J Mol Biol*, **254**, 523-537.

Das, A.T., Brummelkamp, T.R., Westerhout, E.M., Vink, M., Madiredjo, M., Bernards, R. and Berkhout, B. (2004) Human immunodeficiency virus type 1 escapes from RNA interference-mediated inhibition. *J Virol*, **78**, 2601-2605.

Davis, L.I. and Fink, G.R. (1990) The NUP1 gene encodes an essential component of the yeast nuclear pore complex. *Cell*, **61**, 965-978.

De La Cruz, E.M., Mandinova, A., Steinmetz, M.O., Stoffler, D., Aebi, U. and Pollard, T.D. (2000) Polymerization and structure of nucleotide-free actin filaments. *J Mol Biol*, **295**, 517-526.

de la Torre, J.C. (1994) Molecular biology of borna disease virus: prototype of a new group of animal viruses. *J Virol*, **68**, 7669-7675.

De La Torre, J.C., Gonzalez-Dunia, D., Cubitt, B., Mallory, M., Mueller-Lantzsch, N., Grasser, F.A., Hansen, L.A. and Masliah, E. (1996) Detection of borna disease virus antigen and RNA in human autopsy brain samples from neuropsychiatric patients. *Virology*, **223**, 272-282.

de Noronha, C.M., Sherman, M.P., Lin, H.W., Cavrois, M.V., Moir, R.D., Goldman, R.D. and Greene, W.C. (2001) Dynamic disruptions in nuclear envelope architecture and integrity induced by HIV-1 Vpr. *Science*, **294**, 1105-1108.

Defacque, H., Egeberg, M., Antzberger, A., Ansorge, W., Way, M. and Griffiths, G. (2000) Actin assembly induced by polylysine beads or purified phagosomes: quantitation by a new flow cytometry assay. *Cytometry*, **41**, 46-54.

Demidov, V.V., Potaman, V.N., Frank-Kamenetskii, M.D., Egholm, M., Buchard, O., Sonnichsen, S.H. and Nielsen, P.E. (1994) Stability of peptide nucleic acids in human serum and cellular extracts. *Biochem Pharmacol*, **48**, 1310-1313.

Deming, M.S., Linkins, R.W., Jaiteh, K.O. and Hull, H.F. (1997) The clinical efficacy of trivalent oral polio vaccine in The Gambia by season of vaccine administration. *J Infect Dis*, **175 Suppl 1**, S254-257.

Derossi, D., Calvet, S., Trembleau, A., Brunissen, A., Chassaing, G. and Prochiantz, A. (1996) Cell internalization of the third helix of the Antennapedia homeodomain is receptor-independent. *J Biol Chem*, **271**, 18188-18193.

Doyle, D.F., Braasch, D.A., Simmons, C.G., Janowski, B.A. and Corey, D.R. (2001) Inhibition of gene expression inside cells by peptide nucleic acids: effect of mRNA target sequence, mismatched bases, and PNA length. *Biochemistry*, **40**, 53-64.

Dramsi, S. and Cossart, P. (1998) Intracellular pathogens and the actin cytoskeleton. *Annu Rev Cell Dev Biol*, **14**, 137-166.

Drenckhahn, D. and Pollard, T.D. (1986) Elongation of actin filaments is a diffusion-limited reaction at the barbed end and is accelerated by inert macromolecules. *J Biol Chem*, **261**, 12754-12758.

Dupuy-Coin, A.M., Moens, P. and Bouteille, M. (1986) Three-dimensional analysis of given cell structures: nucleolus, nucleoskeleton and nuclear inclusions. *Methods Achiev Exp Pathol*, **12**, 1-25.

Egholm, M., Buchardt, O., Christensen, L., Behrens, C., Freier, S.M., Driver, D.A., Berg, R.H., Kim, S.K., Norden, B. and Nielsen, P.E. (1993) PNA hybridizes to complementary oligonucleotides obeying the Watson-Crick hydrogen-bonding rules. *Nature*, **365**, 566-568.

Egholm, M., Buchardt, O., Nielsen, P.E. and Berg, R.H. (1992) Peptide nucleic acids (PNA). Oligonucleotide analogues with an achiral peptide backbone. *J Am Chem Soc*, **114**, 1895-1897.

Egholm, M., Christensen, L., Dueholm, K.L., Buchardt, O., Coull, J. and Nielsen, P.E. (1995) Efficient pH-independent sequence-specific DNA binding by pseudoisocytosine-containing bis-PNA. *Nucleic Acids Res*, **23**, 217-222.

Ellenberg, J., Siggia, E.D., Moreira, J.E., Smith, C.L., Presley, J.F., Worman, H.J. and Lippincott-Schwartz, J. (1997) Nuclear membrane dynamics and reassembly in living cells: targeting of an inner nuclear membrane protein in interphase and mitosis. *J Cell Biol*, **138**, 1193-1206.

Elliott, G. and O'Hare, P. (1997) Intercellular trafficking and protein delivery by a herpesvirus structural protein. *Cell*, **88**, 223-233.

Evgen'ev, M.B., Corces, V.G. and Lankenau, D.H. (1992) Ulysses transposable element of Drosophila shows high structural similarities to functional domains of retroviruses. *J Mol Biol*, **225**, 917-924.

Fang, G., Yu, H. and Kirschner, M.W. (1998) Direct binding of CDC20 protein family members activates the anaphase-promoting complex in mitosis and G1. *Mol Cell*, **2**, 163-171.

Finzi, D., Hermankova, M., Pierson, T., Carruth, L.M., Buck, C., Chaisson, R.E., Quinn, T.C., Chadwick, K., Margolick, J., Brookmeyer, R., Gallant, J., Markowitz, M., Ho, D.D., Richman, D.D. and Siliciano, R.F. (1997) Identification of a reservoir for HIV-1 in patients on highly active antiretroviral therapy. *Science*, **278**, 1295-1300.

Forget, J., Yao, X.J., Mercier, J. and Cohen, E.A. (1998) Human immunodeficiency virus type 1 vpr protein transactivation function: mechanism and identification of domains involved. *J Mol Biol*, **284**, 915-923.

Fouchier, R.A., Meyer, B.E., Simon, J.H., Fischer, U., Albright, A.V., Gonzalez-Scarano, F. and Malim, M.H. (1998) Interaction of the human immunodeficiency virus type 1 Vpr protein with the nuclear pore complex. *J Virol*, **72**, 6004-6013.

Frankel, A.D. and Pabo, C.O. (1988) Cellular uptake of the tat protein from human immunodeficiency virus. *Cell*, **55**, 1189-1193.

Fricker, M., Hollinshead, M., White, N. and Vaux, D. (1997) Interphase nuclei of many mammalian cell types contain deep, dynamic, tubular membrane-bound invaginations of the nuclear envelope. *J Cell Biol*, **136**, 531-544.

Fuchs, E. and Yang, Y. (1999) Crossroads on cytoskeletal highways. *Cell*, **98**, 547-550.

Gallay, P., Hope, T., Chin, D. and Trono, D. (1997) HIV-1 infection of nondividing cells through the recognition of integrase by the importin/karyopherin pathway. *Proc. Natl. Acad. Sci. USA*, **94**, 9825-9830.

Garenne, M. (1993) Measles vaccine: titre and safety. *Science*, **259**, 441-442.

Gilboa, E., Mitra, S.W., Goff, S. and Baltimore, D. (1979) A detailed model of reverse transcription and tests of crucial aspects. *Cell*, **18**, 93-100.

Goh, W.C., Rogel, M.E., Kinsey, C.M., Michael, S.F., Fultz, P.N., Nowak, M.A., Hahn, B.H. and Emerman, M. (1998) HIV-1 Vpr increases viral expression by manipulation of the cell cycle: a mechanism for selection of Vpr in vivo. *Nat Med*, **4**, 65-71.

Gonzalez-Dunia, D., Cubitt, B., Grasser, F.A. and de la Torre, J.C. (1997) Characterization of Borna disease virus p56 protein, a surface glycoprotein involved in virus entry. *J Virol*, **71**, 3208-3218.

Gosztonyi, G., Dietzschold, B., Kao, M., Rupprecht, C.E., Ludwig, H. and Koprowski, H. (1993) Rabies and borna disease. A comparative pathogenetic study of two neurovirulent agents. *Lab Invest*, **68**, 285-295.

Gosztonyi, G. and Ludwig, H. (1995) Borna disease--neuropathology and pathogenesis. *Curr Top Microbiol Immunol*, **190**, 39-73.

Gottlinger, H.G., Dorfman, T., Sodroski, J.G. and Haseltine, W.A. (1991) Effect of mutations affecting the p6 gag protein on human immunodeficiency virus particle release. *Proc Natl Acad Sci U S A*, **88**, 3195-3199.

Grand, R.J. (1989) Acylation of viral and eukaryotic proteins. *Biochem J*, **258**, 625-638.

Green, M. and Loewenstein, P.M. (1988) Autonomous functional domains of chemically synthesized human immunodeficiency virus tat trans-activator protein. *Cell*, **55**, 1179-1188.

Gu, J., Emerman, M. and Sandmeyer, S. (1997) Small heat shock protein suppression of Vpr-induced cytoskeletal defects in budding yeast. *Mol Cell Biol*, **17**, 4033-4042.

Gundersen, G.G. and Cook, T.A. (1999) Microtubules and signal transduction. *Curr Opin Cell Biol*, **11**, 81-94.

Haggerty, S. and Stevenson, M. (1991) Predominance of distinct viral genotypes in brain and lymph node compartments of HIV-1-infected individuals. *Viral Immunol*, **4**, 123-131.

Hahn, B.H., Shaw, G.M., De Cock, K.M. and Sharp, P.M. (2000) AIDS as a zoonosis: scientific and public health implications. *Science*, **287**, 607-614.

Hayward, W.S. (1977) Size and genetic content of viral RNAs in avian oncovirus-infected cells. *J Virol*, **24**, 47-63.

Heinzinger, N.K., Bukinsky, M.I., Haggerty, S.A., Ragland, A.M., Kewalramani, V., Lee, M.A., Gendelman, H.E., Ratner, L., Stevenson, M. and Emerman, M. (1994) The Vpr protein of human immunodeficiency virus type 1 influences nuclear localization of viral nucleic acids in nondividing host cells. *Proc Natl Acad Sci U S A*, **91**, 7311-7315.

Henderson, L.E., Krutzsch, H.C. and Oroszlan, S. (1983) Myristyl amino-terminal acylation of murine retrovirus proteins: an unusual post-translational proteins modification. *Proc Natl Acad Sci U S A*, **80**, 339-343.

Higgs, H.N. and Pollard, T.D. (2000) Activation by Cdc42 and PIP(2) of Wiskott-Aldrich syndrome protein (WASp) stimulates actin nucleation by Arp2/3 complex. *J Cell Biol*, **150**, 1311-1320.

Hill, C.P., Worthylake, D., Bancroft, D.P., Christensen, A.M. and Sundquist, W.I. (1996) Crystal structures of the trimeric human immunodeficiency virus type 1 matrix protein: implications for membrane association and assembly. *Proc Natl Acad Sci U S A*, **93**, 3099-3104.

Hiskey, R.G. and Adams, J.B., Jr. (1965) Sulfur-containing polypeptides. I. Use of the N-benzhydryloxycarbonyl group and the benzhydryl ester. *J Am Chem Soc*, **87**, 3969-3973.

Hochstrasser, M. and Sedat, J.W. (1987) Three-dimensional organization of Drosophila melanogaster interphase nuclei. II. Chromosome spatial organization and gene regulation. *J Cell Biol*, **104**, 1471-1483.

Hooper, E. (1999) The River: A Journey Back to the Source of HIV and AIDS. *Penguin, London*.

Hull, H.F., Birmingham, M.E., Melgaard, B. and Lee, J.W. (1997) Progress toward global polio eradication. *J Infect Dis*, **175 Suppl 1**, S4-9.

Imreh, G., Beckman, M., Iverfeldt, K. and Hallberg, E. (1998) Noninvasive monitoring of apoptosis versus necrosis in a neuroblastoma cell line expressing a nuclear pore protein tagged with the green fluorescent protein. *Exp Cell Res*, **238**, 371-376.

Iyengar, S., Hildreth, J.E. and Schwartz, D.H. (1998) Actin-dependent receptor colocalization required for human immunodeficiency virus entry into host cells. *J Virol*, **72**, 5251-5255.

Jacinto, A. and Wolpert, L. (2001) Filopodia. *Curr Biol*, **11**, R634.

Jacque, J.M., Triques, K. and Stevenson, M. (2002) Modulation of HIV-1 replication by RNA interference. *Nature*, **418**, 435-438.

Jensen, K.K., Orum, H., Nielsen, P.E. and Norden, B. (1997) Kinetics for hybridization of peptide nucleic acids (PNA) with DNA and RNA studied with the BIAcore technique. *Biochemistry*, **36**, 5072-5077.

Johnson, N., Krebs, M., Boudreau, R., Giorgi, G., LeGros, M. and Larabell, C. (2003) Actin-filled nuclear invaginations indicate degree of cell de-differentiation. *Differentiation*, **71**, 414-424.

Joliot, A., Pernelle, C., Deagostini-Bazin, H. and Prochiantz, A. (1991)

Antennapedia homeobox peptide regulates neural morphogenesis. *Proc Natl Acad Sci U S A*, **88**, 1864-1868.

Jones, A.S., Lewis, P. and Withers, S.F. (1973) The synthesis of carboxymethyl derivates of purines and pyrimidines and their condensation with naturally occuring macromolecules. *Tetrahedron*, **29**, 2293-2296.

Kaelin, K., Dezelee, S., Masse, M.J., Bras, F. and Flamand, A. (2000) The UL25 protein of pseudorabies virus associates with capsids and localizes to the nucleus and to microtubules. *J Virol*, **74**, 474-482.

Kalderon, D., Roberts, B.L., Richardson, W.D. and Smith, A.E. (1984) A short amino acid sequence able to specify nuclear location. *Cell*, **39**, 499-509.

Kashanchi, F., Piras, G., Radonovich, M.F., Duvall, J.F., Fattaey, A., Chiang, C.M., Roeder, R.G. and Brady, J.N. (1994) Direct interaction of human TFIID with the HIV-1 transactivator tat. *Nature*, **367**, 295-299.

Katz, R.A. and Skalka, A.M. (1990) Control of retroviral RNA splicing through maintenance of suboptimal processing signals. *Mol Cell Biol*, **10**, 696-704.

Knudsen, H. and Nielsen, P.E. (1996) Antisense properties of duplex- and triplex-forming PNAs. *Nucleic Acids Res*, **24**, 494-500.

Kohno, T., Goto, T., Takasaki, T., Morita, C., Nakaya, T., Ikuta, K., Kurane, I., Sano, K. and Nakai, M. (1999) Fine structure and morphogenesis of Borna disease virus. *J Virol*, **73**, 760-766.

Korn, E.D. (1982) Actin polymerization and its regulation by proteins from nonmuscle cells. *Physiol Rev*, **62**, 672-737.

Kouyama, T. and Mihashi, K. (1980) Pulse-fluorometry study on actin and heavy meromyosin using F-actin labelled with N-(1-pyrene)maleimide. *Eur J Biochem*, **105**, 279-287.

Laemmli, U.K. (1970) Cleavage of structural proteins during the assembly of the head of bacteriophage T4. *Nature*, **227**, 680-685.

Larsen, H.J., Bentin, T. and Nielsen, P.E. (1999) Antisense properties of peptide nucleic acid. *Biochim Biophys Acta*, **1489**, 159-166.

Larsen, H.J. and Nielsen, P.E. (1996) Transcription-mediated binding of peptide nucleic acid (PNA) to double-stranded DNA: sequence-specific suicide transcription. *Nucleic Acids Res*, **24**, 458-463.

Lasa, I., Gouin, E., Goethals, M., Vancompernolle, K., David, V., Vandekerckhove, J. and Cossart, P. (1997) Identification of two regions in the N-terminal domain of ActA involved in the actin comet tail formation by Listeria monocytogenes. *Embo J*, **16**, 1531-1540.

Le Rouzic, E., Mousnier, A., Rustum, C., Stutz, F., Hallberg, E., Dargemont, C. and Benichou, S. (2002) Docking of HIV-1 Vpr to the nuclear envelope is mediated by the interaction with the nucleoporin hCG1. *J Biol Chem*, **277**, 45091-45098.

Li, E., Stupack, D., Bokoch, G.M. and Nemerow, G.R. (1998) Adenovirus endocytosis requires actin cytoskeleton reorganization mediated by Rho family GTPases. *J Virol*, **72**, 8806-8812.

Liu, B., Dai, R., Tian, C.J., Dawson, L., Gorelick, R. and Yu, X.F. (1999) Interaction of the human immunodeficiency virus type 1 nucleocapsid with actin. *J Virol*, **73**, 2901-2908.

Liu, R., Paxton, W.A., Choe, S., Ceradini, D., Martin, S.R., Horuk, R., MacDonald, M.E., Stuhlmann, H., Koup, R.A. and Landau, N.R. (1996) Homozygous defect in HIV-1 coreceptor accounts for resistance of some multiply-exposed individuals to HIV-1 infection. *Cell*, **86**, 367-377.

Liu, Y., Braasch, D.A., Nulf, C.J. and Corey, D.R. (2004) Efficient and isoform-selective inhibition of cellular gene expression by Peptide nucleic acids. *Biochemistry*, **43**, 1921-1927.

Locker, J.K., Kuehn, A., Schleich, S., Rutter, G., Hohenberg, H., Wepf, R. and Griffiths, G. (2000) Entry of the two infectious forms of vaccinia virus at the plasma membane is signaling-dependent for the IMV but not the EEV. *Mol Biol Cell*, **11**, 2497-2511.

Luby-Phelps, K. (2000) Cytoarchitecture and physical properties of cytoplasm: volume, viscosity, diffusion, intracellular surface area. *Int Rev Cytol*, **192**, 189-221.

Ludwig, H., Bode, L. and Gosztonyi, G. (1988) Borna disease: a persistent virus infection of the central nervous system. *Prog Med Virol*, **35**, 107-151.

Lukacs, G.L., Haggie, P., Seksek, O., Lechardeur, D., Freedman, N. and

Verkman, A.S. (2000) Size-dependent DNA mobility in cytoplasm and nucleus. *J Biol Chem*, **275**, 1625-1629.

Luna, A., Matas, O.B., Martinez-Menarguez, J.A., Mato, E., Duran, J.M., Ballesta, J., Way, M. and Egea, G. (2002) Regulation of protein transport from the Golgi complex to the endoplasmic reticulum by CDC42 and N-WASP. *Mol Biol Cell*, **13**, 866-879.

Machesky, L.M., Atkinson, S.J., Ampe, C., Vandekerckhove, J. and Pollard, T.D. (1994) Purification of a cortical complex containing two unconventional actins from Acanthamoeba by affinity chromatography on profilin-agarose. *J Cell Biol*, **127**, 107-115.

Mallavarapu, A. and Mitchison, T. (1999) Regulated actin cytoskeleton assembly at filopodium tips controls their extension and retraction. *J Cell Biol*, **146**, 1097-1106.

Mangeat, B., Turelli, P., Caron, G., Friedli, M., Perrin, L. and Trono, D. (2003) Broad antiretroviral defence by human APOBEC3G through lethal editing of nascent reverse transcripts. *Nature*, **424**, 99-103.

Massiah, M.A., Starich, M.R., Paschall, C., Summers, M.F., Christensen, A.M. and Sundquist, W.I. (1994) Three-dimensional structure of the human immunodeficiency virus type 1 matrix protein. *J Mol Biol*, **244**, 198-223.

Matarrese, P., Conti, L., Varano, B., Gauzzi, M.C., Belardelli, F., Gessani, S. and Malorni, W. (2000) The HIV-1 vpr protein induces anoikis-resistance by modulating cell adhesion process and microfilament system assembly. *Cell Death Differ*, **7**, 25-36.

McDonald, D., Vodicka, M.A., Lucero, G., Svitkina, T.M., Borisy, G.G., Emerman, M. and Hope, T.J. (2002) Visualization of the intracellular behavior of HIV in living cells. *J Cell Biol*, **159**, 441-452.

McMahon, B.M., Stewart, J.A., Bitner, M.D., Fauq, A., McCormick, D.J. and Richelson, E. (2002) Peptide nucleic acids specifically cause antigene effects in vivo by systemic injection. *Life Sci*, **71**, 325-337.

McMahon, B.M., Stewart, J.A., Jackson, J., Fauq, A., McCormick, D.J. and Richelson, E. (2001) Intraperitoneal injection of antisense peptide nucleic acids targeted to the mu receptor decreases response to morphine and receptor protein levels in rat brain. *Brain Res*, **904**, 345-349.

Mellon, P. and Duesberg, P.H. (1977) Subgenomic, cellular Rous sarcoma virus RNAs contain oligonucleotides from the 3' half and the 5' terminus of virion RNA. *Nature*, **270**, 631-634.

Merrifield, B. (1986) Solid phase synthesis. *Science*, **232**, 341-347.

Merrifield, R.B. (1963) Solid-phase synthesis. I. The synthesis of a tetrapeptide. *J. Am. Chem. Soc.*, **85**, 2149-2154.

Miller, M.D., Farnet, C.M. and Bushman, F.D. (1997) Human immunodeficiency virus type 1 preintegration complexes: Studies of organization and composition. *Journal of Virology*, **71**, 5382-5390.

Miller, M.D., Warmerdam, M.T., Gaston, I., Greene, W.C. and Feinberg, M.B. (1994) The human immunodeficiency virus-1 nef gene product: a positive factor for viral infection and replication in primary lymphocytes and macrophages. *J Exp Med*, **179**, 101-113.

Mitchison, T.J. and Cramer, L.P. (1996) Actin-based cell motility and cell locomotion. *Cell*, **84**, 371-379.

Molling, K., Bolognesi, D.P., Bauer, H., Busen, W., Plassmann, H.W. and Hausen, P. (1971) Association of viral reverse transcriptase with an enzyme degrading the RNA moiety of RNA-DNA hybrids. *Nat New Biol*, **234**, 240-243.

Muriaux, D., De Rocquigny, H., Roques, B.P. and Paoletti, J. (1996) NCp7 activates HIV-1Lai RNA dimerization by converting a transient loop-loop complex into a stable dimer. *J Biol Chem*, **271**, 33686-33692.

Murphy, F.A., Fauquet, C.M., Bishop, D.H.L., Ghabrial, S.A., Jarvis, A.W., Martelli, G.P., Mayo, M.A. and Summers, M.D. (1994) Virus taxonomy: The classification and nomenclature of viruses,. In *Retroviridae*. Springer-Verlag, Vienna.

Nielsen, P.E., Egholm, M., Berg, R.H. and Buchardt, O. (1991) Sequence-selective recognition of DNA by strand displacement with a thymine-substituted polyamide. *Science*, **254**, 1497-1500.

Nielsen, P.E., Egholm, M. and Buchardt, O. (1994a) Peptide nucleic acid (PNA). A DNA mimic with a peptide backbone. *Bioconjug Chem*, **5**, 3-7.

Nielsen, P.E., Egholm, M. and Buchardt, O. (1994b) Sequence-specific transcription arrest by peptide nucleic acid bound to the DNA template strand. *Gene*, **149**, 139-145.

Ottmann, M., Gabus, C. and Darlix, J.L. (1995) The central globular domain of the nucleocapsid protein of human immunodeficiency virus type 1 is critical for virion structure and infectivity. *J Virol*, **69**, 1778-1784.

Paddock, S.W. and Albrecht-Buehler, G. (1986) Distribution of microfilament bundles during rotation of the nucleus in 3T3 cells treated with monensin. *Exp Cell Res*, **163**, 525-538.

Park, P.C. and De Boni, U. (1992) Nuclear membrane modifications in polytene nuclei of Drosophila melanogaster: serial reconstruction and cytochemistry. *Anat Rec*, **234**, 15-26.

Perraut, R., Girault, G. and Moreau, J.P. (2000) Stability-related studies on 17D yellow fever vaccine. *Microbes Infect*, **2**, 33-38.

Peterson-Burch, B.D., Wright, D.A., Laten, H.M. and Voytas, D.F. (2000) Retroviruses in plants? *Trends Genet*, **16**, 151-152.

Piot, P., Bartos, M., Ghys, P.D., Walker, N. and Schwartlander, B. (2001) The global impact of HIV/AIDS. *Nature*, **410**, 968-973.

Pistor, S., Chakraborty, T., Walter, U. and Wehland, J. (1995) The bacterial actin nucleator protein ActA of Listeria monocytogenes contains multiple binding sites for host microfilament proteins. *Curr Biol*, **5**, 517-525.

Pollard, T.D. (1986) Rate constants for the reactions of ATP- and ADP-actin with the ends of actin filaments. *J Cell Biol*, **103**, 2747-2754.

Pollard, T.D. (1999) Introduction to actin and actin-binding proteins. In Kreis, T. and Vale, R. (eds.), *Guidebook to the Cytoskeletal and Motor Proteins.* Oxford University Press, New York.

Pollard, T.D. and Beltzner, C.C. (2002) Structure and function of the Arp2/3 complex. *Curr Opin Struct Biol*, **12**, 768-774.

Pollard, T.D., Blanchoin, L. and Mullins, R.D. (2000) Molecular mechanisms controlling actin filament dynamics in nonmuscle cells. *Annu Rev Biophys Biomol Struct*, **29**, 545-576.

Pollard, T.D. and Borisy, G.G. (2003) Cellular motility driven by assembly and disassembly of actin filaments. *Cell*, **112**, 453-465.

Pollard, T.D. and Cooper, J.A. (1986) Actin and actin-binding proteins. A critical evaluation of mechanisms and functions. *Annu Rev Biochem*, **55**, 987-1035.

Pomerantz, R.J. and Horn, D.L. (2003) Twenty years of therapy for HIV-1 infection. *Nat Med*, **9**, 867-873.

Popov, S., Rexach, M., Ratner, L., Blobel, G. and Bukrinsky, M. (1998a) Viral protein R regulates docking of the HIV-1 preintegration complex to the nuclear pore complex. *J Biol Chem*, **273**, 13347-13352.

Popov, S., Rexach, M., Zybarth, G., Reiling, N., Lee, M.A., Ratner, L., Lane, C.M., Moore, M.S., Blobel, G. and Bukrinsky, M. (1998b) Viral protein R regulates nuclear import of the HIV-1 pre-integration complex. *Embo J*, **17**, 909-917.

Praseuth, D., Grigoriev, M., Guieysse, A.L., Pritchard, L.L., Harel-Bellan, A., Nielsen, P.E. and Helene, C. (1996) Peptide nucleic acids directed to the promoter of the alpha-chain of the interleukin-2 receptor. *Biochim Biophys Acta*, **1309**, 226-238.

Prat, A.G. and Cantiello, H.F. (1996) Nuclear ion channel activity is regulated by actin filaments. *Am J Physiol*, **270**, C1532-1543.

Prats, A.C., Sarih, L., Gabus, C., Litvak, S., Keith, G. and Darlix, J.L. (1988) Small finger protein of avian and murine retroviruses has nucleic acid annealing activity and positions the replication primer tRNA onto genomic RNA. *Embo J*, **7**, 1777-1783.

Rambaut, A., Robertson, D.L., Pybus, O.G., Peeters, M. and Holmes, E.C. (2001) Human immunodeficiency virus. Phylogeny and the origin of HIV-1. *Nature*, **410**, 1047-1048.

Ramboarina, S., Morellet, N., Fournie-Zaluski, M.C., Roques, B.P. and Moreller, N. (1999) Structural investigation on the requirement of CCHH zinc finger type in nucleocapsid protein of human immunodeficiency virus 1. *Biochemistry*, **38**, 9600-9607.

Ratilainen, T., Holmen, A., Tuite, E., Haaima, G., Christensen, L., Nielsen, P.E. and Norden, B. (1998) Hybridization of peptide nucleic acid. *Biochemistry*, **37**, 12331-12342.

Renkema, G.H. and Saksela, K. (2000) Interactions of HIV-1 NEF with cellular signal transducing proteins. *Front Biosci*, **5**, D268-283.

Richman, D.D. (2001) HIV chemotherapy. *Nature*, **410**, 995-1001.

Ridley, A.J. and Hall, A. (1992) The small GTP-binding protein rho regulates the assembly of focal adhesions and actin stress fibers in response to growth factors. *Cell*, **70**, 389-399.

Ridley, A.J., Paterson, H.F., Johnston, C.L., Diekmann, D. and Hall, A. (1992) The small GTP-binding protein rac regulates growth factor-induced membrane ruffling. *Cell*, **70**, 401-410.

Riparbelli, M.G., Dallai, R. and Callaini, G. (1993) The cortical actin cytoskeleton in a Dipteran embryo: analysis of the spatial reorganization of F-actin aggregates during the early nuclear division cycles. *Biol Cell*, **78**, 223-227.

Roberts, J.D., Bebenek, K. and Kunkel, T.A. (1988) The accuracy of reverse transcriptase from HIV-1. *Science*, **242**, 1171-1173.

Roux, P., Munter, S., Frischknecht, F., Herbomel, P. and Shorte, S.L. (2004) Focusing light on infection in four dimensions. *Cell Microbiol*, **6**, 333-343.

Sazani, P., Gemignani, F., Kang, S.H., Maier, M.A., Manoharan, M., Persmark, M., Bortner, D. and Kole, R. (2002) Systemically delivered antisense oligomers upregulate gene expression in mouse tissues. *Nat Biotechnol*, **20**, 1228-1233.

Schiavoni, I., Trapp, S., Santarcangelo, A.C., Piacentini, V., Pugliese, K., Baur, A. and Federico, M. (2004) HIV-1 Nef enhances both membrane expression and virion incorporation of Env products: a model for the Nef dependent Increase of HIV-1 infectivity. *J Biol Chem*.

Schluter, K., Jockusch, B.M. and Rothkegel, M. (1997) Profilins as regulators of actin dynamics. *Biochim Biophys Acta*, **1359**, 97-109.

Schmidt, A. and Hall, M.N. (1998) Signaling to the actin cytoskeleton. *Annu Rev Cell Dev Biol*, **14**, 305-338.

Schneemann, A., Schneider, P.A., Lamb, R.A. and Lipkin, W.I. (1995) The remarkable coding strategy of borna disease virus: a new member of the nonsegmented negative strand RNA viruses. *Virology*, **210**, 1-8.

Schneider, P.A., Briese, T., Zimmermann, W., Ludwig, H. and Lipkin, W.I. (1994) Sequence conservation in field and experimental isolates of Borna disease virus. *J Virol*, **68**, 63-68.

Sei, S., Yang, Q.E., O'Neill, D., Yoshimura, K., Nagashima, K. and Mitsuya, H. (2000) Identification of a key target sequence to block human immunodeficiency virus type 1 replication within the gag-pol transframe domain. *J Virol*, **74**, 4621-4633.

Sheetz, M.P. (1999) Motor and cargo interactions. *Eur J Biochem*, **262**, 19-25.

Sherman, M.P. and Greene, W.C. (2002) Slipping through the door: HIV entry into the nucleus. *Microbes Infect*, **4**, 67-73.

Small, J.V., Herzog, M. and Anderson, K. (1995) Actin filament organization in the fish keratocyte lamellipodium. *J Cell Biol*, **129**, 1275-1286.

Small, J.V., Isenberg, G. and Celis, J.E. (1978) Polarity of actin at the leading edge of cultured cells. *Nature*, **272**, 638-639.

Sodeik, B., Ebersold, M.W. and Helenius, A. (1997) Microtubule-mediated transport of incoming herpes simplex virus 1 capsids to the nucleus. *J Cell Biol*, **136**, 1007-1021.

Soderqvist, H., Imreh, G., Kihlmark, M., Linnman, C., Ringertz, N. and Hallberg, E. (1997) Intracellular distribution of an integral nuclear pore membrane protein fused to green fluorescent protein--localization of a targeting domain. *Eur J Biochem*, **250**, 808-813.

Sohail, M. and Southern, E.M. (2000) Selecting optimal antisense reagents. *Adv Drug Deliv Rev*, **44**, 23-34.

Spector, I., Shochet, N.R., Blasberger, D. and Kashman, Y. (1989) Latrunculins--novel marine macrolides that disrupt microfilament organization and affect cell growth: I. Comparison with cytochalasin D. *Cell Motil Cytoskeleton*, **13**, 127-144.

Stricker, R.B. and Elswood, B.F. (1997) Polio vaccines and the origin of AIDS: an update. *Med Hypotheses*, **48**, 193.

Sune, C. and Garcia-Blanco, M.A. (1995) Transcriptional trans activation by human immunodeficiency virus type 1 Tat requires specific coactivators that are not basal factors. *J Virol*, **69**, 3098-3107.

Suomalainen, M., Nakano, M.Y., Keller, S., Boucke, K., Stidwill, R.P. and Greber, U.F. (1999) Microtubule-dependent plus- and minus end-directed motilities are competing processes for nuclear targeting of adenovirus. *J Cell Biol*, **144**, 657-672.

Symons, M., Derry, J.M., Karlak, B., Jiang, S., Lemahieu, V., McCormick, F., Francke, U. and Abo, A. (1996) Wiskott-Aldrich syndrome protein, a novel effector for the GTPase CDC42Hs, is implicated in actin polymerization. *Cell*, **84**, 723-734.

Tanchou, V., Gabus, C., Rogemond, V. and Darlix, J.L. (1995) Formation of stable and functional HIV-1 nucleoprotein complexes in vitro. *J Mol Biol*, **252**, 563-571.

Taylor, D.L. and Salmon, E.D. (1989) Basic fluorescence microscopy. *Methods Cell Biol*, **29**, 207-237.

Taylor, R.W., Chinnery, P.F., Turnbull, D.M. and Lightowlers, R.N. (1997) Selective inhibition of mutant human mitochondrial DNA replication in vitro by peptide nucleic acids. *Nat Genet*, **15**, 212-215.

Temin, H.M. and Mizutani, S. (1970) RNA-dependent DNA polymerase in virions of Rous sarcoma virus. *Nature*, **226**, 1211-1213.

Thomas, S.A. (2004) Anti-HIV Drug Distribution to the Central Nervous System. *Curr Pharm Des*, **10**, 1313-1324.

Thomson, S.A., Josey, J.A., DCadilla, R., Gaul, M.D., Hassman, G.C., Luzzio, M.J., Pipe, A.J., Reed, K.L., Ricca, D.J., Wiehte, R.W. and Noble, S.A. (1995) Fmoc mediated synthesis of peptide nucleic acids. *Tetrahedron*, **51**, 6179-6194.

Tilney, L.G. (1976) *Actin: its association with membranes and the regulation of its polymerization*. Rockefeller University Press, Boston, MA.

Tilney, L.G. and Portnoy, D.A. (1989) Actin filaments and the growth, movement, and spread of the intracellular bacterial parasite, Listeria monocytogenes. *J Cell Biol*, **109**, 1597-1608.

Towers, G.J., Hatziioannou, T., Cowan, S., Goff, S.P., Luban, J. and Bieniasz, P.D. (2003) Cyclophilin A modulates the sensitivity of HIV-1 to host restriction factors. *Nat Med*, **9**, 1138-1143.

Vacquier, V.D. (1968) The connection of blastomeres of sea urchin embryos by filopodia. *Exp Cell Res*, **52**, 571-581.

Verrier, F.C., Charneau, P., Altmeyer, R., Laurent, S., Borman, A.M. and Girard, M. (1997) Antibodies to several conformation-dependent epitopes of gp120/gp41 inhibit CCR-5-dependent cell-to-cell fusion mediated by the native envelope glycoprotein of a primary macrophage-tropic HIV-1 isolate. *Proc Natl Acad Sci U S A*, **94**, 9326-9331.

Vogt, V.M. (1996) Proteolytic processing and particle maturation. *Curr Top Microbiol Immunol*, **214**, 95-131.

von Schwedler, U., Kornbluth, R.S. and Trono, D. (1994) The nuclear localization signal of the matrix protein of human immunodeficiency virus type 1 allows the establishment of infection in macrophages and quiescent T lymphocytes. *Proc. Natl. Acad. Sci. USA*, **91**, 6992-6996.

Wain-Hobson, S., Vartanian, J.P., Henry, M., Chenciner, N., Cheynier, R., Delassus, S., Martins, L.P., Sala, M., Nugeyre, M.T., Guetard, D. and et al. (1991) LAV revisited: origins of the early HIV-1 isolates from Institut Pasteur. *Science*, **252**, 961-965.

Wang, Y.L. (1985) Exchange of actin subunits at the leading edge of living fibroblasts: possible role of treadmilling. *J Cell Biol*, **101**, 597-602.

Weaver, A.M., Young, M.E., Lee, W.L. and Cooper, J.A. (2003) Integration of signals to the Arp2/3 complex. *Curr Opin Cell Biol*, **15**, 23-30.

Weiss, R.A. (2001) Gulliver's travels in HIVland. *Nature*, **410**, 963-967.

Weiss, S.R., Varmus, H.E. and Bishop, J.M. (1977) The size and genetic composition of virus-specific RNAs in the cytoplasm of cells producing avian sarcoma-leukosis viruses. *Cell*, **12**, 983-992.

Welch, M.D. and Mullins, R.D. (2002) Cellular control of actin nucleation. *Annu Rev Cell Dev Biol*, **18**, 247-288.

Welch, M.D., Rosenblatt, J., Skoble, J., Portnoy, D.A. and Mitchison, T.J. (1998) Interaction of human Arp2/3 complex and the Listeria monocytogenes ActA protein in actin filament nucleation. *Science*, **281**, 105-108.

WHO, U.a. (2003) AIDS epidemic update 2003.

Wilk, T., Gowen, B. and Fuller, S.D. (1999) Actin associates with the nucleocapsid domain of the human immunodeficiency virus Gag polyprotein. *J Virol*, **73**, 1931-1940.

Wills, J.W. and Craven, R.C. (1991) Form, function, and use of retroviral gag proteins. *Aids*, **5**, 639-654.

Wong, J.K., Hezareh, M., Gunthard, H.F., Havlir, D.V., Ignacio, C.C., Spina, C.A. and Richman, D.D. (1997) Recovery of replication-competent HIV despite prolonged suppression of plasma viremia. *Science*, **278**, 1291-1295.

Yan, C., Leibowitz, N. and Melese, T. (1997) A role for the divergent actin gene, ACT2, in nuclear pore structure and function. *Embo J*, **16**, 3572-3586.

Yin, H.L. and Stull, J.T. (1999) Proteins that regulate dynamic actin remodeling in response to membrane signaling minireview series. *J Biol Chem*, **274**, 32529-32530.

Zennou, V., Petit, C., Guetard, D., Nerhbass, U., Montagnier, L. and Charneau, P. (2000) HIV-1 genome nuclear import is mediated by a central DNA flap. *Cell*, **101**, 173-185.

Zhang, H., Yang, B., Pomerantz, R.J., Zhang, C., Arunachalam, S.C. and Gao, L. (2003) The cytidine deaminase CEM15 induces hypermutation in newly synthesized HIV-1 DNA. *Nature*, **424**, 94-98.

Zhao, Y., Yu, M., Chen, M., Elder, R.T., Yamamoto, A. and Cao, J. (1998) Pleiotropic effects of HIV-1 protein R (Vpr) on morphogenesis and cell survival in fission yeast and antagonism by pentoxifylline. *Virology*, **246**, 266-276.

Zhen, Y.Y., Libotte, T., Munck, M., Noegel, A.A. and Korenbaum, E. (2002) NUANCE, a giant protein connecting the nucleus and actin cytoskeleton. *J Cell Sci*, **115**, 3207-3222.

Zhu, T., Korber, B.T., Nahmias, A.J., Hooper, E., Sharp, P.M. and Ho, D.D. (1998) An African HIV-1 sequence from 1959 and implications for the origin of the epidemic. *Nature*, **391**, 594-597.

Zimmermann, W., Breter, H., Rudolph, M. and Ludwig, H. (1994) Borna disease virus: immunoelectron microscopic characterization of cell-free virus and further information about the genome. *J Virol*, **68**, 6755-6758.

6. Annex

Chemical synthesis of pseudoisocytosin

To get a stable triplex formation, pseudoisocytosine (ψiC or 'J bases') is more favorable than cytosine in the Hoogsteen strand because the 'J-base' does not require low pH for N3 'protonation' (see chapter 1.2.1). Pseudoisocytosine is not available by any supplier and in order to design triplex forming PNAs we had to synthesize this particular nucleobase ourselves. The synthesis had to be done in three main steps. In independent reactions the N-(2-aminoethyl) glycine backbone, the 'J-base' and the protecting group (Bhoc) for the exocyclic nitrogen of the 'J-base' had to be synthesized. Finally, all three molecules were meant to be coupled in the last synthesis steps.

Synthesis of the backbone (Thomson et al., 1995)

To a vigorously stirred solution of ethylenediamine (1) (75ml, 1.13mol) in CH_2Cl_2 (500ml) at 0˚C t-butyl bromoactate (20.7ml, 0.13mol) in CH_2Cl_2 (100ml) was added over 5 hours. The resulting mixture was allowed to warm slowly to room temperature (RT) and then stirred overnight. The reaction mixture was washed with water (3 x 125ml), and the combined aqueous wash was back-extracted with CH_2Cl_2 (125ml). Combined organic phases were dried over $MgSO_4$ and filtered. This workup gave *tert*-butyl N-(2-aminoethyl)glycinate (2) with a yield of 14.8g (65%). This material was taken after verification by mass spectrometry on the next step without further purification (m/z 175 $(M+H)^+$).

The Fmoc group was installed on the primary amine selectively. The product (2) (14.8g, 0.085mol) was dissolved in CH_2Cl_2 and diisopropylethylenamine (18.75ml, 0.11mol) was added with mechanical stirring. A solution of N-(9-fluorenylmethoxy carbonyloxy)succinimide (36.25g, 0.11mol) in CH_2Cl_2 (200ml) was added dropwise over 5 hours. The solution was stirred overnight, and then washed with 1N aq. HCl (5 x 100ml) and brine (1 x 100ml). The organic layer was dried ($MgSO_4$) and partially concentrated in vacuo (ca. 250ml). Cooling (-20˚C) overnight resulted in a precipitate, which was collected by filtration and washed with CH_2Cl_2 until the filtrate was colorless. The solids were dried in vacuo (60˚C) to give *tert*-butyl N-[2-(N-9-fluorenylmethoxycarbonyl)aminoethyl] glycinate hydrochloride (3) with a yield of 6.65g (36%) (m/z 397 $(M+H)^+$).

To obtain the free base (3) (4.76g, 0.01mol) was dissolved in $CHCl_3$ washed with aqueous saturated $NaHCO_3$ (2 x 150ml), dried ($MgSO_4$) and concentrated in vacuo.

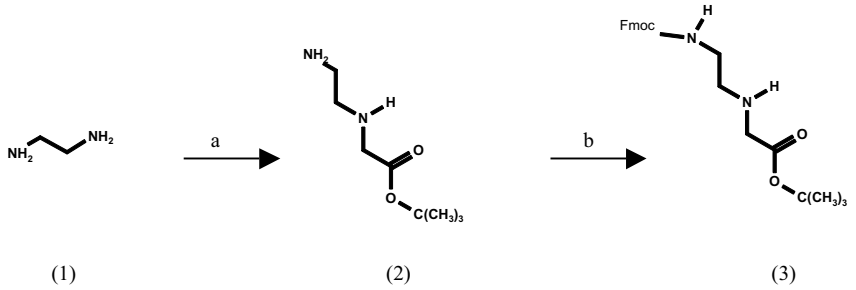

(1) (2) (3)

Figure 31: PNA backbone synthesis

Reagent (a) $BrCH_2CO_2C(CH_3)_3$, CH_2Cl_2; (b) DIEA, N-(9-fluorenylmethoxycarbonyloxy)-succinimide.

Pseudoisocytosine (Egholm et al., 1995)

Sodium methoxide (40.5g, 0.75mol) was suspended in dry ether (500ml) and stirred under N_2 at 0˚C. A mixture of dimethyl succinate (4) (65.4ml, 0.50mol) and methyl-formiate (5) (123ml, 2mol) was added dropwise over 45 min. The reaction mixture was stirred at 0˚C for 2 hours and then at RT overnight. Subsequently, the reaction mixture was evaporated to a viscous brown residue, which was washed once with petroleum ether and then dissolved in 3M HCl (160ml). The solution was then made weakly acidic with concentrated HCl and extracted with dichloromethane (4 x 250ml). The organic phase was dried ($MgSO_4$), filtered and evaporated under low pressure. The resulting residue was distilled at 65˚C and 0,7mbar overnight, yielding 38.7g (57%) of a mixture of methyl α-formylsuccinate (6) and dimethyl succinate (80:20) as a colorless oil. After verification of the product the mixture was used directly in the following preparation (NMR (as described in literature); m/z 174 $(M+H)^+$).

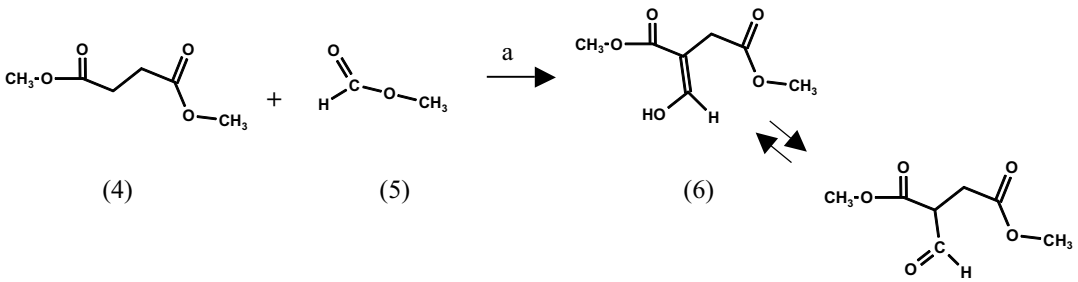

(4) (5) (6)

Figure 32: Step 1: Pseudoisocytosin

Reagent (a) sodium methoxid (CH_3ONa). Reaction was done in CH_2Cl_2 under N_2 atmosphere.

In the second step, sodium methoxide (41.9g, 0.78mol) was dissolved in 200ml methanol, dried with magnesium overnight and distilled immediately before use.

When sodium methoxide was completely dissolved, guanidine hydrochloride (49.4g, 0.52mol) (7) was added and the mixture was stirred for 10 min under nitrogen at RT. Then, a solution of methyl α-formylsuccinate (30.0g, 0.2mol) (6) in dry methanol was added. The reaction mixture was refluxed under nitrogen for 3 hours and then stirred at RT overnight. Subsequently, the reaction mixture was filtered, and the filter cake was washed once with methanol. The collected filtrate and wash fraction were evaporated under reduced pressure. The resulting residue was dissolved in water (80ml) and the solution was acidified with concentrated HCl to pH 4.2. The mixture was again stirred at 0˚C then filtered, the precipitate washed once with water and then freeze-dried leaving 13.54g (46%) of isocytosin-5-ylacetic acid (8) as a white solid (m/z 169 $(M+H)^+$). Then, thionylchloride (3.6ml, 0.05mol) was added to stirred methanol (210ml) at –40˚C under nitrogen, followed by isocytosin-5-ylacetic acid (8) (7.0g, 0.04mol) and the mixture was stirred at RT for 1 hour, at 60˚C for 3 hours and overnight at RT. The reaction mixture was evaporated to dryness and the residue was dissolved in saturated aqueous sodium bicarbonate ($NaHCO_3$, 80ml) giving a foamy precipitate. 4M HCl was added to pH 6.5 and the suspension was stirred at RT for 1 hour. The precipitate was collected by filtration, washed with water, recrystallized from water and freeze-dried yielding 4g (53%) of methyl isocytosin-5-ylacetate as white crystals (9) (NMR (as described in literature); m/z 184 $(M+H)^+$).

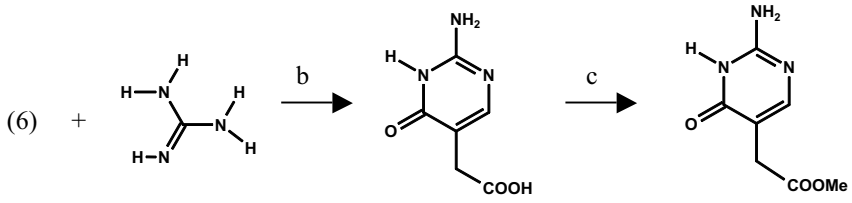

(7) (8) (9)

Figure 33: Step 2: Pseudoisocytosin

Reagents: (b) sodium methoxid ($NaOCH_3$), (c) thionylchloride ($SOCl_2$)

Bhoc synthesis (Hiskey and Adams, 1965)

A mixture containing benzhydrol (10) (9.21g, 0.05mol), pyrimidine (4.065ml, 0.05mol) and 15ml chloroform was cooled in an ice bath and treated dropwise over 30 minutes with 4.3ml methyl chlorothiolcarbonate (11) (5.3g, 0.05mol). The mixture was stirred for 1.5 hours and allowed to warm to RT. Most of the chloroform was removed in vacuo, the residue was dissolved in ether and the pyridine hydrochloride removed by filtration. The ether solution was washed with water and saturated sodium chloride solution and dried with $MgSO_4$. The evaporation of the ether resulted in a yellow liquid benzhydryl methylthiolcarbonate (12), which was dried over calcium chloride. The crude benzhydryl methylthiolcarbonate (12) was dissolved in ether (45ml), cooled and slowly treated dropwise over 1 hour with a solution of 85% hydrazine hydrate (3.75ml, 0.05mol) in 42.25ml methanol. The mixture was stirred for 1.5 hours at RT and then allowed to stand 5 hours at RT. The organic layer was evaporated and dried over silicagel. The solid was recrystallized from ether yielding in 3.9g (36%) of benzhydryloxycarbonylhydrazide (13) as a white solid and used directly in the following preparation (m.p. 101-102˚C; NMR (as described in literature)).

A mixture of (13) (3.9g, 0.02mol), 5.5ml acetic acid and 3ml of water was stirred until solution was completed and then cooled to 0-5˚C. The solution was treated with powdered sodium nitrite (1.37g, 0.02mol) added in portions. Solid azide began precipitating during the $NaNO_2$ addition. The mixture was poured into 80ml of water and extracted with ether. The extract was washed with 200ml of 1M sodium hydrocarbonate solution ($NaHCO_3$) until the washes were alkaline. The extract was then washed with saturated sodium chloride solution, dried and evaporated to a yellow oil. Cooling the oil provided 3.4g (33%) of benzhydryl azidoformate (14) as a pale yellow solid (m.p. 37-39˚C; NMR (as described in literature)).

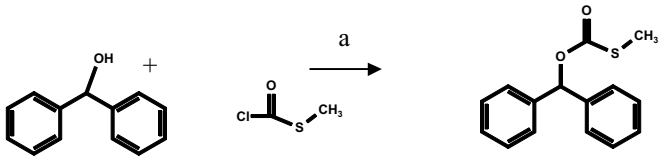

(10) (11) (12)

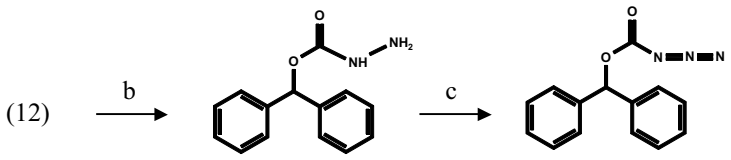

Figure 34: Benzhydryl azidoformate synthesis

Reagent (a) pyridine (C_5H_5N), (b) hydrazine hydrate (N_2H_4) and (c) sodium nitrite ($NaNO_2$).

Coupling of thymin to the Fmoc protected backbone (Jones et al., 1973)

Thymine (12.5g, 0.1mol), potassium hydroxide (27.5g, 0.5mol) and chloroacetic acid (18.75g, 0.2mol) were dissolved in water (250ml) and the solution boiled for 1 hour. The solution was cooled and the pH was adjusted to 3.5. The resulting precipitate was filtered off and recrystallized twice from water to give 1-carboxymethylthymine (15) with a yield of 6.65g (36%) (m/z 185 $(M+H)^+$)

The free base of (3) (7.8g, 0.02mol) was dissolved in DMF (100ml) then 1-carboxy methylthymine (15) (4.8g, 0.03mol) was added and the mixture was stirred until the substance was dissolved. EDC (4.8g, 0.03mol) was added in two equal portions over 30 minutes, and the mixture stirred overnight. The solution was concentrated in vacuo, and water (200ml) was added to the resulting thick oil. The mixture was shaken vigorously for several minutes to precipitate a fine white solid. The solids were collected by filtration, stirred with water (200ml), filtered, washed with cold water, and dried in vacuo. Purification by flash chromatography (5% MeOH/CH_2Cl_2) gave *tert*-butyl N-[2-(N-9-fluorenylmethoxycarbonyl)aminoethyl]-N-[(thymin-1-yl)acetyl]glycinate (16) with a yield of 6.8g (66%). To a suspension of (16) (4.5g, 7.9mol) in anhyd CH_2Cl_2 (40ml) was added 4N HCl (4ml) in 1,4-dioxane (60ml) and the mixture was stirred overnight. The solid was collected by filtration, washed with hexane and dried in vacuo to give N-[2-(N-9-fluorenylmethoxycarbonyl)aminoethyl]-N-[(thymin-1-yl)acetyl]glycinate (17) with a yield of 0.85g (21%) (m/z 507 $(M+H)^+$) (Thomson et al., 1995). The final product (the T-PNA-monomer) was used for the PNA synthesis on the automated synthesizer Syro II (chapter 2.1).

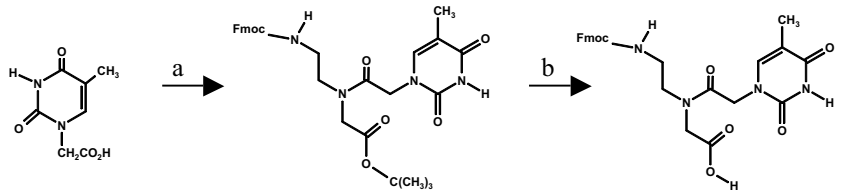

Figure 35: Coupling of thymin to the backbone

Reagents: (a) EDC (1-ethyl-3-(3-dimethylaminopropyl) carbodiimide) and the free base of (3) (b) HCl/ 1,4-dioxane.

Coupling of methyl isocytosin-5-ylacetate to Bhoc protecting group (Hiskey and Adams, 1965)

Finally we wanted to introduce the Bhoc protecting group on the exocyclic nitrogen of methyl isocytosin-5-ylacetate. Therefore benzhydryl azidoformate (14) (3.4g, 0.007mol), methyl isocytosin-5-ylacetate (1.34g, 0.007mol) and magnesium oxide (0.54g, 0.013mol) were mixed in 15ml of water and 30ml of dioxane and shaken for ~60 hours. The filtrated solution was diluted with 150ml of water and extracted with ethyl acetate (3 x 80ml). The aqueous layer was cooled to 0˚C, acidified to pH 1-2 with 4N HCl and again extracted with ethyl acetate (3 x 80ml). The extract was washed with water (3 x 100ml) and saturated sodium chloride solution (1 x 100ml), dried with $MgSO_4$ and evaporated to a pale yellow oil.

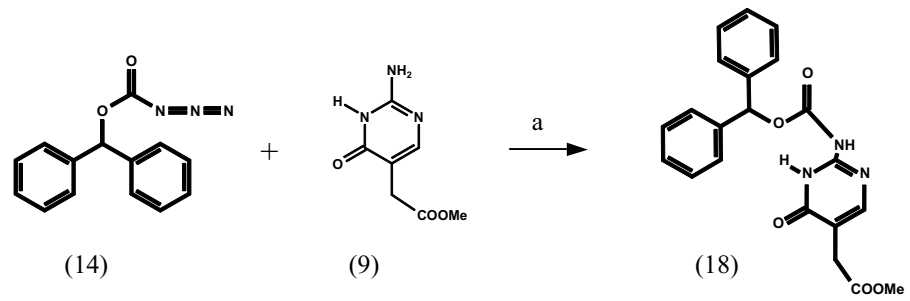

Figure 36: Introduction of the protecting group (Bhoc)

Reagents: (a) magnesium oxide (MgO)

The product (18) should have crystallized from a n-pentan/ ether mixture after the reaction was completed. But unfortunately, no crystals were arising from the solution. Even after further purification with chromatography (10% MeOH/CH_2Cl_2) the correct product was not obtained (checked by mass spectrometry and NMR). The synthesis was stopped at this point, because it became clear that the PNA approach to inhibit the replicative cycle of HIV would not be further considered.

CD-BODIPY labeling of a motile living cell

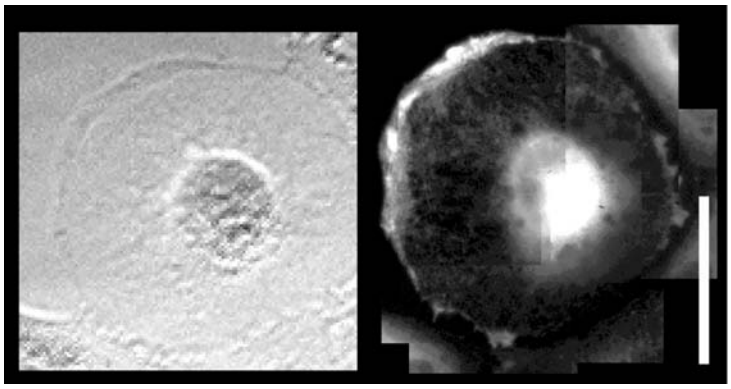

Figure 37: CD-BODIPY labeling of a U87 glioblastoma cell

The panel shows a bright field image of a migrating U87 glioblastoma cell displaying strong membrane ruffling, and the corresponding fluorescence image showing the partitioning of CD-BODIPY (50nM) into the membrane ruffles of the lamellipodia. In addition, high levels of CD-BODIPY are observed around the nucleus. Note: the image is a montage of magnified fields comprising a mosaic across the cell, and due to different intensities in different regions individual frames have been contrast adjusted to accommodate different intensity levels (scale bar: 24μm).

Tracking of single NPCs of Vpr-expressing cells *in vivo*

To quantify membrane ruffling in Vpr expressing cells, we performed a series of *in vivo* experiments imaging the punctuated pattern of the NPCs. For this purpose HeLa cells were transfected with Vpr-GFP or a control plasmid. Approximately 5-6 hours later, 4D image sequences of single nuclei were acquired (one z-stacks every ~15-30 minutes). We were using an imaging system most appropriate for *in vivo* fluorescence microscopy, with fast acquisition time and a high power objective. The series of images were then deconvolved and reconstructed for further analysis to track single NPCs in the global context of the nuclear envelope.

Due to the small size of single NPCs (~7 nm in width and 50 nm in length) the tracking is a very challenging project. Using any light-based microscopy, the best objectives available offer planar (*x*,*y*) resolution in the range of ~200 nm. This means that we are no longer able to spatially distinguish (resolve) two points closer than this distance (the so-called 'diffraction limit'). But fluorescent light of a subresolutional point is emanating into focal planes above and underneath and can be collected by the objective and projected to the light detector, a CCD (charge-coupled device) camera.

The light from the sample is a highly complex representation of the subresolution point inside the sampling voxel volume. Therefore even a subresolution object, such as single NPC, can in fact be detected by its fluorescence (for review see (Roux et al., 2004)).

After deconvolution and reconstruction, the movement of single spots, corresponding to NPCs, was analyzed with an automated algorithm (developed by A. Genovesio). To obtain useful results, the fluorescence of the spots must be strong and stable over time. The preliminary result of the tracking of single NPCs is shown in Figure 38.

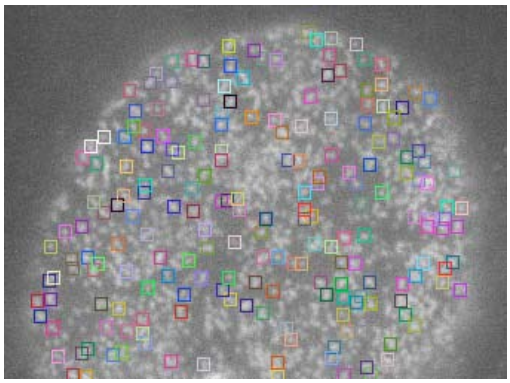

Figure 38: Tracking of single NPCs of a HeLa cell expressing Vpr-GFP

HeLa cells were transfected with a plasmid containing Vpr-GFP. About 6 hours after transfection 4D image series were recorded and subsequent processed for the tracking of single NPCs. The program was engendered to track single points through the volume and timeframe. The colored squares indicate the NPCs recognized as single points by the algorithm of the tracking program.

These first experiments are very encouraging, but in order to have statistically reliable data a certain amount of single nuclei have to be recorded and analyzed.

Visualization strategy of viral particles

To visualize HIV PICs *in vivo*, Annette Boese, a postdoc in the laboratory in Paris (BCN, Pasteur Institute) has engineered GFP labeled viral particles. She constructed an expression vector encoding a fusion protein from GFP-lacI and Vpr, both joined by a peptide that represents the cleavage site for the HIV-1 protease (named pGFP-lacI-HCS-Vpr). This fusion protein is co-expressed during particle production, incorporated into the budding particle via the Vpr moiety and cleaved during

maturation into the Vpr protein (that can subsequently exert its viral functions as it lacks any tags) and GFP-lacI. GFP-lacI binds the lacO-repeats in the retroviral genome after completion of reverse transcription to label the PIC until the site of integration into the genome.

Erklärung

Ich erkläre hiermit, dass ich die vorgelegte Dissertation selbst verfasst und mich dabei keiner anderer als der von mir ausdrücklich bezeichneten Quellen und Hilfen bedient habe.

Heidelberg, den 04. Juni 2004

(Sylvia Münter)